Characterisation of Spreadability Behaviour of Ti6Al4V Powders for Additive Manufacturing

Fatemeh A. Talebi

Submitted in accordance with the requirements for the degree of Master of Research

The University of Leeds

School of Chemical and Process Engineering

April 2021

Acknowledgements

Special thanks to my supervisors Dr. Ali Hassanpour and Prof. Andrew Bayly, without whom this work would have not been possible. I am grateful for your advice, support and guidance throughout the course in the middle of the pandemic.

To my parents and brother, words cannot describe how grateful I am for you. Thank you for believing in and supporting me in every shape and form and providing me with the wings to fly. None of this would have ever been possible without you.

Abstract

Powder-bed based Additive Manufacturing (AM), also known as 3D printing, is an emerging technology to produce high quality end-parts at a cost and time effective manner as compared to the traditional subtractive manufacturing processes. The study of metal powder-bed processes usually involves two critical steps which includes the spreading of the powder and the fusion of the layers. Spreadability of powders is an essential characteristic in determining the total build time and quality of the final product. The spreadability is thought to be linked to the powder characteristics, mostly the flow behaviour, which is influenced by the individual particle properties and environmental conditions.

This thesis endeavours to investigate the spreading behaviour of two samples of titanium alloy (Ti6Al4V) powders, produced by Gas Atomisation (GA) and Hydrogenation-dehydrogenation (HDH) methods. The spreading behaviour of each sample has been investigated using an in-house spreading rig set up at University of Leeds, with a set of parameters, including the gap size between the blade and build plate (ranging between 191 μm to 508 μm) and spreading velocity (ranging between 50mm/s to 200mm/s) as the variables, while the mass of the fed powder as a constant. The bulk layer density and mass per area are the two measures of spreadability introduced in this study.

It is found that the quality of the spread layer is significantly influenced not only by the powder properties, but also the process parameters. GA powder exhibited spherical shapes, which in turn created homogeneous layers due to improved packing behaviour compared to HDH powder which were characterised by irregular shapes impeding powder flow. Additionally, the bulk layer density of GA powder decreased when the spreading velocity was increased, but this correlation was not established for HDH powder. This owes to the fact that HDH powders are of irregular morphologies, hence they consist of particular particle arrangements under the spreader at certain velocities. An increase in the spreading velocity also resulted in a gradual reduction in the values of the mass per area, suggesting that higher velocities jeopardise the quality of the spread layer. Due to the limitations of spreader rig, only a specific amount of powder to cover the build plate was utilised, however, in reality an infinite amount of powder is fed for spreading the layers.

It is concluded that GA powders outperform HDH powders in terms of reliability and creating higher bulk layer densities, which is essential in ensuring quality layers and, consequently, defect-free end parts. The quality of the layer is determined by calculating the average bulk layer density. In AM, a higher bulk layer density is desirable as it demonstrates better packing quality , homogenous layers of low porosity, which consequently results into end parts of high density and increased mechanical strength.

Table of Contents

List of Tables

List of Figures

Abbreviations

AM	Additive manufacturing
DEM	Discrete element method
PBF	Powder bed fusion
LPBF	Laser-based powder bed fusion
DMLS	Direct metal laser sintering
EBM	Electron beam melting
SHS	Selective heat sintering
SLM	Selective laser melting
SLS	Selective laser sintering
PSD	Particle size distribution
GA	Gas atomisation
WA	Water atomisation
PREP	Plasma rotating electrode process
PA	Plasma atomisation
HDH	Hydrogenation-dehydration
AR	Aspect ratio
AoR	Angle of repose
HR	Hausner ratio
CI	Carr's compressibility index

CHAPTER ONE

Introduction

1.1 Focus of the Research

1.2 Aims of the Research

1.3 Objectives of the Research

1.4 Overview of the Research

1. Introduction

Additive manufacturing (AM) has become an increasingly popular method of production over the last few years. It eliminates the traditional subtractive methods of production by depositing materials layer-by-layer to fabricate parts that comprise of complex geometries with exceptional properties [1-3]. Additive manufacturing consists of seven manufacturing technologies including VAT photopolymerisation, material jetting, binder jetting, material extrusion, sheet lamination, directed energy deposition (DED) and powder bed fusion (PBF) [4]. Powder-bed based processes employ a laser or electron beam as a source of energy to sinter feedstock material in the form of powders, and consists of different printing methods, such as, but not limited to: direct metal laser sintering (DMLS), electron beam melting (EBM), selective heat sintering (SHS), selective laser melting (SLM) and selective laser sintering (SLS) [5, 6]. The above mentioned printing techniques have different binding mechanisms by either completely or partially melting the metal powders [7]. Additionally, laser-based powder bed fusion (LPBF) is a common manufacturing technology employed by industry to produce high quality metal products [8].

Additive manufacturing is used in an array of disciplines to accelerate market adoption, especially in the areas of medicine and engineering [9]. High performance alloys such as Ti-6Al-4V are used within the aerospace industry due to their reduced “buy-to-fly ratio”; however, the price of these AM powders is a major drawback [10]. The buy-to-fly ratio is defined as ratio of the raw material required to produce a part to the actual final part output [11]. One of the many advantages governing direct metal additive manufacturing is its compensation for the high prices due to minimal wastage of AM powders, as only the required amount is used to sinter the “near net shape” and the rest can then be recycled for reuse [10].

To further develop this area and ensure high-quality end parts, the spreading process of AM powders need to be investigated. This is commonly known as “spreadability” in literature, and unlike “flowability” of powders, it is not extensively covered. To date, there is neither a definition agreed by the general consensus nor a characterisation method to analyse “spreadability” of powders. Keeping in mind that the two terminologies are very different, a parallel can be established between them to further understand the term “spreadability”. Generally, the term

"spreadability" has been defined as the ease in powder movement under narrow openings or gaps to form thin, uniform layers of high packing densities [12, 13], while flowability is defined as the "ability of the powder to flow" [14]. Spreadability of powders is directly linked to the quality of the deposited layer, hence, different factors such as powder properties (i.e. particle size and shape distribution, morphology and flow behaviour), process parameters (i.e. spreading velocity, gap size, material and type of spreader) and environmental conditions (i.e. humid and higher temperatures) can significantly influence the spreading behaviour of powders. The quantification of the spread layer quality in terms of the layer's bulk density, surface roughness and spread coverage as parameters provides valuable information for the development of spreadability metrics. Hence, experimental and simulation work has been carried out by some researchers to investigate the effect of spreadability on both the powder layers and consequently the final fabricated product, and will be thoroughly discussed in this work.

This work endeavours to investigate the effects of process parameters such as spreading velocity and gap size on the quality of spread layers by utilising an in-house spreading rig, and to further quantify the spread quality using the "bulk layer density" and "percentage of spread coverage" of layers on the build plate.

1.1 Focus of the Research

The focus of this thesis is to scrutinise the effects of powder properties and process parameters on the spread layers created in additive manufacturing, especially within the powder bed fusion processes. Powder properties such as particle shape, size distribution, packing behaviour and flow behaviour have shown to have a significant effect on powder spreading. Additionally, process parameters such as spreading velocity, gap size and laser energy have proven to also have ramifications on the quality of spread layers.

1.2 Aims of the Research

The aim of this research is to acknowledge the gap within literature regarding the spreadability of powders and to potentially quantify this term. To date, there are no viable metrics for spreadability. Two samples of GA and HDH, grade 5 Ti-6Al-4V powders are utilised in this work. The different production methods are highly likely to result in different spreading profiles.

In order, to analyse and compare the differences in the spreading of these powders, a set of objectives are established. These are thoroughly mentioned in the following section.

1.3 Objectives of the Research

1. To undertake a thorough review of literature and identify the knowledge gap. This is of importance as the dynamics of powder spreading is yet to be established.
2. To undertake experimental work, using an in-house spreading rig that emulates the re-coating behaviour in powder bed-based processes. The powders will be spread and tested against a set of parameters such as spreading velocity and gap sizes.
3. To further quantify the spread layer in terms of the bulk layer density and mass per area.
4. To further perform a comparative analysis between HDH and GA Ti-6Al-4V powders by investigating the effects of the dimensionless shear rate on the bulk layer density.
5. To perform image analysis using an over-head camera and visually observe the quality of the spread layers at different velocities and gap sizes.
6. Finally, to formulate a matrix to identify the optimal gap size and velocities for each of the powders. The matrix will enable comparison of the two powders at different gap sizes and velocities.

1.4 Overview of the Research

This thesis will consist of the following structure to meet the aims and objectives proposed:

- **Chapter one** consists of the introduction, where general information regarding additive manufacturing as an emerging industry is provided. The different manufacturing technologies associated with AM are briefly described. Furthermore, the aims and objectives of the research are stated and expanded upon.
- **Chapter two** consists of the literature review, where some articles regarding powder production technologies and powder characterisation in AM are thoroughly reviewed. The effects of Ti-6Al-4V powder properties and process parameters on the quality of the spread layer are further expanded upon and a summary of the knowledge gap is reported.

- **Chapter three** consists of the materials and methodology, where the experimental procedure undertaken for the spreading tests is specified. The quantification methods for the bulk layer density, mass per area and dimensionless shear rates are further explained.
- **Chapter four** consists of the qualitative observations where the standard operating procedures are mentioned, and the spread profiles captured from the overhead camera are analysed. The angle of repose on the built plate is also analysed and quantified for comparative analysis.
- **Chapter five** analyses the effects of spreading velocity and gap size on the spreading behaviour of Ti-6Al-4V layers by introducing two spreading metrics, namely the bulk layer density and mass per area. The combined effect of the spreading velocity and gap size in the form of the dimensionless shear rate is further discussed to compare the HDH and GA Ti-6Al-4V powders.
- **Chapter six** provides the conclusions gathered in this work where a comparative analysis between HDH and GA powders is reported.
- **Chapter seven** comprises of the future work where suggestion and recommendation are reported, such as the in-house rig upgrade and testing powders in different environmental conditions to further understand the spreading dynamics.

CHAPTER TWO

Literature Review

2.1 Methods of Powder Production in Additive Manufacturing (AM)

2.2 Powder Characterisation in Additive Manufacturing (AM)

2.3 Effects of Powder Properties on the Quality of Spread Layer

2.4 Effects of Process Parameters on the Quality of Spread Layer

2.5 Characterisation of Ti-6Al-4V Powders in Additive Manufacturing

2.6 Summary of the Knowledge Gap

2 Literature Review

2.1 Methods of Powder Production in Additive Manufacturing (AM)

The production method for AM powders plays a crucial role on the overall performance of the production process and inevitably the final quality of the end product [15]. There are a variety of powder production technologies that include mechanical methods and physical-chemical methods [15, 16]. These technologies include but are not limited to atomisation, electrolysis and plasma spheroidisation; for the purpose of this research, atomisation, which is a common metal powder production method in AM, will be expanded upon. The atomisation process involves the disintegration of a very thin stream of metal in a molten form by exposing it to gas, high water pressure, rotating forces or plasma [17]. As the molten metal is subjected to the previously mentioned factors, it disperses into droplets that crystallise before reaching the atomiser walls [17].

There are different types of atomisation processes that can be implemented, however, the three common techniques include: gas atomisation (GA), water atomisation (WA) and plasma rotating electrode process.

2.1.1 Gas Atomisation (GA)

Gas atomisation (GA) is the most common method for AM powder production, even though it is relatively expensive compared to water atomisation (WA). This method is opted for due to its production of spherical particles which is a crucial factor for overall flowability, loose powder packing and powder spreading [15, 18, 19]. This method involves a stream of molten metal that is pulverised by a jet of pressurised gas, which is later solidified and collected at the bottom of the system [15, 19]. The microstructure of these powders tends to be metastable due to the very rapid cooling rates that occur in the system [19]. However, gas entrapment during solidification is a weakness to this system [20].

2.1.2 Water Atomisation (WA)

This production method involves water sprays at high pressures ranging from 3-20 MPa, where it impinges on to the molten metal causing it to disintegrate into droplets. There are different water

spray configurations and pressures that can be utilised to produce powders of different particle sizes [21, 22]. The molten droplets then solidify to produce metal powders which are collected at the bottom of the atomisation chamber [21]. The main advantage of water atomisation is not only its cost effectiveness, but also high powder production rates. However, the powders produced through this technique are often irregularly shaped [16]. This can be due to their higher cooling rates compared to powders produced through gas atomisation [15].

2.1.3 Plasma Rotating Electrode Process (PREP)

In this process, the molten metal is "centrifugally atomised in the form of droplets" where they later solidify into spherical shaped particles in an atmosphere filled with an inert gas [23]. Powders produced through this process are characterised by increased purity, low porosity and uniform spherical shapes with absence of defects such as satellites [24-26]. In a study that compared PREP and GA Ti-6Al-4V powders, it was gathered that PREP powders exhibited greater deposition rates, low surface roughness of deposited layer, three times less porosity of powders and lower interlayer porosity [27]. Therefore, PREP produces high quality powders which enhances flowability due to their smooth surfaces and uniform particle size distribution. However, this AM powder production method is deemed not only expensive with lower yield of the atomisation process, but also typically consists of coarser particles and wider size distributions that are not desired for AM applications [28, 29]. It is important to distinguish between plasma atomised (PA) powders and PREP powders as plasma atomisation involves the use of "non-transferred direct-current arc plasmas to accelerate the atomisation gas", where titanium alloys in the form of wires are fed "into the apex of the multiple plasmas" where the metal wires are melted and atomised simultaneously to produce smooth spherical particles of an average size of 40 μm with excellent filling densities [30]. However, PA processes have major drawbacks, such as low productivity and incredibly high production costs in comparison to other powder manufacturing methods [26].

2.1.4 Spheroidisation

Plasma spheroidisation is a technique implemented after powder production processes, where the powders are further treated with high-temperature plasma in a plasma induction furnace [15, 31]. Spheroidisation results in more spherical powders with smaller sized and narrower particle size distribution [31, 32]. Additionally, this post-processing procedure further improves the flowability

of powders, which in turn increases their overall packing density. As the individual particles are exposed to high-temperature plasma, the internal porosity of particles is reduced due to the melting process which results in greater particle hardness and bulk density [33, 34].

2.1.5 Hydrogenation-Dehydration (HDH)

The hydrogenation-dehydration method for producing Ti-6Al-4V is based on a reversible reaction of titanium and hydrogen. Titanium forms stable hydrides during its interaction with hydrogen at elevated temperatures above 650°C [35]. The titanium hydride (TH_2) formed has a brittle property which allows easy milling to produce finely-crushed hydride powders [35, 36]. The fine powders are then reheated at temperatures above 350°C under vacuum conditions, where the hydrogen is removed, producing dehydride titanium powders of the desired particle size distribution [35]. It is important to note that HDH method of powder production is not a refining technique hence the impurities remain unchanged [35]. Additionally, the price of Ti-6Al-4V AM powders is a major bottleneck within the AM industry where a kilogram of this powder will cost a minimum of $400 due to expensive equipment and low rates of production; meanwhile, hydrogenation-dehydration (HDH) powders cost about $30 per kilogram with a wider range of particle size distributions and higher production rates [35, 37]. However, HDH-Ti powders are often characterised by irregular morphologies and low flowability which makes them unsuitable for direct printing in the unmodified state [38].

To summarise, different powder production methods produce particles of different shapes which may be suitable for different applications. HDH particles exhibit irregular shapes and rough surfaces due to the milling process and particle fracture [39]. Atomisation process produces smooth, spherical particles due to the solidification of molten droplets; however, GA powders are characterised by less spherical particles with microsatellites compared to plasma atomised powders (PA) as droplets in PA processes are exposed to longer, higher temperatures before solidification [39]. Additionally, GA particles generally display wider size distributions while PREP powders present pure, spherical shapes consisting of narrower particle size distributions [26]. Figure 1 below illustrates Ti-6Al-4V powders produced by some of the above-mentioned powder manufacturing methods.

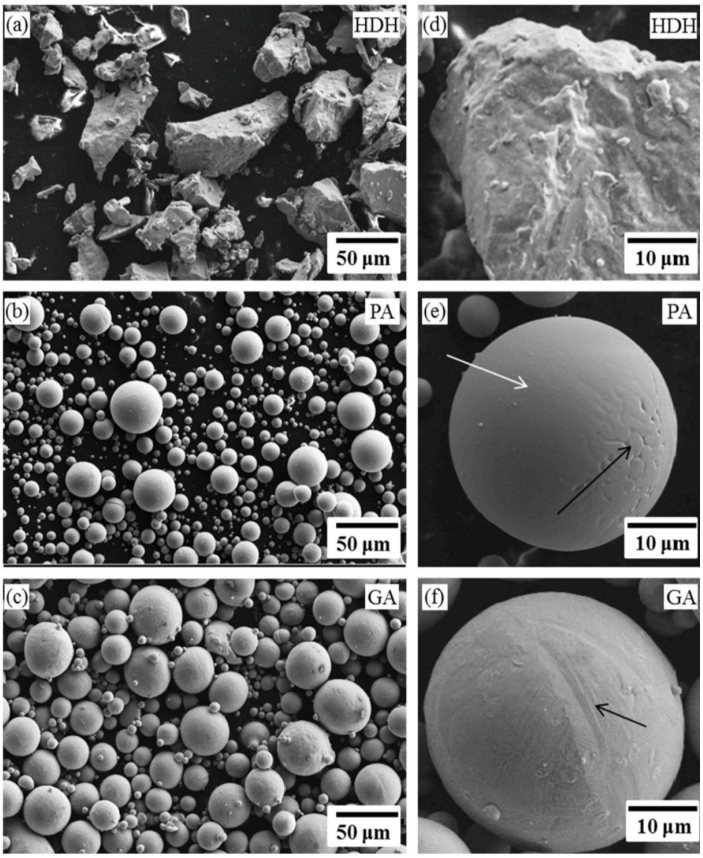

Figure 1: SEM images of TI- 6Al-4V (a) HDH, (b) PA, (c) GA powder and High magnification images of Ti-6Al-4V (a) HDH, (b) PA and (c) GA powders [39].

2.2 Powder Characterisation in Additive Manufacturing (AM)

Characterisation of powders is imperative in the AM industry as the production of suitable and reliable AM parts is only made possible by consistent and repeatable powder layers. Powder feedstocks are required to have "repeatable characteristics" which is achieved and measured using standardized methods [40]. This section will discuss some of the powder characterisation methods.

2.2.1 Particle size and distribution

Particle size and distribution plays a crucial role in determining the overall quality of the AM end product as it directly impacts the quality of the powder layer through the packing density and uniformity of the surface [41-45]. Utilising finer particles can result in considerable advantages, such as increased surface layer quality and particle packing [42, 46]. Moreover, smaller particles

will lead to a reduction in surface roughness which curtails the stair-stepping effect in the AM part [47]. However, fine particles have the propensity to easily agglomerate leading to flowability issues such as discontinuities and voids within the powder layers [44, 48, 49]. Additionally, agglomeration tends to impede particle flow during the spreading process as it increases the interparticle friction, creating inhomogeneous layers of low density which can result in a phenomenon known as the balling effect [50, 51]. This effect can lead to increased layer porosity due to the variable deposition of powder on the bed, where some regions may have more powder compared to the rest [52, 53]. Moreover, Meier et al. employed a computational model to examine powder cohesiveness in the recoating process of AM powders based on the behaviour of plasma-atomised Ti-6Al-4V [41]. They gathered that smaller particle sizes increases cohesiveness, which results in low quality powder layers due to uneven surfaces and varying packing fractions of the layer [41]. However, Spierings et al. suggested that the presence of finer particles is required to ensure optimised layer densities and end parts of high mechanical strength as they are easily sintered, while the amount of larger particles is restricted to the effective powder layer thickness [54]. They continued, stating that the advantages of employing larger particles will enhance the breaking elongations [54]. Moreover, larger particles are governed by gravitational forces instead of interparticle forces, which enhances their rolling movement allowing for a more compacted packing [55, 56].

Furthermore, Ma et al. also established that a certain amount of fine particles will fill the interstitial sites of the larger particles which will result in denser powder layers; however, this effect will be reversed if the fine fraction (Ψ) exceeds a threshold of 1.5% [44]. As stated previously, the excessive use of fine particles will result in flowability issues, as light finer particles tend to agglomerate and clump together due to the dominant Van der Waals force [44]. Chen et al. further confirmed that during the spreading mechanism of powders smaller than a specific size (45 μm for 316L stainless steel in their study), the cohesion effect as a result of Van der Waals will dominate the spreading, leading to a decrease in the packing density of the layer due to the agglomeration of fine powders [57].

Sutton et al. stated that the effects of both larger particles (greater than 150 μm) and finer particles (less than 10 μm) need to be individually tested in order to attain an optimum particle range [52]. They further stated that the upper threshold in a size range is dependent on the layer thickness such that all the powders, regardless of the size, will be deposited on the bed if the layer thickness is greater than the maximum particle size. On the contrary, there will be preferential fine powder deposition if the layer thickness is smaller than the maximum particle size [52]. Abd-Elghany and Bourell specified that increasing the layer thickness will not only lead to a decrease in layer densities, but also increase the surface roughness due to the unsintered large particles [58]. Therefore, it is critical to choose a suitable layer thickness that is not much lower than the mean particle size as larger particles are pushed away causing changes in the actual particle size distribution during powder spreading [48].

Liu et al. mentioned that different particle size distributions, broad and narrow, behave differently in powder-bed fusion processes and inevitably result in end-parts of different qualities [59]. Averardi et al. and Simchi stated that low attainable density is a result of agglomeration that tends to occur in finer powders with narrow particle size distribution, and segregation that occurs in coarser powders with wide particle size distribution [48, 60]. Wide particle size distribution results into powder beds of high density due to their high packing capacity, producing smooth parts of high density, while narrow particle size distribution enhances flowability that allows the production of parts with high ultimate tensile strength [59]. On the other hand, a study suggested that the use of wide particle size distribution created inhomogeneous spread layers that ultimately produced parts of high surface roughness [61]. Parteli and Pöschel, also found that utilising a wide particle size distribution will increase the packing porosity and surface roughness of the deposited powder layer due to the agglomeration of fine particles [62]. A study by Muñiz-Lerma et al. suggested that a narrow particle size distribution consisting of larger particles reduced the powder cohesion, which resulted in higher apparent density and better powder flow [63]. Jacob et al. studied the influence of spreading metal powders with different particle size distributions and gathered that wide particle size distributions with particles sizes in the range of the effective layer thickness resulted in higher powder bed densities as opposed to distributions with a greater fine powder ratio [64].

To summarise, a wide particle size distribution consists of both fine and large particles, where the finer particles tend to fill the voids between the larger particles (increasing tapped density), while a narrow particle size distribution either entails a higher percentage of fine or large particles [65]. A narrow particle size distribution with a greater ratio of large particles tends to increase powder flow but results in AM parts of lower density, while a narrow particle size distribution biased to finer particles tend to produce parts with smooth surfaces but are more prone to agglomeration [65]. It is therefore imperative to utilise a "graded" powder batch with an optimum particle range to ensure smooth layers of high bulk layer density. Figure 2 below summarises the types of particle size distributions where they are categorised under narrow and broad PSD, in accordance with their application.

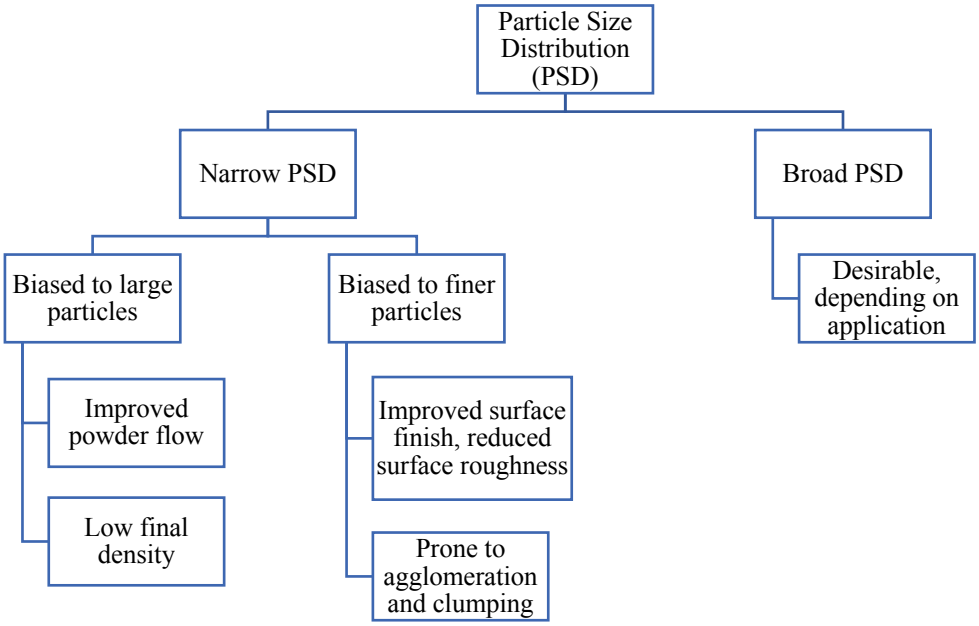

Figure 2: Types of particle size distributions.

2.2.2 Powder Morphology

Powder morphology is directly related to the shape and size of powders, and can be defined as the degree of packing in the layer-by-layer process of powder bed fusion [66]. According to Sutton et al. and Beretta and Evans, the size, shape and surface roughness of particles are also related to the morphology of the powders that influences the powder performance and flow characteristics, such as its packing efficiency and flow behaviour [52, 67]. Cordova et al. further added that powder

morphology is an important parameter affecting the spreadability of powders on the powder bed [68]. As stated in section 2.1, the powder production method has a significant role in determining the shape of the AM powders, where they can either be spherical or non-spherical. It is important to note that particle shapes are not limited to the above mentioned as there is a broad range of shapes such as elliptical, porous, dendric, rod-like, flake and angular [69]. Vock et al. conducted a comprehensive review on powders in powder bed fusion, where they established that large, smooth, spherical particles tend to have a better flow behaviour compared to rough, angular, non-spherical powders [70]. Attar et al. postulated that non-spherical powders tend to inhibit uniform powder deposition on the bed as they are prone to mechanical interlocking that often results in porous layers [66]. Moreover, Olakanmi, suggested that homogenous layers of high density is achieved by utilising spherical particles [71]. Additionally, Spierings et al. suggested that the packing density of elliptical particles will be lower than spherical particles [72]. Angular and fibrous particles tend to be more cohesive [73] while spherical particles tend to easily flow owing to the low internal friction resulting in defect-free layers [74, 75]. Pleass and Jothi also confirmed that spherical particles enhance flowability, owing to their minimal surface area to volume ratio and lack of mechanical interlocking [76]. They also stated that forces that inhibit powder flow, such as frictional forces between particles, interparticle forces or mechanical interlocking, are dependent on powder morphology [76]. Figure 3 below, portrays the different variations of particle shapes.

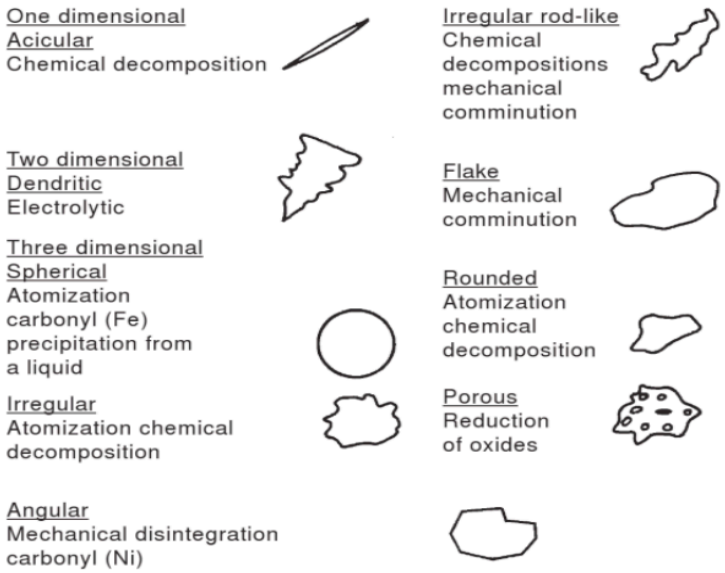

Figure 3: Different particle morphologies [69].

2.2.2.1 Aspect Ratio (AR)

The most common shape factor used in AM is the aspect ratio (AR), where it is defined as the measure of the particle elongation, or the ratio of the width to the height of a particle [52, 77]. This shape factor does not provide information about surface topography of particles and is typically used for "not very elongated" particles which is applicable to the majority of AM powders [78]. In addition, a perfect sphere will consist of an AR value of one, however, similar values of the width and length of a particle does not necessarily correspond to a circular shape, as symmetrical particles tend to have high aspect ratios [79]. The AR is calculated using the following equation, where x_{Fmin} is the minimum Feret's diameter (shortest distance between two parallel tangents of a particle) and x_{Fmax} is the maximum Feret's diameter (longest distance between two tangents of a particle) [79]:

$$AR = \frac{x_{F\,min}}{x_{F\,max}} \qquad \text{Equation 1}$$

Strondl et al. examined new and recycled Ti-6Al-4V powders regarding their particle shape and concluded that, upon recycling, any slight change in the aspect ratio of particles will significantly impact the dynamic flow behaviour of powders, which will inevitably result in defected powder layers [80]. Furthermore, Dang and Davé conducted a dynamic simulation on the packing behaviour of particles suggesting that regardless of the size of the particles, porosity remains unchanged with powders of fixed aspect ratios when cohesive forces are absent in the system [81]. However, it was found that porosity and surface energy increase when the aspect ratios increase, and size of particles decrease [81]. Nasato and Pöschel, examined the influence of particle shape in additive manufacturing, and gathered that at low velocities elongated particles consisting of low aspect ratios perform better in terms of compacted powder layers, while spherical particles have better performance at high velocities owing to their enhanced flow behaviour [82]. Additionally, Haeri et al. investigated powder spreading process in additive manufacturing and concluded that larger aspect ratios (AR) of powders at high velocities result in to low bed quality due to greater surface roughness and lower volume fraction [83]. They further documented shape segregation in

a batch of powders with different aspect ratios, where powders of larger aspect ratios accumulated on the upper bed layers [83].

2.2.2.2 Circularity (C)

Circularity is another shape factor used to characterise powder feedstock and is defined as the "measure of the particles' sphericity" [77]. In other words, to what degree the particle resembles a circle. Circularity is also an indicator of the smoothness of the particle's perimeter where it measures the roughness and overall form [79]. Therefore, a lower circularity value suggests that the particle is farthest from a smooth, spherical particle. Thus, a circularity value of one suggests a perfectly round, smooth particle, while a value of zero provides the complete opposite. Circularity is the ratio of the area, A to the square of the perimeter, P shown in the equation below [79]:

$$C = \frac{4\pi A}{P^2} \qquad \text{Equation 2}$$

Sun et al. characterised novel titanium powder precursors for AM applications and gathered that the roundness or circularity of particles decreased with successive layer iterations due to the presence of agglomerates [52, 84]. Moreover, Vock et al. conducted an extensive review on powders for powder bed fusion where they stated that smooth spherical particles (suggesting circularity values closer to one) exhibit better flow behaviour compared to sharp-edged, non-spherical particles [70].

2.2.2.3 Convexity (C_x)

Convexity is defined as the particle's roughness. The perimeter for particles with rough surfaces tends to increase, resulting in low convexity values. The particle roughness is dependent on the amount and size of irregularities present on the particles surface [79]. Therefore, particles with rougher surfaces will carry convexity values closer to zero, while particles with smoother surfaces will consist of values closer to one [79]. This is calculating using the following equation which is the ratio of convex hull perimeter, P_c (the envelope perimeter) to the actual perimeter (encompasses all the extrusions and intrusions on a single particle), P, of the powder [79]:

$$C_x = \frac{P_c}{P}$$ Equation 3

Landauer et al. emphasised on the importance of detailed particle shape analysis such as convexity for the transportation, mixing and fluidisation operations of powders [85]. They further hypothesised that convexity as a descriptor of particle shape is influential on both the packing behaviour, bulk and tapped densities [85]. They concluded that there was no significant difference between concave and convex particles on the bulk and tapped densities, however, this was not the case for the angle of repose as it demonstrated differences in these morphologies. They reported that concave particles were characterised by low bulk densities and very high angle of repose, however, no definitive pattern was established [85]. This raises the need to further investigate the effects of such shape descriptors on the flow behaviour of powders which inevitably affects the quality of the deposited layers.

2.2.3 Powder Flow Behaviour

Prescott and Barnum define powder flowability as the "ability of the powder to flow" [14]. They explained that a single value or index cannot be used to define flowability, as it is not an inherent powder property [14]. By the same token, Van den Eynde mentioned that there is a great challenge in assessing powder flow, as the majority of methods provide a measure of "indices rather than intrinsic material properties"[74]. An index is a value that is dependent on both the powder and equipment, which only makes it a comparative value to assess powders.

Krantz et al. conducted a series of experiments in testing powders under different stress conditions and concluded that the technique of powder characterisation has to match the final process [49]. They also suggest that employing a single method is insufficient to fully characterise a powder, hence both static and dynamic techniques have to be utilised individually; in other words, combining results from different techniques to form a single index will lead to inaccurate results [49]. Thus, measuring powder flowability is imperative as it significantly affects the quality of powder spreading.

2.2.3.1 Angle of Repose (AoR)

Angle of repose is a parameter among many used to assess the flow behaviour of bulk powders. According to ASTM B213, the angle of repose (AoR) is a measure of powder flowability, where a specific powder is poured through a funnel onto a plate forming a heap [86]. The angle of repose is then calculated by measuring the inclination angle between the base plate and the powder heap. Gerald et al. stated that there are multitude methods established for measuring the angle of repose, however, the general consensus agrees on two main types, the static and dynamic angles [87]. They further state that different methods provide different values of angle of repose [87]. Table 1 indicates values for measuring flowability suggested by Carr [88]. It is important to note that, the angle of repose is just a mere measurement providing some information on the flow behaviour of powders, and is insufficient to implement in design and equipment selection [89]. The angle of repose is employed in AM as an indicator of flowability, where a lower angle of repose indicates a free flowing powder, while higher angles indicate poorer powder flow as a result of greater inter-particle forces, which can significantly influence the spreading behaviour [74, 90]. The effects of the angle of repose is explained in section 2.3 of this thesis. Figure 4 below represents the apparatus used to measure the angle of repose of powders.

Table 1: Angles of repose as a guide to measure flowability [88]

Angle of Repose (°)	Flowability Index
<25	Very, excellent flow
25 - 30	Excellent flow
31 - 35	Good flow
36 - 40	Fair flow
41 - 45	Passable
46 - 55	Poor
56 - 65	Very poor
> 66	Very, very poor

Figure 4: Angle of repose instrument.

A static angle of repose is measured when the heap is at rest and is calculated by numerous methods such as poured angle of repose or funnel technique, where the powder is poured through an orifice and the inclination angle is calculated [74]. The limitation to this method is not only the obstructed flow when using cohesive powders but also the lack of aeration which actually occurs during the production processes [87, 89]. Additionally, the dynamic angle of repose is measured when the heap is in motion, in a rotating drum, and is the inclination angle when the cohesive and gravity forces are in balance [74, 89]. The major weakness to this method is the amount of time required to not only measure the angles but also cleaning the equipment to eliminate the risk of contamination [87].

2.2.3.2 Packing Behaviour of Particles

Packing behaviour of particles directly affects the bulk layer density and generally the apparent and tapped densities can be used as parameters to further understand this dynamic. Abdullah and Geldart, defined the term apparent or bulk density as the mass of the powder divided by its occupied volume [91]. The volume occupied by the particles includes both the interstices between particles and envelope volumes [91]. The bulk density to some extent can be used to understand the flow behaviour of powders and is measured by two common techniques; the aerated bulk density (random loose packing), and the tapped bulk density (random dense packing) [91]. The aerated bulk density was measured by taking the weight of a powder in a cylinder divided by the volume it occupies under the force of gravity, while the tapped density was calculated by taking the weight of a powder divided by the volume upon tapping [92]. Wong studied the flow behaviour of glass beads ranging from 20-170 μm and established that the aerated bulk density (ρ_A) remained unchanged for larger particles above 90 μm and decreased for finer powders below the size of 90 μm [92]. The unaffected ρ_A in larger particles was a result of the counterbalance of the weight and interparticle forces, while the reduced ρ_A in finer particles was due the dominant interparticle forces [92]. Notably, finer particles tend to have relatively low densities at the aerated state, hence tapping will allow particles to rearrange as interparticle forces are overcome, resulting in a more compacted form with increased layer bulk densities [92, 93]. Markusson further added that tapping, which mimics vibrations caused by powder processing and handling, will increase the density compared to the bulk density of the powder due to the process of consolidation; and the difference of these two values will suggest the sensitivity of powders to such vibrations [94].

In addition to that, Rausch et al. analysed the process window for Ti-6Al-4V powders and concluded that low powder bulk densities will result in increased energy consumption, surface roughness and porosity of layers [70, 95]. Poor packing of individual layers also led to irregular and unstable melt pool shapes [95]. Furthermore, highest relative bulk densities are achieved through utilising spherical particles as it enhances the flow behaviour and even distribution across the powder bed [96, 97]. Averardi et al. emphasised on the importance of uniformly packed bed as it significantly impacts the process parameters and the repeatability of packing fractions. They further expanded by stating that consistent packing fractions across all layers is sufficient enough to produce desirable end parts, even if the powder bed does not have a fully closed packed arrangement [60]. Amado et al. also confirmed that increased powder packing and homogenous layers are a result of reliable processing conditions i.e. powder deposition on the bed [98]. Moreover, Karapatis quantified layer quality by measuring the layer density of powders and concluded that the layer densities were greater than the apparent densities, which signified the occurrence of minimal compaction upon powder deposition [99].

The bulk density provides valuable indicators for flowability, such as the Hausner Ratio (HR) and the Carr's Compressibility Index (CI). Grey and Beddow defined the Hausner Ratio as the "ratio between the tap density and apparent density of a moving powder mass" [100]. The Hausner Ratio is a measure of the friction occurring in a bulk powder [100]. Hausner Ratio and Carr's Compressibility Index are calculated by the following equations [89]:

$$HR = \frac{\rho_b\ tapped}{\rho_b\ aerated} \qquad \text{Equation 4}$$

$$CI\ (\%) = \frac{\rho_b\ tapped - \rho_b\ aerated}{\rho_b\ aerated} \times 100 \qquad \text{Equation 5}$$

Table 2 below provides information regarding the flowability index with the respective HR and CI values.

Table 2: HR and CI as indicators to measure flowability [88]

Hausner Ratio	Carr's Compressibility Index (%)	Flowability Index
1.00 - 1.11	≤ 10	Free-flowing to excellent flow
1.12 - 1.18	11 - 15	Free-flowing to good flow
1.19 - 1.25	16 - 20	Fair to passable flow
1.26 - 1.34	21 - 25	Passable
1.35 - 1.45	26 - 31	Cohesive powders - poor flow
1.46 - 1.59	32 - 37	Cohesive powders - very poor flow
>1.60	>38	Cohesive powders - very, very poor flow

Zou and Yu carried out experiments under loose and dense random packing and gathered that the Hausner Ratio decreases with increasing sphericity for mono-sized particles [101]. Zocca et al. stated that free-flowing powders have high bulk densities in their aerated condition (absence of vibration); thus there is no significant increase in their tapped densities compared to low or cohesive powders, hence why they have lower values of HR [102]. On the contrary, Spierings suggests that HR fails to correlate the visual evaluation of flowability as different powders are not thoroughly distinguished [78]. He also states that in additive manufacturing, the layer-by-layer deposition of powders does not involve any tapping or compression [78]. It is therefore crucial to note that HR and CI only provide a simple indication of the powders' flow behaviour during handling, but it is not at all sufficient [89].

Furthermore, the flow function introduced by Jenike can be used as a numerical characterization of flowability where ff_c is the ratio calculated by taking the consolidation stress of a bulk solid, σ_1, to the unconfined yield strength, σ_c [103]. This is expressed by the equation below:

$$ff_c = \frac{\sigma_1}{\sigma_c}$$ Equation 6

Flowable powders are characterised by larger ff_c values, suggesting that the unconfined yield strength, σ_c, which related to the interparticle forces exiting in the shearing zone [104] is smaller than the consolidation stress, σ_1, which is the vertical applied stress [105]. Schulze, with the aid of Jenike's classification, defined and classified the flow behaviour of powders as shown in Table 3 and Figure 5.

Table 3: Characterisation of flowability using the flow function [105]

ff_c Ratio	Flowability Index
$ff_c < 1$	Not flowing
$1 < ff_c < 2$	Very cohesive
$2 < ff_c < 4$	cohesive
$4 < ff_c < 10$	Easy-flowing
$10 < ff_c$	Free-flowing

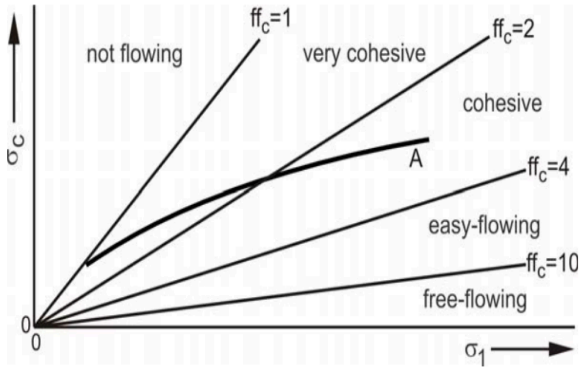

Figure 5: Flow Function [105].

It is clearly depicted from Figure 5 above that the ratio of ff_c of a bulk powder is dependent on the consolidation stress, σ_1, where an increase of the consolidation stress will result in an increase in ff_c [105]. Schulze further states that the flowability of bulk powders is significantly influenced by the consolidation stress, hence flowability is greater at higher consolidation stresses [105]. However, flowability cannot be analysed using a single value due to its dependence on the consolidation stress, σ_1 [105].

Additionally, the shear cell, uniaxial tester and ball indentation can be employed to produce the flow function of powders. However, uniaxial testers are not utilised for free-flowing powders, and the application of the shear cell in additive manufacturing is restricted due to the history of consolidation of AM powders. Shear cells have consolidation levels of 1000-2000 Pa while the heap deposited in front of the spreader has very low stress and consolidation levels between 20 to

200 Pa. Hence, standard conventional shear cells cannot be employed as they do not cover such low ranges, however low stress Schulze shear cell could potentially be suitable but has not been utilised in literature to correlate data with AM.

2.2.3.3 Hall Flowmeter

This method is used to indicate the flow behaviour of powders by determining the mass flow rate, where a mass of powder is poured on to a funnel and the time is simultaneously recorded. Slotwinski and Garboczi mentioned that Hall flowmeter as a powder characterisation method measures the coefficient of friction, however its major limitation is its lack of sensitivity and accuracy for detecting miniscule differences in such values [106]. Mellin et al. further adds that Hall flowmeter method has a major drawback when it comes to utilising cohesive powders, and that the Gustavsson flowmeter should be opted for when characterising powders [107]. Additionally, Schulze commented that the method of powder pouring by the operator has a significant influence on the accuracy of measurements and that some powders fail to pass through the 0.1" diameter, even though they are suitable for AM [108]. This presents a great challenge to gather precise results in distinguish different powders. Figure 6 below illustrates a schematic drawing of the Hall flowmeter.

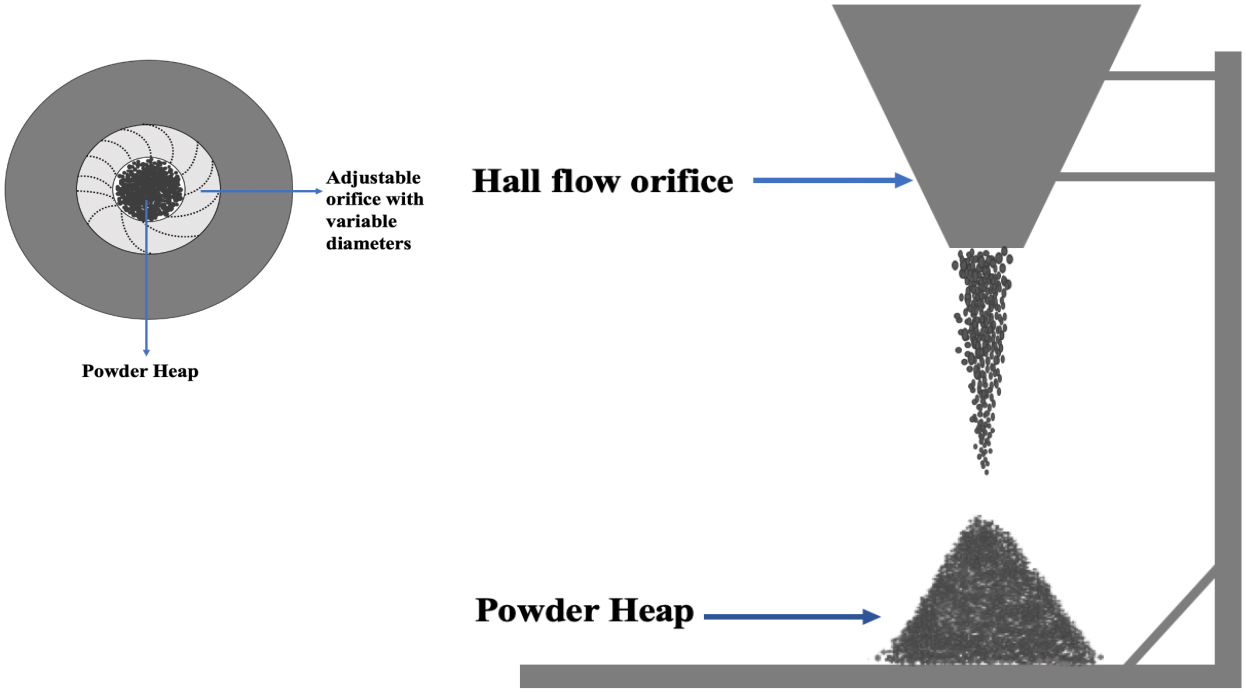

(a) (b)

Figure 6: Schematic drawing of (a) top view and (b) side view of the Hall flowmeter.

2.2.3.4 Dimensionless Shear Rate ($\gamma^{\circ *}$)

It is established that powders can flow in various rheological states depending on their interaction with each other [109]. During the spreading mechanism, powders are spread at various velocities and inevitably different shear rates. The shear rates based on the particle size will be in the form of dimensionless rate which then determines the flow regime.

Additionally, Tardos et al. emphasised the difference of flow behaviour of powders to that of fluids, where powders exhibit interparticle friction rather than viscosity [110]. A schematic representation of the flow regimes was first introduced by Tardos et al. in terms of the dimensionless shear rate [110]. The differences in the dimensionless shear rate represents powders in different flow regimes which affects the stress-strain relationship. The following expression was introduced by Tardos et al. to measure the dimensionless shear rate [110]:

$$\boldsymbol{\gamma}^{\circ *} = \dot{\gamma}\,[d/g]^{1/2} \qquad \text{Equation 7}$$

Where the shear strain rate, $\dot{\gamma} = \left(\frac{Velocity\ (v)}{Gap\ height\ (h)}\right) s^{-1}$, d is the particle's diameter taken as d_{50} and g is the gravitational acceleration. Figure 7 below represents a tentative schematic of the different flow regimes consisting of the static, quasi-static, intermediate flow and rapid granular flow regimes [110].

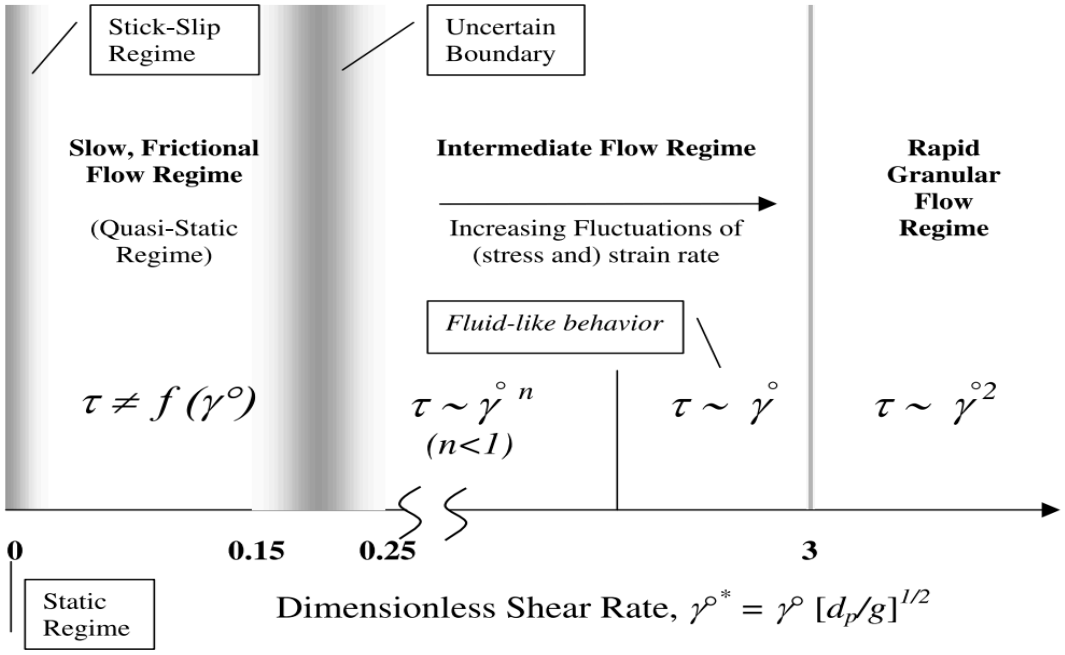

Figure 7: Schematic depiction of different powder flow regimes based on the dimensionless shear rate [110].

The static regime occurs when the powder bed has no shear exerted on them; in other words, the powders are at static equilibrium. The stresses within the powder bed can be calculated by using the static equilibrium and the yield conditions. The yield point refers to the onset of powder deformation, in the presence of stresses [109].

The quasi-static regime occurs when the particles are influenced by friction and exhibit very slow movements. The particles in this flow regime tend to lose their energy from the sliding effects during powder collisions. This occurrence owes to the collision of closely packed arrangement of powders at negligible velocities, where contact friction from sliding governs the particles' flow. This flow regime occurs at dimensionless shear rates of 0.15-0.25, where the upper boundary of this rate is still ambiguous and requires additional work for further understanding [109, 110].

The intermediate flow regime is the regime occurring between the quasi-static and rapid granular flow regimes. The powder flow in this regime is caused by the different variations in the stress and strain rates. The particles in this regime exhibit not only frictional forces but also collisional forces. Through the experimental work, it was deduced that powder flow in the intermediate region manifest fluctuations in stresses and deformations [109, 110]. They exhibit dimensionless shear rates of higher than zero but approximately less than three.

The rapid granular flow regime consists of powders moving at very high velocities, where only the collisional forces are accounted for and the frictional forces ignored. The particles in this regime lose their energy as a result of inelasticity. Powders in this flow regime experience stochastic motion and high energies similar to gas molecules. Thus, the kinetic theory of gas can be implemented on these particles in this region for analysis [109, 110].

2.2.4 Other Properties of AM Powders

Improved surface properties of AM powder are requisites to ensure the deposition of quality spread layers and ultimately defect-free AM parts. X-ray computed tomography (XCT) is an appealing technique that enables the measurement of a powder's surface topography as well as the internal structure, an area difficult to reach [111]. This subsection will cover a few factors that can significantly influence the properties of individual layers and mechanical strength of end parts.

2.2.4.1 Porosity

Porosity in AM is often described as an effect occurring during the processing of AM powders such as the sintering stage, however, porosity is also generated by the presence of voids within the microstructure of powders [52]. The inherent porosity of powders can exhibit complications on

both the spread layer and final fabricated product as it generates micro-porosity [84]. Benson and Synders emphasised on the significance of powder characteristics such as porosity on the flow behaviour of powders and commented on how powder porosity affects the sinterability during processing [112]. Cunningham et al. investigated the porosity of Ti-Al-4V using synchrotron-based X-ray microtomography and found that the particle porosity can be related to "raw materials-related defects" that occur during the powder manufacturing stage, where the culprit for these microstructural pores are due to "trapped gases" [113]. They suggest that better selection of powder feedstock will aid in eliminating powder induced porosity such as utilising PREP powders that consist of fewer internal porosities owing to the inert gas conditions [113, 114].

Galarraga et al. examined the effects of microstructure and porosity on the properties of Ti-6Al-4V alloys and detected two types of morphological pores, namely; spherical pores and non-spherical pores [115]. The spherical pores were a result of entrapped gases due to the atomisation process while the non-spherical pores that occurred parallel to the scanning layer were due to un-melted particles within the layers [115]. This agreed with the study conducted by Iebba et al. that spherical pores emerged from the presence of entrapped gasses while non-spherical pores were caused by discontinuities within the scan tracks [116]. Iebba et al. concludes that controlling the atomisation process of the initial powder is fundamental to eliminate internal porosities and created defect free layers [116].

2.2.4.2 Roughness

The surface roughness of a powder can greatly affect the functional property of AM parts, including their mechanical strengths [117]. The production method also plays a crucial role in determining the surface roughness of powders. Mehrabi et al. studied two samples of Ti-6Al-4V powders, produced by GA and HDH methods [118]. They clearly stated that GA powders were characterised by smoother surfaces while HDH powder exhibited "high degree of surface roughness" [118]. In addition to that, satellites that can be formed during the atomisation process [119] play an influential role in determining the surface quality of powders. Hebert commented that changes on the surface roughness of a powder is also due to the environmental conditions in the storage containers, as well as the processing stages with the AM machines [120]. This will inevitably impact the desirable densities and flow behaviour [120]. Pyka et al. suggested that the

combination of chemical etching (CH) and electrochemical polishing (EP) for porous Ti-6Al-4V structures will discard attached powders and enhance homogeneity [121].

2.2.4.3 Surface Adhesion

Generally, adhesive forces tend to be of more prominence between finer particles due to the dominant Van der Waals forces. Hamaker, numerically computed the forces between two spherical particles as the function of the particles' diameter and the distance between them and concluded that even if particles are surrounded by fluid, they will still exhibit these attractive forces [122]. Chu et al. examined the influence of satellite on the processability of AlSi10Mg powders, and also gathered that some of the satellite particles were a result of the Van der Waals forces that increases the cohesion and agglomeration of particles [123]. This will inescapably result in the formation of irregular morphologies inhibiting powder flow and consequently affecting uniform powder deposition [123].

2.3 Effects of Powder Properties on the Quality of Spread Layer

It is well established that powder properties as discussed in previous sections significantly affect the spread layer. This section will cover a review regarding these effects on the spreadability of powders in PBF by looking at the conclusions gathered by different authors.

Ahmed et al. introduced a simple technique to analyse the spreadability of powders in additive manufacturing, and defined the term spreadability as a complex powder characteristic influenced by powder properties to generate uniform thin layers free from rough surfaces, agglomerates and empty patches [13]. They stated that spreadability is significantly affected by the flow behaviour of powders in restricted areas where the shearing zone is a few multiples of the particle size, making powder properties such as particle size, shape and surface texture dominant characteristics that affect transient jamming during spreading [13]. They further mentioned that the particles should be small to ensure effective sinterability during powder bed-based processes, but not too small that they are prone to agglomeration, which impedes powder flow [124, 125]. Snow et al. stated that highly flowable powders exhibit exceptional coverage on the built layer resulting in higher packing density [77]. On the contrary, powders with lower flowability resulted in lower packing fractions as the powders were pushed off the built plate instead of being deposited on top

[77]. They also stated that by increasing the angle of repose both the percent coverage and deposition rates will decrease, suggesting the direct influence of the angle of repose on the spreading quality of the layer. They drew the conclusion that the angle of repose is the major powder property determining the spreadability of powders, and for any improvements in the spreadability, the powder feedstock needs to be changed while maintaining the same process parameters [77].

Haeri et al. investigated powder spreading through both experimental and simulation (discrete element method) work, where they suggested that the particle shape as a powder property influences the quality of the spread layer in terms of the layer's surface roughness and solid volume fraction [83]. The surface roughness and solid volume fractions are crucial parameters as increased surface roughness results in greater porosity and weaker bonds between layers, ultimately creating undesirable end products [83]. They characterised the shape of three different PEK and PEEK (Poly-Ether Ether Ketone) particles and decided on a rod-shaped particle for numerical simulation [83]. They concluded that generally particles with higher aspect ratios (AR) tend to produce powder beds of lower density and high surface roughness.

Chatham et al. on the review of the process physics in powder bed fusion additive manufacturing also stressed on the importance of powder size and morphology [126]. They stated that the diameter of powders influenced the flow behaviour such that particles below the size of 25 μm are overpowered by the surface energy that impedes powder flow [55, 126]. They further mentioned the importance of utilising free flowing powders as they produce high powder bed packing densities, which is essential for defect-free layers of high density. As stated previously, spherical particles are desirable for additive manufacturing, as irregular particles are accompanied with voids in between which drastically reduces the packing density [126].

Additionally, Meier et al. on the influence of particle size and cohesion stated that finer particles with a mean diameter of 17 μm are dominated by Van der Waals forces which increases the cohesiveness of powders [41]. As a result, the powder layers exhibit non-homogeneity with varying packing fractions. They further stated that the effects of cohesiveness are due to surface energy and mean size of particles. They also mentioned that inefficient energy process is a

drawback associated with reduced packing fractions due to the reduction of laser energy absorption and thermal conductivity of layers [41]. They further provide a solution for improving the surface roughness of powder layers by employing a spreader with low adhesive interaction [41].

Berretta et al. examined the effects of powder properties, such as particle shape and size distribution, on the flow behaviour of SLS and non-SLS polymers [127]. They obtained a significant difference in the AoR between the two polymer classes, were the SLS powders exhibited lower AoR values of between 38° and 42°, while the non-SLS powders had a value of 52°. Such discrepancies within the AoR values were a result of morphological differences between the powders [127]. Low AoR suggests powders with high flowability indicating spherical shapes while high AoR indicates low flowable, angular, flaky particles consisting of lower densities, which deteriorates the surface quality of layers. They further stated that the powder's morphology has a significant effect on the flowability compared to the particle size distribution, and the thorough application of additives may enhance flowability [127]. Additionally, Esmaeilizadeh et al. investigated the effect of virgin and spatter particles distribution on the quality of AM parts and deduced that spatter particles significantly affect the layers and consequently final AM parts [128]. It was concluded that spatter particles increase the layer thickness and creates irregularities within the layer hindering efficient sinterability of powders [128]. This will ultimately result in inadequate fusion and formation of pores between layers. This study also highlights the necessity of sieving powders during the recycling process [128].

Karapatis et al. also stated that the density of the powder layers before processing is imperative to ensure the production of desirable end parts, which is dependent on the particle size distribution [42]. They proposed different fractions of fine and coarse powders and analysed the optimal ratio that produced the highest layer density. They observed an increase of layer density from 53% to 63% when 30% of fine powders were added to the coarser ones, suggesting a ratio of 1:10 for coarse-to-fine powders [63]. Contreras et al. on the improvements of rheological properties using tailored particle size distribution reiterated the importance of employing a broad particle size distribution [129]. They presented the advantages of broad PSD's in terms of better packing, low viscosity and enhanced optimal solids loading [129]. Solid loading was stated to reduce defects

such as shrinkage during the sintering process, which creates homogenous layers and consequently end parts of high dimensional accuracy [129].

2.4 Effects of Process Parameters on the Quality of Spread Layer

The effects of process parameters on the spreadability of powders has been studied by several authors, which will be discussed in this section. Spreading velocity, gap size and type or material of the spreader are some of the process parameters that directly affect the spreadability and consequently the quality of the spread layer.

Ahmed et al. conducted an experiment on powder spreadability using a Stanton cutter blade with gap sizes of 45 μm, 67.5 μm, 90 μm, 112.5 μm and 135 μm to manually spread a powder heap and analyse the formation and size of empty patches due to particle jamming [13]. They observed that the frequency of the empty patches decreased significantly when the gap sizes increased, suggesting a more uniform spread layers at larger gap sizes [13]. Their work was closely related to Nan et al. where they examined the transient jamming of particles during powder spreading using numerical simulation, Direct Element Method (DEM) [130]. Nan et al. described jamming as a "manifestation of empty patches", which adversely impacts the spread quality as well as the speed of the fabrication process [130]. The frequency of these empty patches was analysed as a function of the gap size (D_{90}). They pointed out several findings such as the linear increase of the total volume of spread particles and the reduced frequency of jamming with increased gap sizes [130]. They also commented on the position of particles on the powder bed such that particles' velocity before the blade will substantially decrease, especially towards the base, when the gap sizes increase. Additionally, particles positioned underneath the spreader experienced "dragging", thus gaining velocity to jump to the front of the spreader [130]. However, they mentioned that the large gap sizes between the build plate and spreader will jeopardize the dimensional accuracy of AM parts; hence, spreading must be evaluated at smaller gap sizes to maintain the quality of spread layers [130].

Snow et al. attempted to establish a spreadability metrics through experimental and statistical work by employing an in-house spreader rig that mimics the conditions of PBF systems [77]. Their experimental design consisted of three input factors: the gap size, rake velocity, and the spreader

material [77]. They discovered that the material of the spreader – tool steel or silicone – had a direct effect on the quality of the spread layer. They further mentioned that the tool steel blade provided desirable coverage on the build plate for powders with low angles of repose while the silicone blades provided better results for powders with lower flowability [77]. Moreover, by increasing the rake velocity from 50 mm/s to 150 mm/s, they spotted an increase in the deposition rate and rate of change in the avalanche angle as the recoating time was reduced [77]. However, Chen et al. studied the effects of a counter-rolling spreader on the quality of the powder layer and found that as the rake velocity increased, the surface roughness of the layer increased while the packing density decreased [131]. This proves that high rake velocities are detrimental to the quality of the powder layer. In addition to that, increase rake velocities tend to enhance the pressure between the powder heap and substrate leading to a reduced coordination number. The downside to a low coordination number is a loose powder heap during spreading, which consequently reduced the packing quality of the layer [131].

Additionally, Haeri et al. suggested two process parameters, the spreader type and velocity, to control the quality of the spread layer when utilizing rod shaped particles [83]. They mentioned that adopting a roller instead of a blade will be beneficial for the quality of the spread layer, as blades have inadequate contact with powders, resulting in particle "dragging" and low bed qualities [83]. They also stated that improved bed qualities are created when employing low translational velocities [83]. Moreover, Haeri performed direct element method (DEM) simulation to optimise the geometry of blade type spreaders to achieve the lowest void fraction [132]. Similarly to Haeri et al., he mentioned that effective spreader-to-bed contact is necessary to ensure high quality spread layers in terms of surface roughness and solid volume fraction [132]. In principle, blades result in "dragging" of the powder heap positioned in front of the spreader, which then degrades the powder layer; hence, the alteration and modification of the geometry of these blades can significantly improve the surface quality. Haeri proposed a new class of spreaders consisting of super-elliptic edges, where the width, height and shape was controlled [132]. Furthermore, the new optimised blade showed similar results in that of a roller in terms of the volume fraction; however, it outperformed a roller as it was less sensitive to high translational speeds, indicating increased production rates without jeopardizing the quality of the spread layer [132]. Additionally, Beitz et al. also revealed that the shape of the blade plays a crucial role on the

surface quality of the powder bed, stating that a flat bottom shaped blade was more desirable compared to sharp and slightly rounded ones [12]. This was due to the even compression due to the horizontal contact zone between the powder bed and spreader producing layers of increased uniformity and density [12]. Moreover, Budding and Vaneker tested powder compaction with three different spreader types: a doctor spreader, a counter-rotating roller and a forward-rotating roller [133]. They concluded that the counter-rotating roller presented optimised results in terms of high bulk density and high surface quality, while the combination of the doctor blade and forward-rotating blade presented relatively high surface qualities [133]. The doctor blade had poor performance when attaining bulk densities and average surface qualities were only possible with the aid of compaction [133].

Furthermore, Fouda and Bayly attempted a DEM study for the spreading of spherical, mono-sized, non-cohesive Ti-6Al-4V powders in an idealised coating system. They stated that the deposited powder layer will consist of a lower packing fraction that the original powder heap due to three dominant mechanisms, including: shear- induced dilation in the initial spreading stage, rearrangement and dilation of powders underneath the spreader and finally the powder inertia within the spread layer [134]. They emphasised that process conditions such as gap size and spreader velocity are the main factors that influence the three mechanisms, and that controlling these conditions is imperative to ensure spread layers of high packing density. Their study analysed gap sizes ranging from 2 to 6 particle diameters, where the packing fraction of the layer increased linearly with the gap sizes [134]. Additionally, they tested the powder spreading with five velocities, including 10, 30, 50, 80 and 100 mm/s at a constant gap size of 4 particle diameter and gathered that the packing fraction of the spread layer decreased when the spreader velocity increased [134]. To reduce the production time, it is desirable to use higher spreader velocities; however, it has been established that higher velocities degrade the quality of the spread layer. Nan and Ghadiri analysed the powder flow during the spreading process using numerical simulation where they examined the effects of gap size and rake velocity [135]. They stated a linear relationship between increased gap sizes and the mass flow rate through the gap and that the rake velocity follows two regimes, where initially the mass flow rate increases linearly with higher velocities, but later reaches an asymptotic point where no changes in the rate of mass flow are detected. This implies a restriction to the limit of rake velocity within the spreading process [135].

Xiang et al. conducted a discrete element method simulation using three variations of the particle size distribution including mono-size, bimodal, and Gaussian distribution [136]. They analysed the packing density and coordination number with a range of gap sizes, including 100 μm, 150μm, 200 μm, 250 μm, 300μm and 350μm which meets the range of normal AM systems (80μm - 300μm) [136]. It was found that the packing density and the average coordination number, defined as the number of particles in contact with a certain particle, both increased but reached a stable value with increased gap sizes [136, 137]. They also analysed the effect of compression on powder beds indicating improved packing density and increased coordination number, and stating that such effects were greater in lower gap sizes [136]. They concluded that the compression process enhances and stabilises the particle's contact state and density [136].

2.5 Characterisation of Ti-6Al-4V Powders in Additive Manufacturing

In addition to previous sections that also covered the implementation of Ti-6Al-4V powders in additive manufacturing, the following sub-section will only focus on the characterisation and performance of Ti-6Al-4V powders covered by some authors within the literature.

Desai and Higgs studied the effects of industrial Ti-6Al-4V powders with different spreader speeds using numerical simulation. They characterised the spread layer with a roller in terms of the "mass of the powder within the sampling region (Ms), spread throughput (Qs), surface roughness of the spread layer (Rq) and porosity of the spread layer (ϕ)" [138]. They investigated the changes in the mass (Ms) with varying spreader speeds, which included translational speeds of 40, 55, 70, 85 and 100 mm/s, and rotational speeds of 0, 5, 10, 15, 20, -5, -10, -15 and -20 rad/s. They stated that the mass of powder (Ms) will increase if the rotational speed decreases from a positive value to zero owing to the reduced energy transferred from the roller to the powder [138]. They also detected a sharp increase in the mass of powder (Ms) when the rotational speeds changed to negative values as more than one layer of powder was deposited. Similarly, the spread throughput (Qs) increases as the rotational speed changes from a positive value to zero while a sudden increase in Qs is also detected when the rotational speeds change from positive to negative [138]. This is owing to the fact of multiple layer deposition when utilising negative roller rotational speeds, while only a single layer of powder is deposited during positive roller rotational speeds. The surface roughness

of the layer (Rq) is minimal when there are zero rotational speeds at a constant translational speed; however, as the magnitude of the rotational speed increases, the surface quality deteriorates [138]. Moreover, an increase in the porosity (ϕ) of the deposited layers was recognised with higher translational speeds, at constant rotational speeds [138].

Additionally, Shaheen et al. implemented direct particle simulation to study the spreading process of Ti-6Al-4V powders that influenced the quality of the spread layer and ultimately the final product [139]. Their study included varying parameters such as cohesion, sliding and rolling friction to identify their effects on the spread layer in terms of density and uniformity. The analysis was based on interparticle friction of powders as a measurement of their irregularities; the sliding friction (μs) as surface roughness and rolling friction (μr) as particle shape. They concluded that increased interparticle friction resulted in non-homogenous layers of low density, high porosity and "dragged" particles, which created a defected powder bed [139]. They also revealed that the sliding friction had an insignificant effect on the uniformity of the spread layer, however, it highly influenced the segregation of particles [139]. On the other hand, they mentioned that the rolling friction of particles impacted the uniformity of layers. They briefly reported that an increase in the spreader velocity from 10 mm/s to 50 mm/s generated higher porosity within the layers [139]. Sieving was recommended to reduce irregularities within powders to allow improvements in layer quality [139].

Meier et al. examined the effects of particle size and cohesion of plasma atomised Ti-6Al-4V powders during the spreading processes using numerical simulation [41]. They reported that reduced particle sizes increase cohesiveness, which negatively impacts the packing fraction and uniformity of the spread layers. They stated that for finer particles with an average particle size of 17 μm, the cohesive forces dominated the gravitational force by two orders of magnitude, producing layers of low quality [78]. They also stated that any impairment between the powder and substrate adhesion, such as contamination or oxidation, will result in a further deterioration of the spread layer quality. Dynamic powder-post flow was reported when the spreader velocity increased, consequently reducing the average layer thickness [41]. This effect was mitigated by employing higher nominal layer thickness and reduced powder flowability, the thickness of the layer before and after sintering is known as nominal and effective layer, respectively. In addition

to that, an increase in the nominal layer thickness results in improved layer qualities, and optimum results are obtained by utilising a minimum layer thickness of two or three times the maximal particle diameter. Designing a spreader blade of minimal adhesive interaction was suggested to further improve the surface uniformity of layers [41].

Mehrabi et al. performed an X-ray microtomography study on the particle morphology and packing behaviour of two samples of Ti-6Al-4V, produced by gas atomisation (GA) and hydrogenation-dehydration (HDH) methods during filling, compaction and ball indentation process [118]. Their aim was to implement a three-dimensional analysis of the ball indentation process to further recognise the effects of powder packing and flow behaviour [118]. As previously mentioned in section 2.1, gas atomisation produces powder of spherical morphology while hydrogenation-dehydration produces irregularly shaped powders. They characterised powder flow by methods of indentation of the powder bed under low consolidation stresses, where the hardness was measured as the ratio between the maximum applied force of the indenter to the projected imprint area [118]. Additionally, the indentation hardness provided important information about powders and their resistance to plastic deformation. They quantitatively analysed the packing fraction within the central and radial zones during the filling, compaction and ball indentation phases, and reported low packing fractions for HDH powders compared to GA due to their irregular morphologies and rough surfaces [118]. They also observed that the position of the indentation can influence the value of hardness during loose or low compaction owing to the different powder morphologies [118].

Sun et al. conducted a comparative study of six different virgin Ti-6Al-4V powders in additive manufacturing, where powders from different vendors were examined. The common particle size distribution for Ti-6Al-4V powders used in electron beam powder processing are 45-105 μm, 53-125 μm or 45-125 μm, while laser-based powder bed fusion utilises smaller particles in the range of 20 μm to 60 μm [140]. The powders acquired were from AP&C, Hoeganaes, Puris, TIMET, ATI and Praxair. Puris, ATI, and TIMET were of grade 5 condition, AP&C and Praxair were categorised as grade 23, ELI (extra low-interstitial) and Hoeganaes was grade C [140]. The TIMET powder was produced by the PREP method while the rest were manufactured using different atomisation processes [140]. Differences in the particle size were observed such that the Puris and

ATI powders exhibited finer particles compared to AP&C and Praxair powders. TIMET powders portrayed very smooth surfaces, possibly owing to the PREP manufacturing process, while the rest were accompanied with satellites. They also emphasised that high or low flowability does not necessarily indicate the suitability of the powder for additive manufacturing as too much flowability might negatively influence the spreading process, however, this effect must be examined in future works [140]. Additionally, Sun et al. highlighted the advantages of Ti-6Al-4V as they consist of phenomenal mechanical and corrosion properties [140]. It is important to note that any impurities within the alloys can significantly change the mechanical properties regarding the ductility, fatigue behaviour and yield strength. The impurities within titanium are hydrogen, oxygen, nitrogen and carbon, which can originate from the powder manufacturing stage [140]. The predominant cause of impurities in gas atomisation and PREP are the initial processing of the ingot and further atomisation steps. As the titanium and titanium alloys are produced through the atomisation step, they are prone to surface oxidation; however, different atomisation processes exhibit varying impurity uptakes [140].

In addition to that, Chen et al. undertook a comparative study of Ti-6Al-4V AM powders using three different powder production methods, including gas atomisation (GA), plasma rotating electrode process (PREP) and plasma atomisation (PA) [141]. It was reported that the particle size significantly influenced the micro-morphology of powders in terms of pore size, porosity and argon content. They concluded that PREP powders exhibited the lowest porosity and argon content for particle sizes less than 150 μm, while GA powders produced the highest values [141]. They further stated that for particles below the size of 50 μm the porosity was negligible for all three powders. Additionally, for all of the three above mentioned powders, the reduction of particle size resulted in a decrease in the pore population, size and porosity, while the argon content increased with larger particle sizes [141]. Finally, they detected an increase in pore sphericity for GA and PA powders compared to powders produced by the PREP method due to the varying gas pressures within powders created during the atomisation process. They stated that the operating gas pressure in PREP is much lower than that used in GA and PA [141]. Therefore, close attention must be paid in investigating and controlling the production method of powders and their properties to enable the production of repeatable and reliable end parts with desirable performance.

Moreover, Gong et al. analysed the defects generated in Ti-6Al-4V products in powder bed-based fusion including SLS and EBM and highlighted the importance of process parameter control to ensure high quality end parts [142]. They utilised Raymor Ti-6Al-4V (Grade 23) for SLM (inert gas atmosphere) processes and Arcam Titanium Ti-6Al-4V ELI powder for EBM (vacuum atmosphere) systems. The characterisation of Raymor powders provided the following information: bulk density of 2.55 g/cm^3, where most powders exhibited a spherical shape and particle size not exceeding 45 μm, with a D_{10} of 17.36 μm and D_{90} of 44.32 μm. Arcam powders exhibited spherical particles with a bulk density of 2.70 g/cm^3, D_{10} of 46.94 μm and D_{90} of 99.17 μm [142]. The different particle size distribution is crucial for these processing systems as EBM requires electrons to penetrate the surface of the powders into the grains so as to convert their kinetic energy into thermal energy for powder melting, while in SLS, powders absorb heat from the laser beams (photons) [142]. Additionally, laser spots have a much finer size than the electron beam, hence EBM systems require larger particles and larger electron beam sizes to eliminate any repelling between particles as they end up charging from the electron beam. Thus, EBM produces parts that are much larger than SLM parts in term of resolution, feature size and surface quality. They reported that the generation of defects are a result of both the powder properties and system performance such that any fluctuation in the laser beam will create challenges in the melting process [142, 143]. For instance, reduced laser power inhibits in-depth penetration resulting in un-melted particles underneath melt pools. A solution to improve the quality of SLS Ti-6Al-4V products was to increase the inert gas velocity across the chamber as the gas would eliminate fine powders [144]. Moreover, spherical pores that occurred in EBM Ti-6Al-4V products were a result of entrapped gases during the powder production process. Thus, to eliminate the generation of defects within the products, the processing conditions and inherent powder properties need to be regulated [142]. Similarly, Iebba et al. also conducted a study in the effects of Ti-6Al-4V powders on the generation of porosity in AM components; in other words, a correlation between powder characteristics and defect generation was established [116]. They established that Ti-6Al-4V powdered produced by gas atomisation (GA) exhibited internal porosities occupied by trapped gases and further affirmed that particular attention must be paid to the initial powder manufacturing process to eliminate porosity defects [116].

2.6 Summary of the Knowledge Gap

The complete understanding and dynamics of powder spreadability is yet a challenge imposed within the additive manufacturing industry. To date, there are no viable metrics established to characterise the spreadability of powders, and only measurements of flowability have been utilised to further expand on the powder spreading dynamics. However, flowability measures do not provide an accurate representation of the spreading process in powder bed-based fusion but are still essential to be accounted for during the spreading of thin powder layers [68].

Even though a parallel can be formed between the flowability and spreadability of powders, they are still very different powder properties, hence, thorough investigation is necessary to distinguish and develop characterisation methods for spreadability. Some researchers have attempted to define spreadability as a "complex characteristic feature of a powder" that allows the uniform spread of powders without the formation of empty patches, agglomerates and rough surfaces [13], while others defined it as the "ability of powders to spread over itself", its interaction with the spreader, build plate and partially built parts [145].

As previously mentioned, Snow et al. experimentally attempted to establish spreadability metrics in terms of percent coverage on the build plate, powder deposition rate, and the rate of change of the avalanching angle by utilising an in-house spreader rig with varying rake velocities [77]. They obtained valuable information regarding powder properties and process parameters. They stated that the high angles of repose results in poor spreading qualities and, interestingly, the percent coverage showed no dependence on the rake velocity but rather on the material of the spreader [77]. However, there was a lack of quantification of the powder bed's packing fraction which is essential to determine the quality of the spread layer. They only described qualitatively that flowable powders result in high packing densities while powders with poor flowability created low layer packing densities. Furthermore, Ahmed et al. investigated the ease of powder flow through different gap sizes and their effects on the quality of spread layers in terms of the frequency of jamming [13]. However, they manually spread the powders, which may lead to errors due to user dependency in regard to the positioning and velocity of the spreader. Additionally, there is a lack of in-depth analysis of the packing fraction through controlled chambers within their work. It is

important to note that the experimental studies covered in this work is limited to only a single layer of powder spreading, which is not the case in usual PBF processes.

Moreover, Fouda and Bayly examined the spreadability of Ti-Al-4V powders in additive manufacturing using discrete element method, where they utilised mono-size spherical powders with varying gap sizes and velocities [134]. This assumption may lead to inaccurate results of the packing fraction as mono-sized particles can possibly cause crystal structures within the powder layers. Additionally, Desai and Higgs reported the effects of Ti-6Al-4V powders with varying speeds using simulation, where the packing fraction and quality of spread layer was determined [138]. The major weakness gathered from the simulation studies is the implementation of very ideal conditions such as utilising spherical particles by ignoring their true actual shapes that significantly impacts the spreading behaviour. In addition to that, there is a lack of experimental validation to support and confirm the results of numerical simulations.

Therefore, the experimental studies have not only been limited to a single spread profile that lacks multi-layer depth analysis but also restricted to testing against a few process parameters at a time. The effects of the entirety of process parameters such as rake velocity, gap size, spreader type and material need to be tested at the same time to fully understand their effects on the spreading dynamics. Additionally, studied related to Ti-6Al-4V powders are limited to simulation work and differences in particle properties due to various production methods. Future work will encompass powder spreading by testing the Ti-6Al-4V powders against all the process parameters and in different environments such as inert, humid and higher temperature conditions. Numerical simulation will then be implemented to support the experimental data.

CHAPTER THREE

Materials and Methodology

3.1 Scanning Electron Microscopy (SEM) and X-Ray microtomography (XMT)

3.2 Aspect Ratio (AR) and Angle of Repose (AoR) of HDH and GA Ti-6Al-4V Powders

3.3 Experimental Procedure

3.4 Qualitative Observation

3.5 Image Analysis using ImageJ

3.6 Quantification of the Bulk Layer Density

3.7 Quantification of Layers in terms of Mass per Area

3.8 Angle of Repose on the Build Plate

3.9 Dimensionless Shear Rate

3 Material and Methodology

Titanium alloys are used in an array of industries such as aerospace and medicine owing to their exceptional properties such as resistance to corrosion, outstanding strength-to-weight ratios, enhanced biocompatibility and increased fracture toughness [146]. As previously mentioned, the major drawback associated with the wider application of Ti-6Al-4V powders are their high costs of production. The materials used in this work are two samples of grade 5, Ti-6Al-4V powders produced by HDH and GA methods, supplied by GKN Ltd, UK. The costs of these production methods differ greatly, where HDH powders provide a cost-effective solution but generates irregular powders while GA as a costlier alternative produces spherical particles. The different production methods are covered in section 2.1 of this thesis. Figure 8 below depicts the two different samples, where HDH and GA powders are in left and right containers, respectively. The material properties of Ti-6Al-4V powders have been measured by Mehrabi et al. [118] and due to their strong relevance to this work, they have been reported, mentioned and further correlated to the spreading behaviour.

All the material characterisation including XMT and SEM images illustrated in this work have been conducted by Mehrabi et al. [118], where 20,000 particles were individually characterised in terms of shape (AR and sphericity), which provided accurate and repeatable results for both samples.

Figure 8: HDH powders (left side) and GA powders (right side).

3.1 Scanning Electron Microscopy (SEM) and X-Ray microtomography (XMT)

Scanning electron microscopy is a static image analysis method employed to obtain the absolute range of sizes and the degree of dispersion [147]. SEM and XMT are utilised for the analysis and classification of dry powder surface properties such as porosity and roughness. Scanning electron microscopy (SEM) provides important information regarding the particle's size, shape and surface properties of the two samples. It is important to note that close attention must be paid to the sample preparation stage when employing SEM, such as the approach of dispersion and ensuring particle segregation and aggregation is prevented. Furthermore, the orientation of irregular particles on the substrate under observation can have a significant effect on the imaging results [147]. Sample preparation usually involves actions such as grinding, polishing and etching which is both time consuming and invasive as powders of interest are prone to destruction during the sampling process. Therefore, employing a non-destructive characterisation method such as x-ray microtomography (XMT) enables a three-dimensional characterisation of powders (i.e. shape, size distribution, morphology and porosity) that produce high resolution images used to quantitatively characterise internal features of the powder [148, 149]. SEM and XCT images of the two samples for the shape analysis in this work was provided by Mehrabi et al. [118].

Figure 9 below illustrates the SEM images of the two samples. It is clear from visual observations that the HDH powders consist of irregular shapes with uneven, flake-like rough surfaces, while the GA powders exhibit smooth surfaces with spherical shapes. Such differences may mainly be due to their different powder production methods. As reported earlier in this work, gas atomisation produces more spherical powders compared to the hydrogenation-dehydration method. It was visually deduced from section 4.2.2, that GA powders produced better spreading profiles compared to HDH powders, which may be due to their shape morphologies. Spherical particles are characterised by enhanced flowability [70] while non-spherical particles are prone to mechanical interlocking which impedes powder flow creating non-uniform powder layers [66].

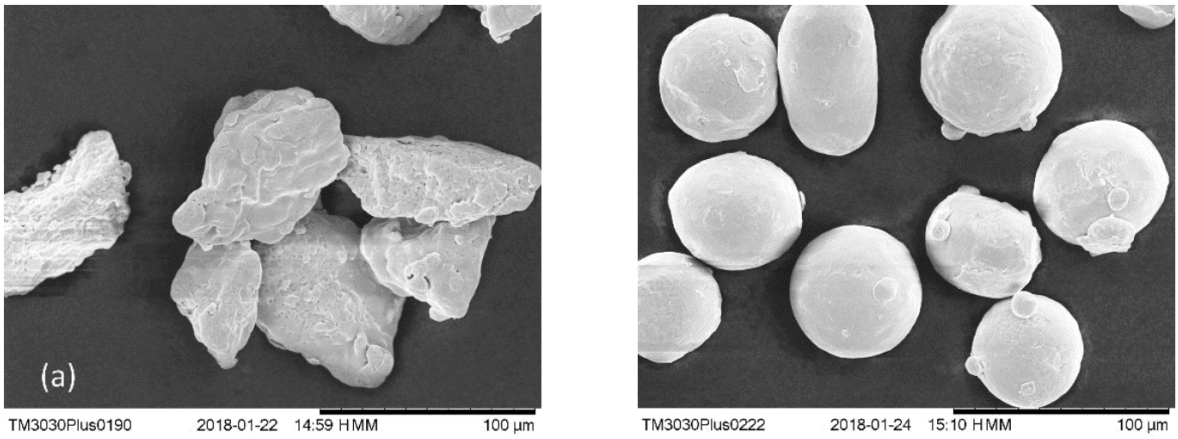

(a) (b)

Figure 9: SEM images for (a) HDH and (b) GA Ti-6Al-4V powders [118].

Furthermore, XCT images were provided by Mehrabi et al. [118] which clearly portrayed the differences within the GA and HDH Ti-6Al-4V powders. Figure 10 below illustrates the reconstructed close-up images of GA and HDH particles.

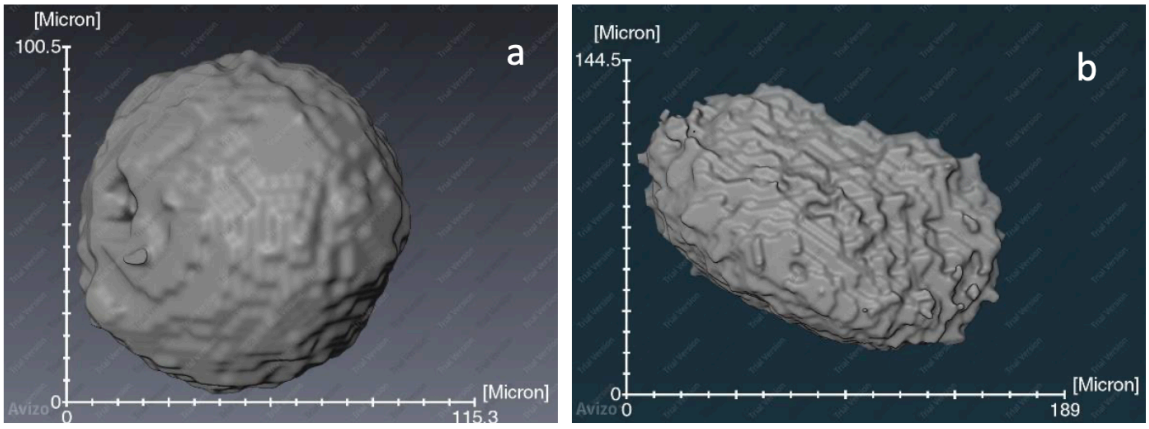

Figure 10: XMT images for (a) GA and (b) HDH Ti-6Al-4V powders [118]

The differences between the two samples are also clearly detected from the XCT images above, where the GA particle consist of a smoother and spherical morphology with the presence of some satellite particles and surface pores, while the HDH powders comprise of elongated shapes with increased surface roughness. In addition to that, the sphericity values for the two samples were also provided, which can be used as an additional indicator of the spread behaviour of powders across the build plate. Figure 11 below provides useful information on the sphericity values of the two samples.

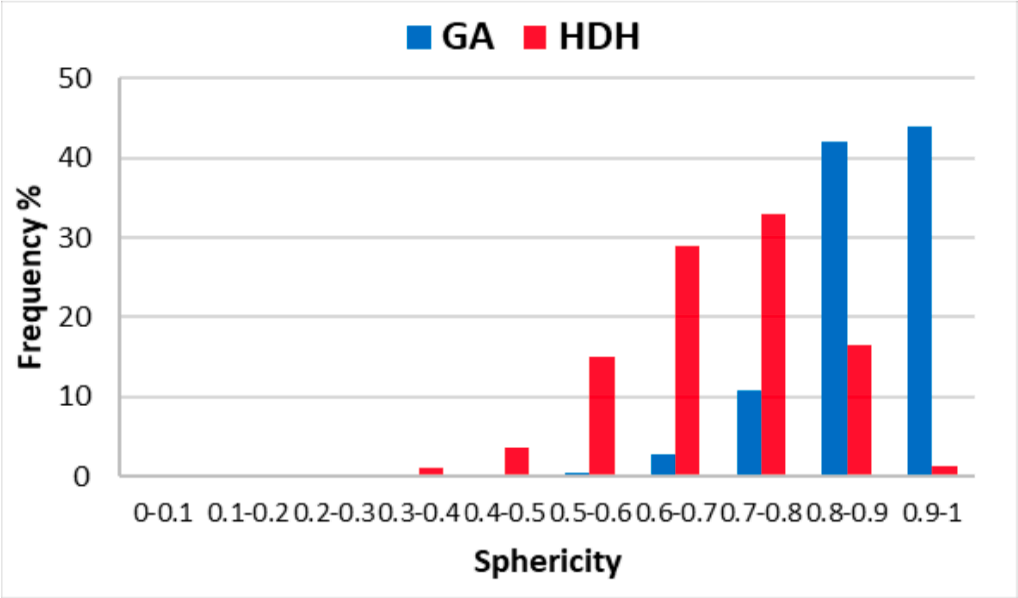

Figure 11: Sphericity values for GA and HDH, Ti-6Al-4V powders [118]

As portrayed by Figure 11 above, the sphericity values for majority of the GA powders is in the range of 0.8 to 1, contrary to the HDH powders were most of them lie within the range of 0.6 to 0.8. This further confirms the image analysis generated by the SEM and XCT images. Mehrabi et al. [118] further reported the factors influencing the sphericity values within the GA powders where GA powders exhibited satellites, concavity and pores which resulted in lower sphericity values in the range of 0.8 to 0.9 [118]. They further generated the following XCT images, Figure 12, to demonstrate some of the different particle shapes present within the GA powders. Such

projections, indentations and porosity on the particles consequently reduced the value of sphericity.

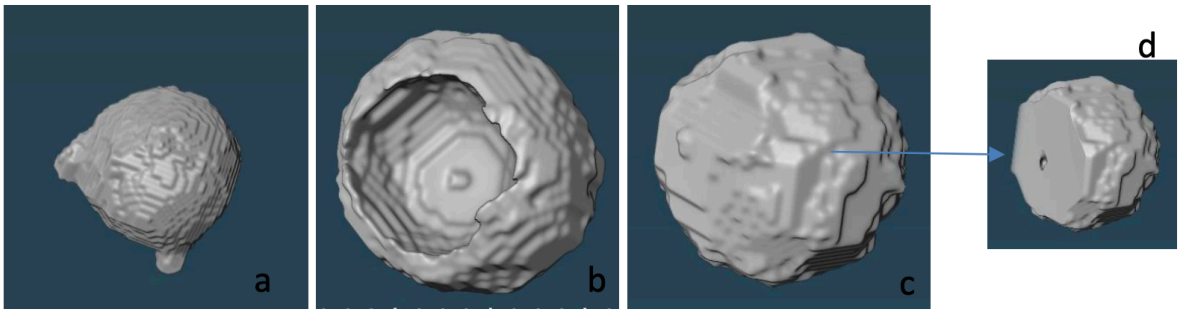

Figure 12: GA powders of different morphologies (a) presence of satellites, (b) concave particles, (c) particle exhibiting porosity and (d) internal porosity, cross-section of image (c) [118].

3.2 Aspect Ratio (AR) and Angle of Repose (AoR) of HDH and GA Ti-6Al-4V Powders

The aspect ratio (AR) also provides a quantitative analysis of the shape of the particle which can further be used to analyse the spreading behaviour. Mehrabi et al. [118] measured the aspect ratios (AR) of the two samples as illustrated in Figure 13 below.

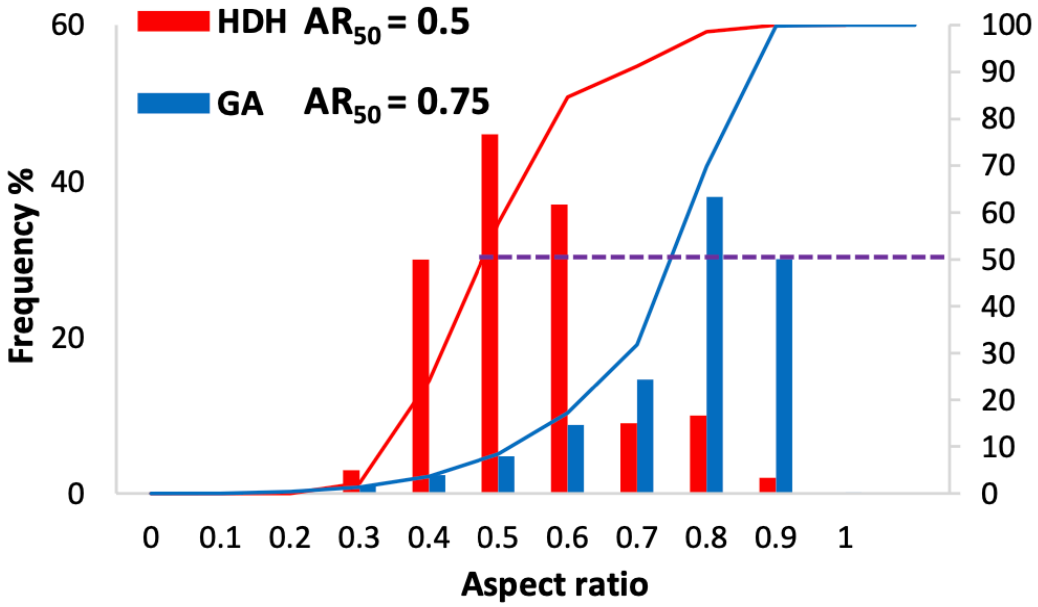

Figure 13: Aspect ratio for GA and HDH, Ti-6Al-4V powders [118].

From Figure 13 above, it can clearly be observed that majority of the HDH particles consist of an AR values of about 0.5 while most of the GA powders are in the range of 0.8 to 0.9. This further affirmed the irregularities in shape of HDH powders, where they exhibit elongated projections rather than spherical shapes. It is important to note that the above-mentioned parameters may not provide decisive results regarding the true shape of particles, as hollow particles may exhibit spherical envelope surfaces but in reality, consist of low sphericity values due to internal pores, hence, caution has to be taken for comparative shape analysis of the two samples [118].

As stated previously, the angle of repose (AoR) is a measurement utilised to provide an indicator of the flow behaviour of powders [89]. A smaller value of the AoR indicates powders of high flowability while greater values indicate powders of poorer flowability. Mehrabi et al. [118] provided the AoR values for the bulk samples as shown in Table 4 below. The AoR of GA powders are much lower than that of HDH powders, indicating improved flow behaviour of powder.

Table 4: Angle of repose of bulk Ti-6Al-4V powders [118]

Samples	Angle of Repose (°)	Flowability Index
GA	27.1 ± 0.05	Excellent
HDH	37.6 ± 0.03	Good

Figure 14 below provides information on the characterisation of powders provided by Mehrabi et al. in regard to the particle size distribution of the two samples [118].

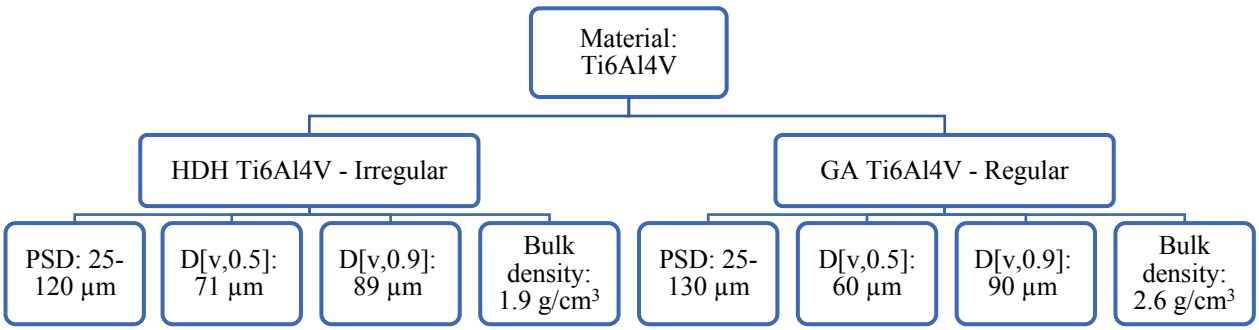

Figure 14: Summary of the material characteristics [118].

3.3 Experimental Procedure

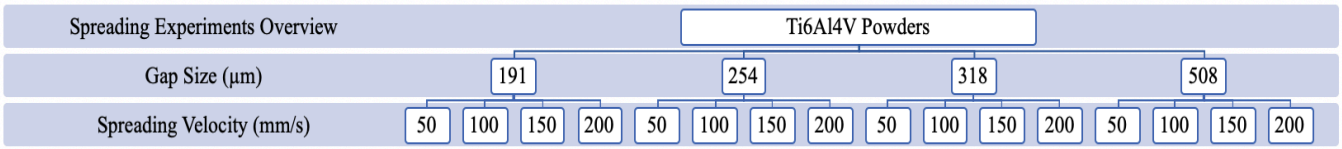

An in-house spreading rig depicted by Figure 15 across mimics the recoating systems in PBF, was set up by previous researchers and was utilised in this work to investigate the spreading profiles of HDH and GA Ti-6Al-4V powders. The spreading rig consists of a fixed blade type spreader and an aluminium build plate with a total bed area of 115mm by 60mm (measured by a calliper), which is motorised through the MSP software. The dimensions of the plate can vary accordingly with the size of the in-house rig. The gap sizes, which is the distance between the spreader and the built plate, are manually adjusted using a gauge, while the velocity is inputted into the software. To determine the gap size, the gauge with the gap of interest is placed between the build plate and the spreader and manually adjusted until a slight friction is sensed on the gauge.

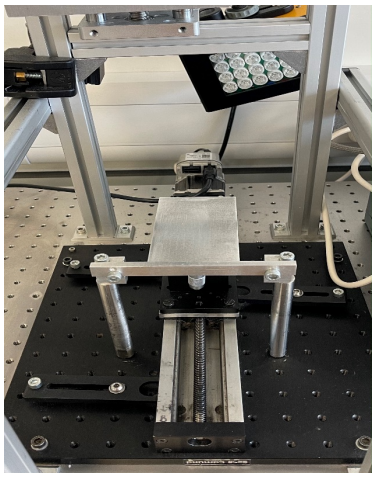

Figure 15: ImageJ analysis to calculate spread area.

The experimental work was designed to examine the spread profiles against a set of parameters, where the mass was a constant while the gap size and velocity were variables. The choice on the gap size was primarily based on the D_{90} of the particles, which included 191 µm, 254 µm, 318 µm and 508 µm. The spreading velocity was selected on the basis of the operating conditions used

within PBF systems and included 50 mm/s, 100 mm/s, 150 mm/s and 200 mm/s. The standard operating procedures include the mass of the powder which was determined through conducting a series of trial and error tests in accordance with the gap size and highest velocities. There was a minimum of five iteration for each test to minimise errors and ensure repeatability. Furthermore, the experiments were done at ambient humidity (34-38%) and room temperatures (21-22°C).

Figure 16 below illustrates the mechanism of powder spreading with the in-house spreading rig. The initial stage includes the feeding stage, where the powder of a certain mass is poured with the aid of a funnel as depicted by Figure 16 (a). A powder heap is then formed when the feeder is removed as portrayed by Figure 16 (b) and then the spreading process is commenced as depicted in Figure 16 (c).

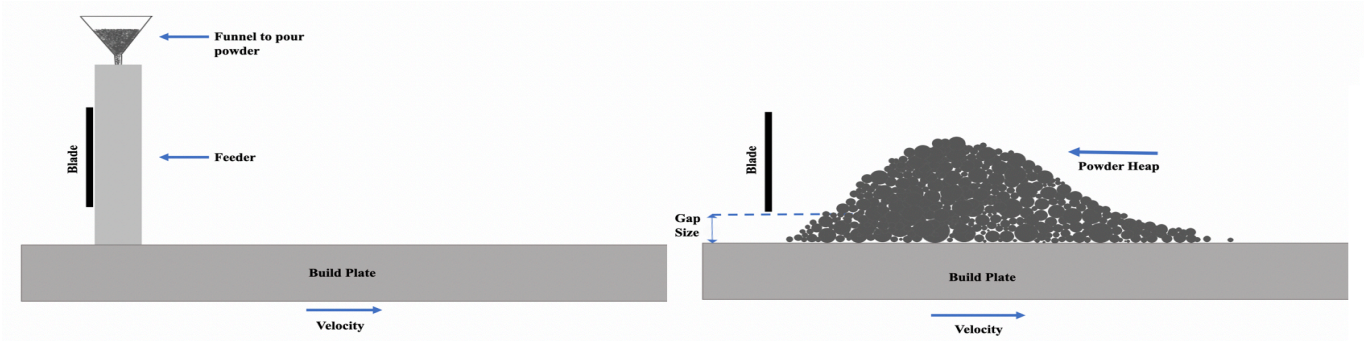

(a) (b)

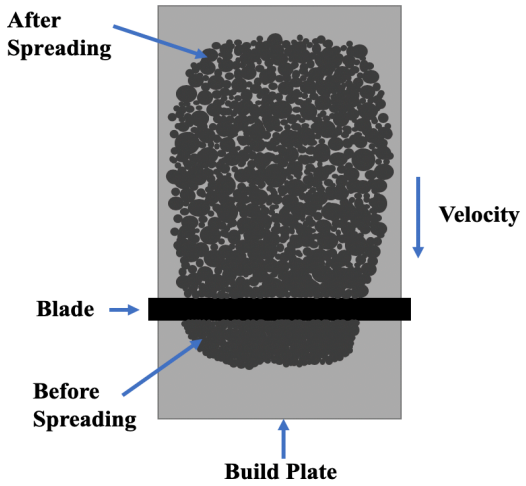

(c)

Figure 16: (a) Side view of feeding stage, (b) side view of powder heap and (c) top view of the spreading stage.

3.4 Qualitative Observation

Qualitative observations provide useful information about the spreading profiles. Each gap size was tested against the four spreader velocities, which was reported in the previous section, where each produced individual spreading profiles. An overhead camera was employed to capture images of each of these individual profiles and observe the differences on the powder layers associated with the different gap size and velocities.

3.5 Image Analysis using Image

The images captured by the overhead camera were then transferred into ImageJ for further analysis. The images were scaled in order to covert the units from pixels to millimetres, which could then be utilised for further additional calculations. ImageJ provided important data regarding the area covered by the spread powder, which was essential for quantifying the layer quality. The steps undertaken to calculate the area of the spread layer are as follows:

i. The image of the spread layer (top view) was uploaded onto the ImageJ software.
ii. The correct scales were inputted by using the "set scale" option under the analyse bar. The length of the build plate was taken as the scale reference, measured at 115mm.
iii. After the scale was set, an accurate outline around the spread profile was drawn using the "polygon selection" option. This is illustrated by the yellow outline in Figure 17 across.
iv. The "measure" option was then used to calculate the final area covered by the spread profile.

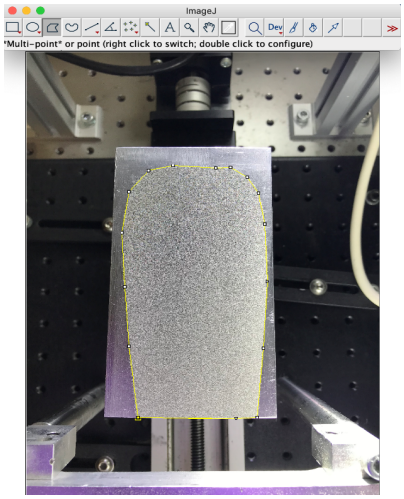

Figure 17: ImageJ analysis to calculate spread area.

3.6 Quantification of the Bulk Layer Density

For the quantification of the layer density, a gravimetric analysis was employed, where a series of calculations were performed using Excel software. This subsection will describe each of the individual experimental steps employed to achieve these results. It is important to note that before the powders were weighed, they were continuously exposed to rotational movements using an apparatus known as "advanced vortex mixer" to mitigate any form of powder segregation.

i. A digital weighing scale was used to measure an amount of mass that was used for spreading.
ii. A plastic thickness gage with a range of 25-762 μm was used to identify the individual gap sizes, by placing it between the spreader and build plate while manually adjusting it until a slight friction is felt on the gage.
iii. A funnel was then placed on top of the feeder, bound in position with tape. This was then placed in front of the spreader which was the initial stage of powder spreading.
iv. The powder was then poured through the feeder on to the powder bed, which then created a powder heap.
v. The powder heap was then spread across the build plate, while the excess powder, namely "dropped powder" was collected at the end of the plate. Collection was only possible on a single side. The spreading velocity for the in-house rig is associated with the movement of the build plate rather than the blade.
vi. The dropped powder was then weighed on the digital scale and the amount was recorded.
vii. The spread powder on the build plate was later collected and weighed. It is important to note that the width of the spread layer remains non-uniform due to the limitations imposed by the in-house rig, hence only a particular amount of powder can be deposited on the built plate.

The percentage (%) of spread powder was then calculated by taking the ratio of the weight of the spread powder to the initial fed mass multiplied by 100%. The following expression was used:

$$Percentage\ of\ spread\ Powder\ (\%) = \frac{Weight\ of\ spread\ powder}{Weight\ of\ initial\ fed\ mass} \times 100 \qquad \text{Equation 8}$$

The average bulk layer density was then calculated by taking the ratio of the mass of spread powder to the volume. The volume was calculated by using the area of the spread powder obtained from ImageJ multiplied by the gap size. It is important to note that the volume is based on the assumption that the gap size throughout the spread layer remains constant for ease of calculations, which is not necessarily the case is real experimental work. In other words, the gap size dictates the thickness. The gap size across the built plate can be measured using different techniques such as laser profilometry and confocal microscopy which will be implemented in future studies.

The following expression was employed to calculate the bulk layer density:

$$Bulk\ layer\ density\ (g/cm^3) = \frac{Weight\ of\ spread\ powder}{Volume\ of\ spread\ layer}$$ Equation 9

3.7 Quantification of Layers in terms of Mass per Area

In addition to the bulk layer density, another measurement of spreadability was introduced; namely, the mass per area. The mass per area of each layer at different gap sizes and velocities were calculated by multiplying the bulk layer density by the corresponding gap size. This metric simply eliminates the gap size as the variable. The following expression is used to calculate the mass per area of individual layers:

$$Mass\ per\ area\ (g/cm^2) = Bulk\ layer\ density \times\ gap\ size$$ Equation 10

3.8 Angle of Repose on the Build Plate

The angle of repose as stated previously is an indicator of flowability, which is a useful information to develop an understanding regarding the spreading dynamics of powders. The angle of repose of the two samples was previously provided by Mehrabi et al. [118], however, an additional measure of the angle of repose was undertaken to compare the results at a smaller scale i.e. build plate scale. ImageJ was employed to measure the height and base of the powder heaps, where the average of

the angles of repose obtained for the left and right side of individual heaps was taken. The following expression was used to measure the angles of repose:

$$Angle\ of\ Repose\ (°) = Tan^{-1}\left(\frac{Height}{Base}\right) \qquad \text{Equation 11}$$

3.9 Dimensionless Shear Rate

The dimensionless shear rate as explained in section 2.2.3.4 provides important information on the flow behaviour of powders in different rheological states. It forms a relationship between the stresses exerted on powders and its corresponding deformations. Equation 7 is applied to calculate the dimensionless shear rate $\gamma^{\circ *}$ at different gap sizes and spreader velocity. The particle diameter used in the equation corresponds to the D_{50} of the two samples.

The following expression as introduced by Tardos et al. is utilised to measure the dimensionless shear rate [110]:

$$\boldsymbol{\gamma}^{\circ *} = \dot{\gamma}\,[d/g]^{1/2} \qquad \text{Equation 7}$$

Where the shear strain rate, $\dot{\gamma} = \left(\frac{Velocity\ (v)}{Gap\ height\ (h)}\right) s^{-1}$, d is the particle's diameter taken as d_{50} and g is the gravitational acceleration. For the detailed calculations refer to the appendix.

CHAPTER FOUR

Qualitative Observations

4.1 Standard Operating Procedures

4.2 Observations from the Overhead Camera

4.3 Angle of Repose (AoR) of the Deposited Heap on the Build Plate

4 Qualitative Observations of Spreadability

This section focuses on the qualitative results such as images of the spread layers obtained from the overhead camera.

4.1 Standard Operating Procedures

As briefly discussed in section 3.1, the amount of mass for the respective gap sizes was chosen based on a series of trial and error tests. The trial and error tests were based on the maximum deposition of powder that could be collected on one side of the built plate (due to the limitations imposed by the in-house rig). The amount of mass differed for each individual gap size but remained constant for the two sample to allow comparison.

Initially, a certain amount of powder was assumed and tested against the highest spreader velocity of 200 mm/s, as the rate of powders being pushed away is highest at this velocity. If the powders dropped from the sides of the build plate as depicted by Figure 18 below, then that amount of mass was not accepted due to limitations imposed on powder collection at the sides. This process was repeated several times until the desirable mass of powder was obtained in accordance with the gap size. Table 5 below summarises the amount of mass that was used for each of the gap sizes.

Table 5: The initial fed mass for the formation of powder heap

Gap size (µm)	Initial Fed Mass (g)
191	3.5
254	3.8
318	4
508	5

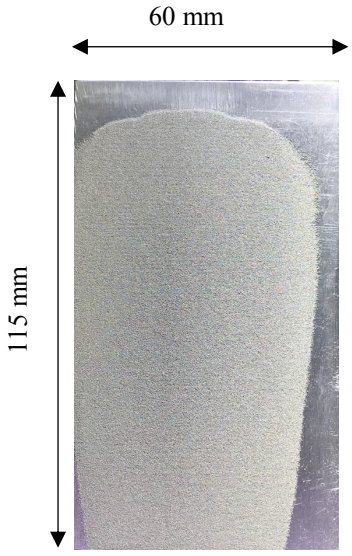

Figure 18: Dropped powder on the side of the build plate.

4.2 Observations from the Overhead Camera

Individual profiles at each of the gap sizes and velocities were captured to detect any visual changes on the powder bed. Initially five gap sizes were included in the experimental work, including 102 μm, 191 μm, 254 μm, 318 μm and 508 μm. However, 102 μm was eliminated as severe jamming was detected on the powder bed.

Figure 19 across illustrates the occurrence of jamming on the powder layer, which is an undesirable effect. The vertical lines on the powder layer may be due to particle drag, which negatively impacts the mechanical properties of the final part, the drag lines on the built plate indicate non-homogeneity of the layer which ultimately generates porous layers. This is potentially due to the rigidity of the blade, which could be mitigated by employing flexible spreaders made of silicone, that will be part of the future works.

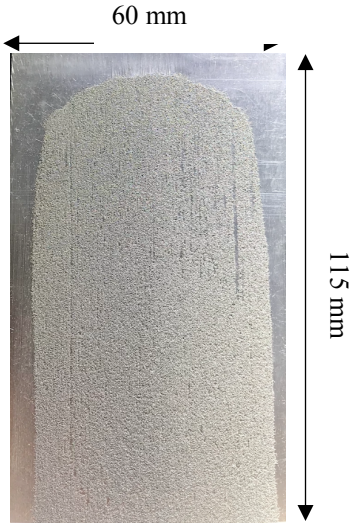

Figure 19: Occurrence of jamming at 102 μm.

The profiles at each individual gap size and spreading velocity are depicted in sections 4.2.1, Figure 20 and 4.2.2, Figure 21 for HDH and GA powders respectively. The quality of the spread layers in terms of drag lines and uneven surfaces tends to deteriorate as the spreading velocity increases. The occurrence of jamming is prevalent at smaller gap sizes and higher velocities as depicted by the spreading profiles of HDH powders. Empty patches and drag lines were clearly observed for HDH powders at 191 μm with a spreading velocity of 200mm/s. Additionally, as the gap size increased, the coverage area by the spread powder reduced, implying an increase in the total volume of the powder layer [130]. From literature, it was gathered that an increased total volume of layers enhances the particle packing, which results in uniform powders layers and consequently end parts of desirable mechanical properties. However, very big gap sizes may compromise the dimensional accuracy of the end part due to unsintered large particles that can result into inhomogeneous surfaces. Furthermore, from the qualitative analysis of the spread profiles below, portrays that GA powders consists of very even and smooth layers, that may be an indicator of a desirable spreading mechanism compared to HDH powders.

4.2.1 Spread Profiles for HDH Ti-6Al-4V

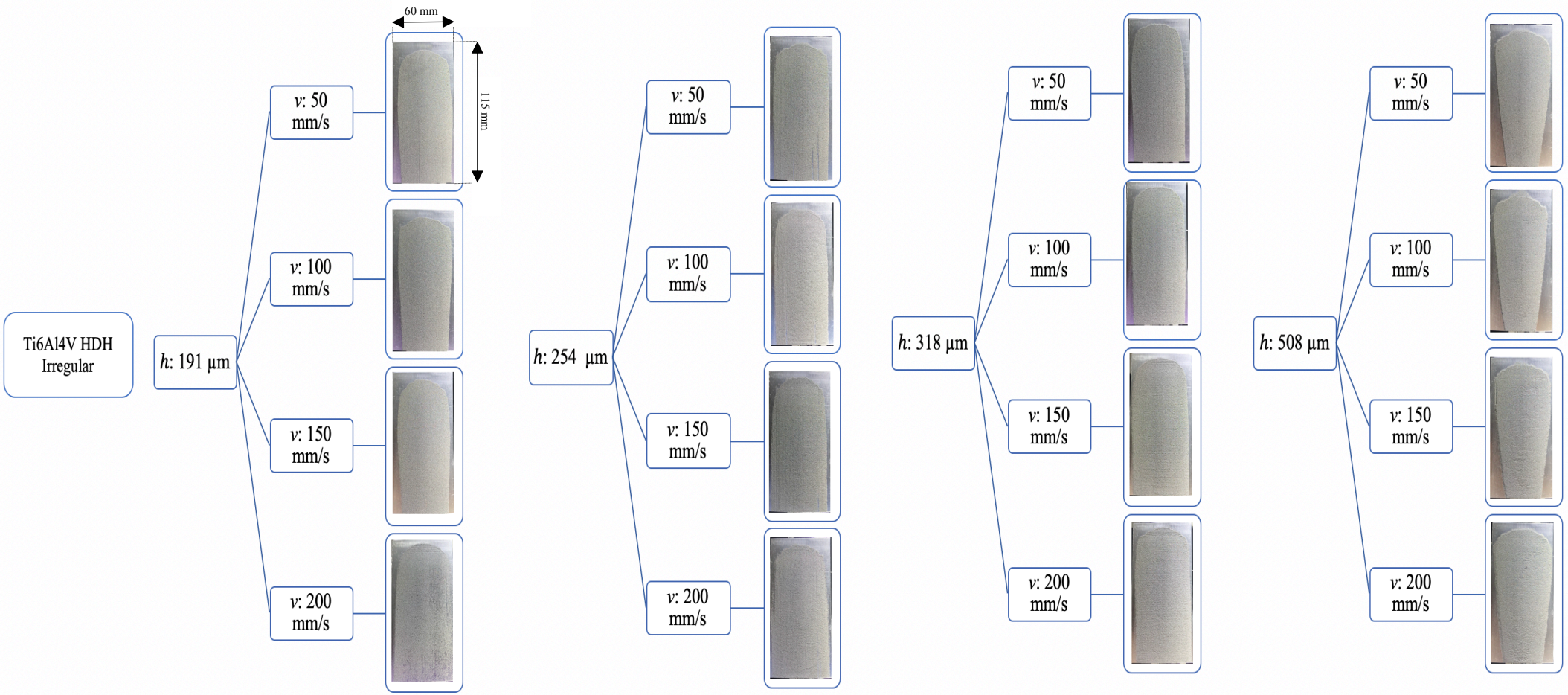

Figure 20: Spread profiles of HDH Ti-6Al-4V powders.

4.2.2 Spread Profiles for GA Ti-6Al-4V

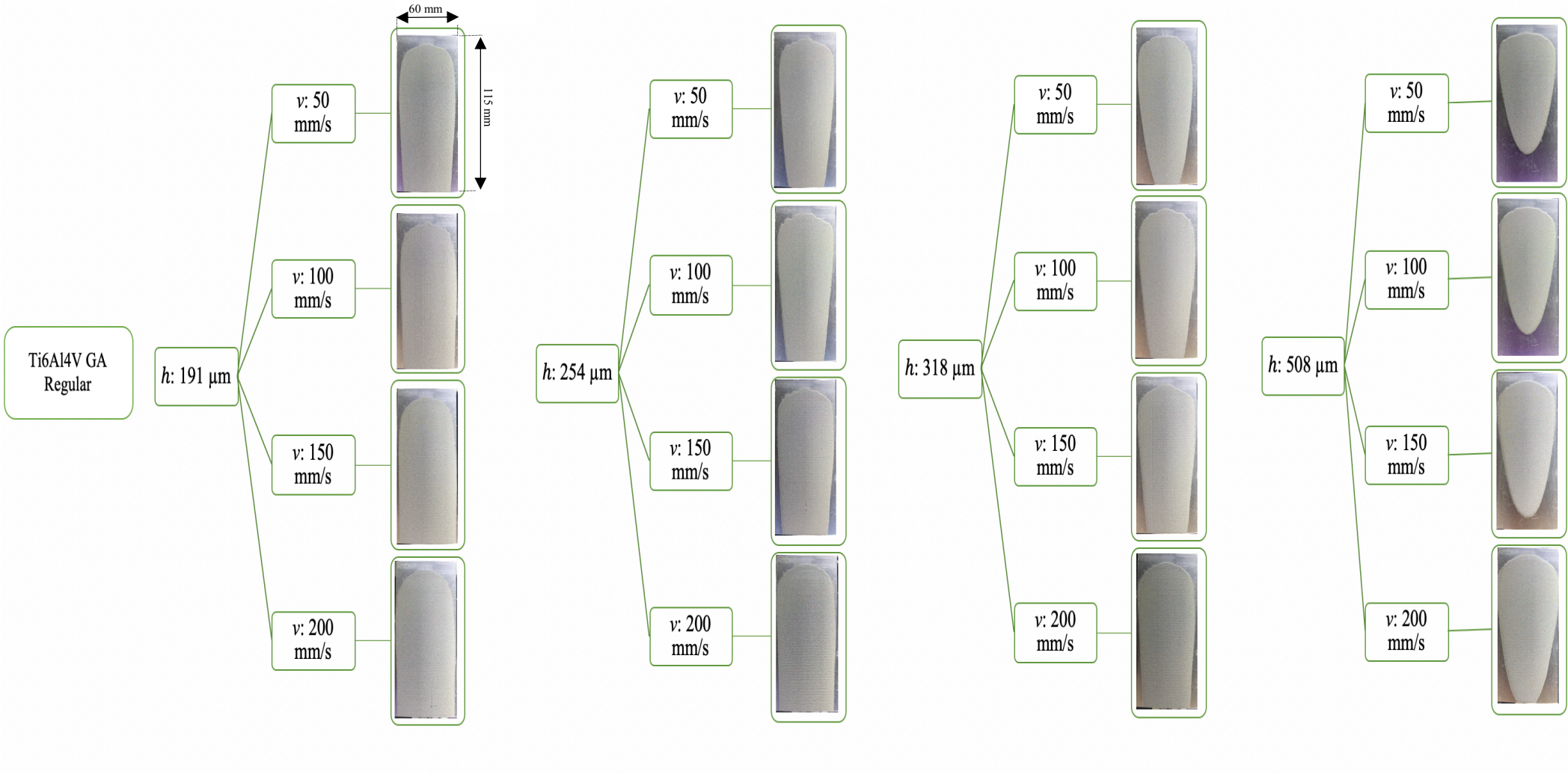

Figure 21: Spread profiles of GA Ti-6Al-4V powders.

4.3 Angle of Repose (AoR) of the Deposited Heap on the Build Plate

An additional measure of the angle of repose was tested on a smaller scale, to analyse the flow behaviour of powders on the powder bed. This provided an approach at measuring the angles of repose at a realistic powder bed scale. Figure 22 depicts the powder heap on the build plate, where the AoR was measured with the aid of ImageJ software. Table 6 below provides the results of the AoR for both samples at the powder bed scale tested with a constant mass of 3.5 grams.

Table 6: Angle of repose of Ti-6Al-4V powders on the build plate

Samples	Angle of Repose (°)	Flowability Index
GA	21.6 $\pm$ 1.35	Excellent
HDH	28.0 $\pm$ 1.31	Excellent

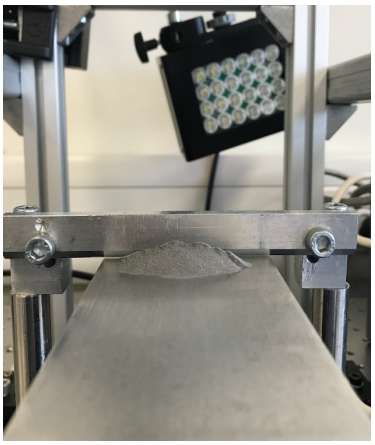

Figure 22: Build plate powder heap.

At the powder bed scale, both powders exhibit excellent flowability; however, GA powders in comparison still have better performance. This further confirms the relative homogenous profiles illustrated in section 4.2.2, suggesting better spreading behaviour of GA powders, which is desirable outcome within the additive manufacturing industry.

CHAPTER FIVE

Effects of Spreader Velocity and Gap Size on the Spreading Behaviour of Ti-6Al-4V Layers

5.1 Bulk Layer Density

5.2 Mass per Area

5.3 Combined Effect of Spreading Velocity and Gap Size

5 Effect of Spreading Velocity and Gap Size on the Spreading Behaviour of Ti-6Al-4V Layers.

This section primarily focuses on the effects of spreader velocity and gap size as process parameters on the quality of the spread layer. As discussed in literature, process parameters significantly influence the quality of the spread layer and consequently the end product [13, 83, 130]. Two metrics for measuring spreadability was introduced in this thesis, the bulk layer density and the mass per area of the spread layers.

5.1 Bulk Layer Density

The bulk layer density as a measure of spreadability is calculated by taking the ratio of the weight of spread powders to the volume it occupies on the build plate. In other words, an attempt is made on defining the term spreadability as the measure of the bulk layer density. Figures 23-26 demonstrate the trends in the bulk layer density of the two samples at different gap sizes and velocities.

Figure 23 illustrates the bulk layer density at 191 µm with respect to different velocities. Generally, GA powders have a better performance in generating powder layers of higher densities compared to HDH powders. The performance of GA powders is optimised at lower velocities of 50 mm/s, producing a bulk layer density of 2.48 g/cm^3 which is close to its bulk density of 2.6 g/cm^3. On the contrary, HDH powders exhibit a different behaviour such that it generates a relatively high layer density of 1.97 g/cm^3 that is greater than the bulk density of 1.9 g/cm^3 at the spreading velocity of 100 mm/s. However, there is a drastic fall in the layer densities after 100 mm/s which is undesirable in additive manufacturing.

Figure 24 portrays the trends of the two samples at the gap size of 254 µm where GA powders behave in a similar manner to the previous gap size, where the highest bulk layer density of 2.55 g/cm^3 is obtained at the spreading velocity of 50 mm/s. It is important to note that the bulk densities obtained with respect to the four different velocities are significantly higher than the ones calculated at 191µm. However, HDH powders reveal an anomalous behaviour with a significant reduction of the bulk layer density in all corresponding velocities. Interestingly, the percentage of

spread is also much lower compared to the results obtained at 191 μm, which is an anomalous situation as usually with any increase in gap size, the percentage spread also increases as there is more powder deposition onto the build plate.

Figure 25 and 26 depict the results gathered at the gap size of 318 μm and 508 μm, respectively for the two samples, where both powders follow a similar pattern to the results obtained for 191 μm. GA powders exhibited high bulk layer densities at lower velocities, however, an increase in the spreading velocity resulted in reduced layer densities which is deemed to have a negative impact on the quality of both the layer and end product. On the other hand, HDH powders demonstrated improved performance at the gap size of 318 μm, where the highest bulk layer density was obtained compared to the other gap sizes. They did follow similar patterns in such a way that the highest bulk layer densities were achieved at a spreading velocity of 100 mm/s.

Therefore, the highest bulk layer densities – which is a measure of spreadability – are obtained when utilising GA powders, owing to their spherical morphologies that enhances flow behaviour and spreading dynamics. For GA powders, the percentage of spread increased as the gap size increased, but this relationship was not established for bulk layer densities. For instance, the highest bulk layer density was obtained at 254 μm with a spreading velocity of 50 mm/s, however, at higher velocities of 150 mm/s and 200 mm/s, the gap size of 508 μm provided higher relative bulk layer densities compared to other gap sizes at 150 mm/s and 200 mm/s. Additionally, the bulk layer density of GA powders decreased with an increase in spreading velocity suggesting that they are repeatable and reliable powders. On the contrary, HDH powders exhibited higher bulk layer densities and percentage of spreads at 100 mm/s except for the gap size of 254 μm, which will be treated as an anomaly. This suggests that HDH powders reveal optimised performance at this specific velocity of 100 mm/s. This could be due to a specific arrangement of particles under the blade that results into optimised behaviour at this velocity, where further exploration is required within the future works. In addition to that, the HDH powders had better performance in terms of layer density at 191 μm and 318 μm compared to the largest gap size of 508 μm. Very large gap sizes such as 508 μm may not be desirable to utilise in PBF processes as very thick layers may prevent efficient laser interaction and result in un-melted particles that further jeopardizes the dimensional accuracy of the final part.

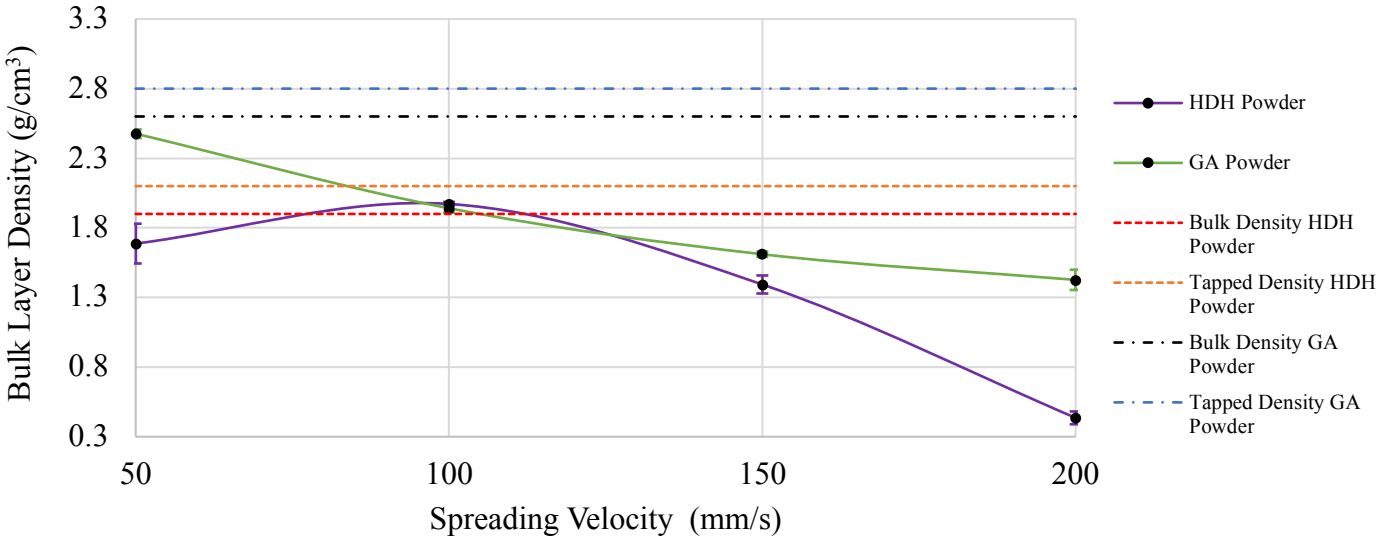

Figure 23: Spreading velocity (mm/s) against Layer Density (g/cm^3) for Gap Size 191µm.

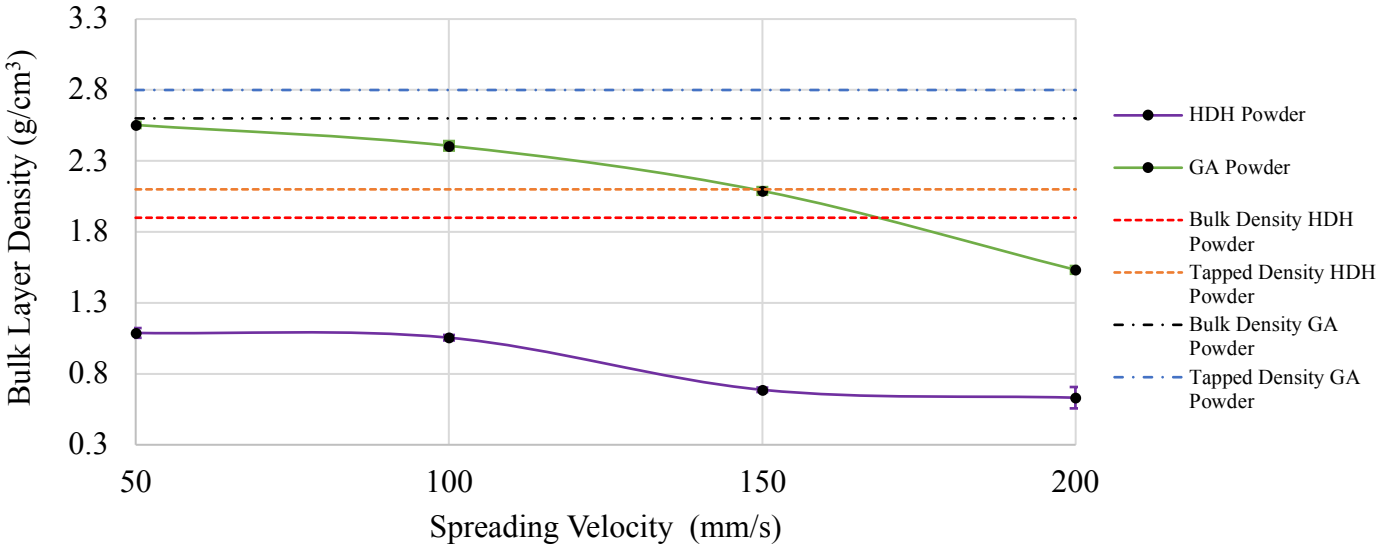

Figure 24: Spreading velocity (mm/s) against Layer Density (g/cm^3) for Gap Size 254 µm

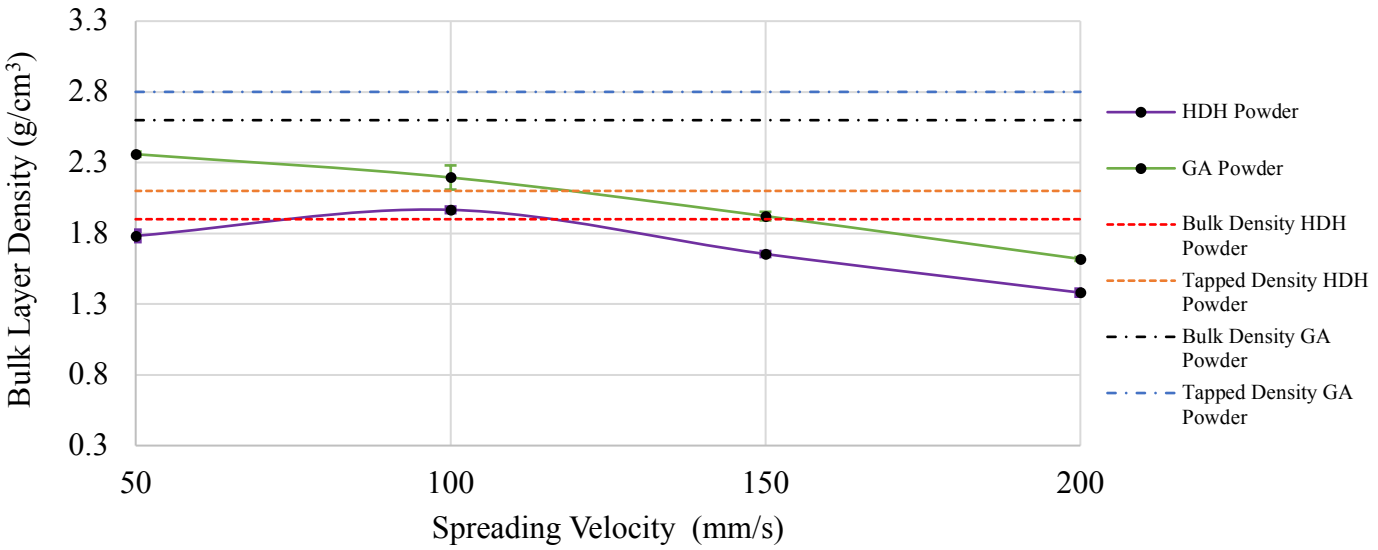

Figure 25: Spreading velocity (mm/s) against Layer Density (g/cm^3) for Gap Size 318 µm

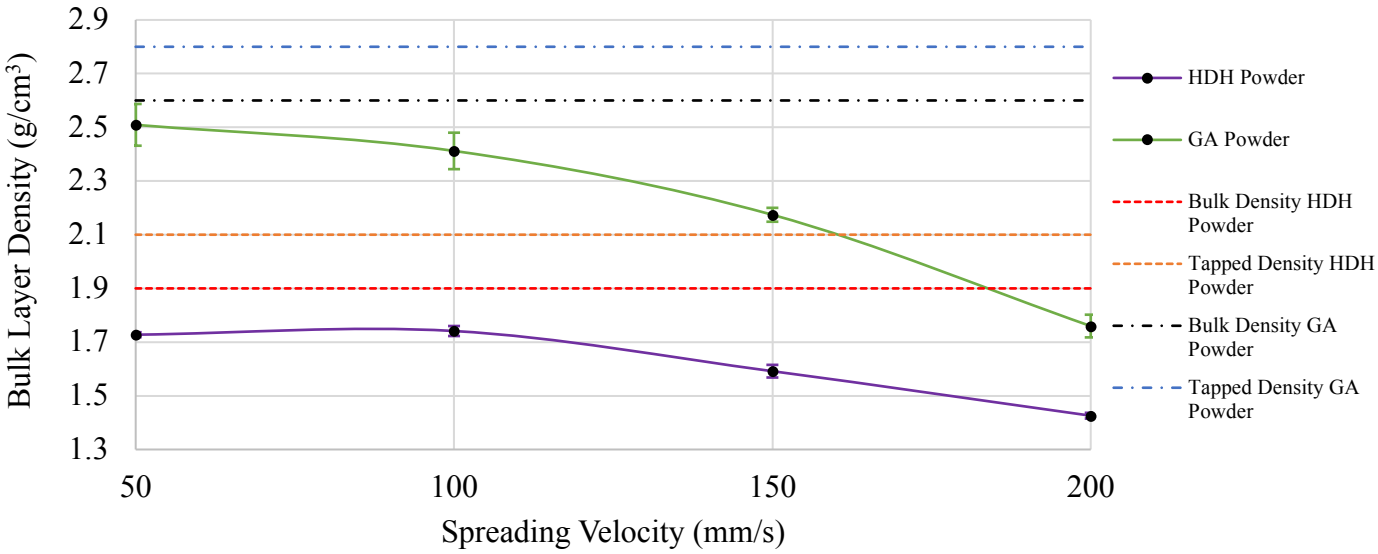

Figure 26: Spreading velocity (mm/s) against Layer Density (g/cm^3) for Gap Size 508 µm

5.2 Mass per Area

Mass per area is an additional metric introduced to characterise the spreadability of powders. This method involves eliminating the gap size from the equation by multiplying the bulk layer density by the corresponding gap size. The gap size across the bed is assumed to remain constant, which is not necessarily the case due to the existence of miniscule variations, hence, the mass per area attempts to redefine spreadability so as to mitigate such inaccuracies. A greater value of the mass per area is an indicator of enhanced powder spread dynamics, as increased mass deposition across an area suggest improved arrangement of particles that could result in uniform and high density layers. Figures 27-30 demonstrates the trends of the mass per area across 191 μm, 254 μm, 318 μm and 508 μm respectively. In most cases, an increase in the gap size will result in an increase in the values of the mass per area as the amount of mass poured on to the bed increases gradually and particles tend to effectively rearrange and easily flow through larger gap sizes [13, 134].

Figure 27 illustrates the mass per area obtained at 191 μm, where GA powders generally exhibits much greater values of mass per area compared to HDH powders except at the velocity of 100 mm/s. The higher mass per area values can be closely linked to the flow behaviour of powders, such that free-flowing powders tend to arrange effectively and spread across the build plate. As established in previous sections, GA powders comprises of better flowability compared to HDH powders, hence, their relative higher mass per area. As the spreading velocity increases, the mass per area of GA powders gradually decreases, implying a negative effect by increased spreader velocities on the spreading mechanism of powders. Figure 28 depicts the trends associated with the gap size of 254 μm, where GA powders outperforms HDH powders at different spreading velocities. Similar to section 5.1, HDH powders exhibits atypical results of extremely low values of the mass per area, hence this will be treated as an anomaly. Figure 29 and 30 portrays the trends at gap sizes 318 μm and 508 μm respectively, where they follow a similar trend to that of 191 μm. HDH powders indicates greater sensitivity to increased spreading velocities, but has its best result at the spreading velocity of 100 mm/s suggesting that they have optimised performance at a standard operating velocity of 100 mm/s.

To sum, mass per area may be used as a metric for spreadability, by eliminating the gap size as a variable so as to mitigate inaccuracies resulting from fluctuations of the gap size across the build

plate. They follow very similar trends to the results obtained for the bulk layer density, however, the values for the mass per area increases as the gap size increases except for HDH powder at 254 µm that will be treated as an anomaly. Increase in the spreading velocity results in a gradual reduction of mass per area values for GA powders, while a relatively drastic reduction for HDH powders except at 100 mm/s. The effects of spreading velocity as a process parameter has been covered in literature, where its increase results in the deterioration of the quality of the powder layer [134, 135, 138]. Additionally, owing to improved flow behaviour, GA powders surpass HDH powders in term of higher values of mass per area, which can be linked to enhanced and uniform layer densities and an indication of improved spreading performance.

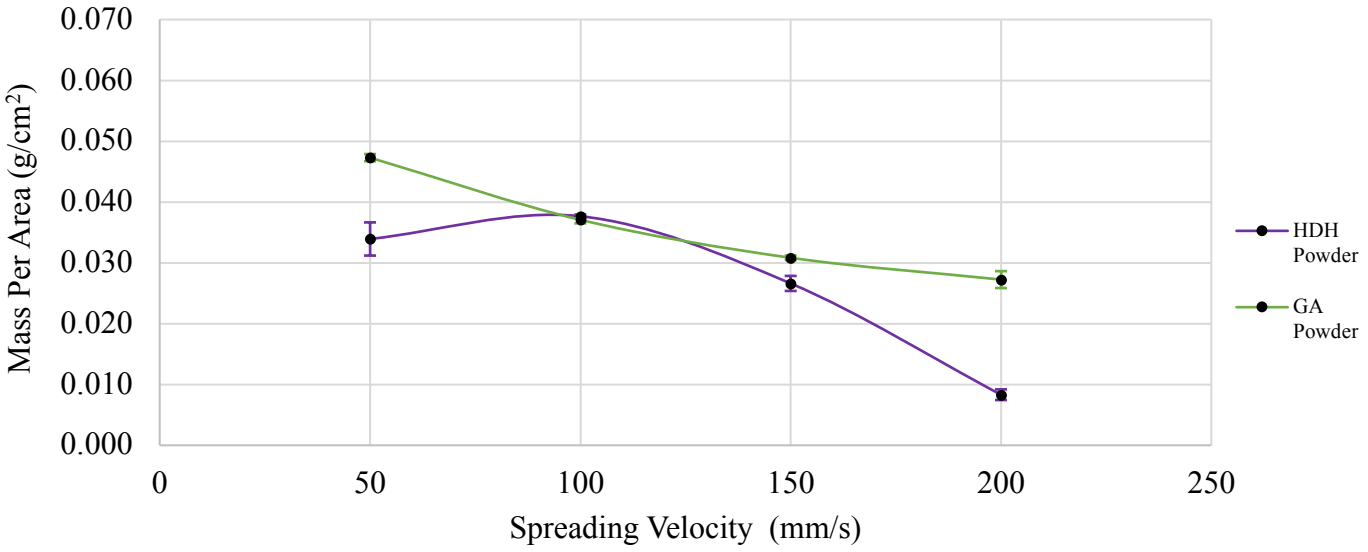

Figure 27: Spreading velocity (mm/s) against mass per area (g/cm^2) for Gap Size 191 µm

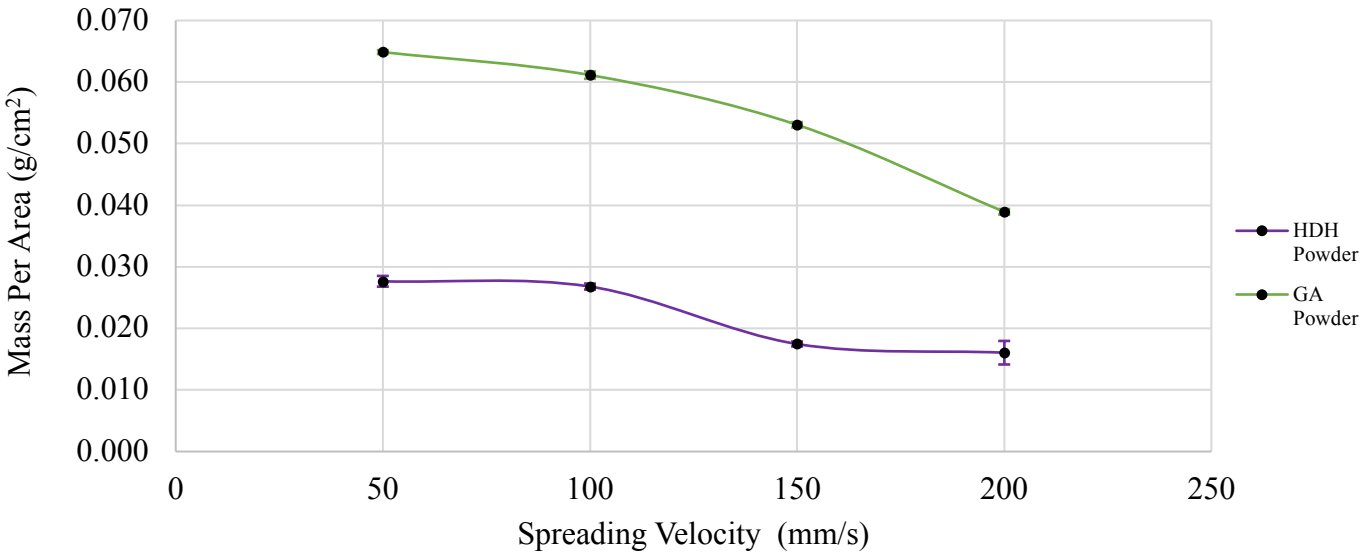

Figure 28: Spreading velocity (mm/s) against mass per area (g/cm^2) for Gap Size 254 µm

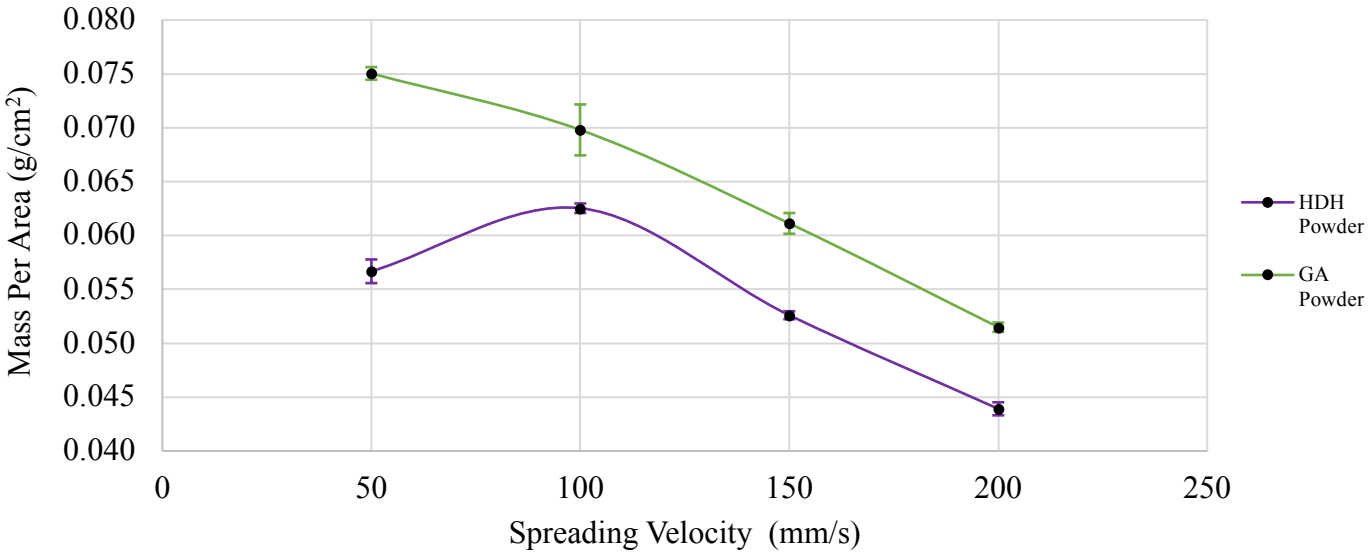

Figure 29: Spreading velocity (mm/s) against mass per area (g/cm^2) for Gap Size 318 µm

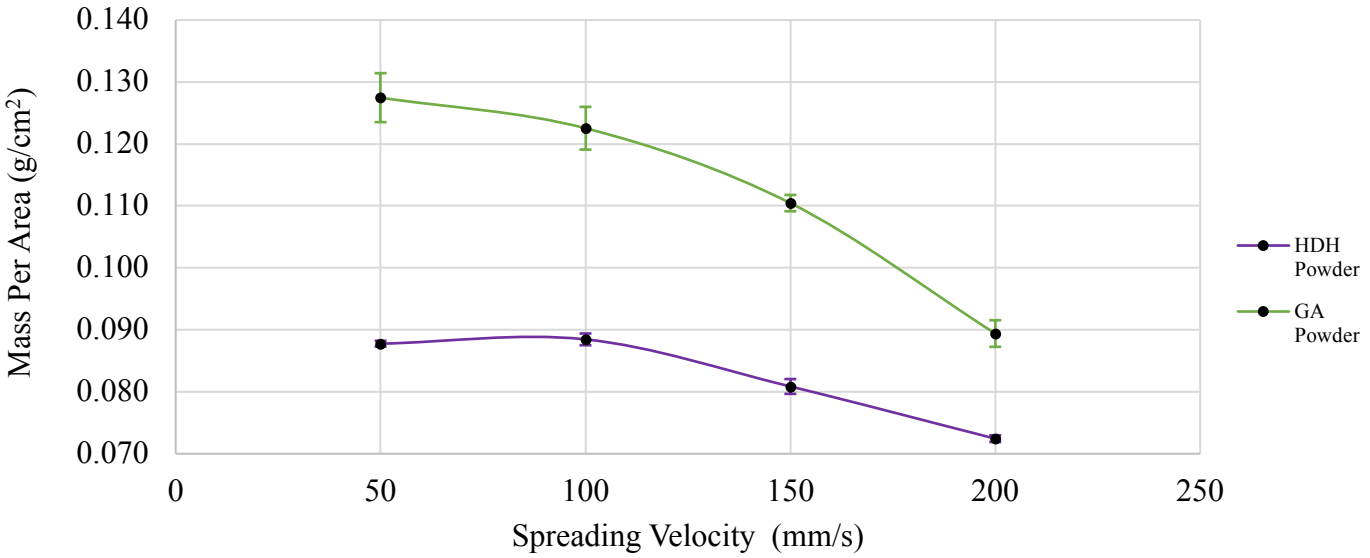

Figure 30: Spreading velocity (mm/s) against mass per area (g/cm^2) for Gap Size 508 µm

5.3 Combined Effect of Spreading Velocity and Gap Size

In addition to the bulk layer density and mass per area, the combined effect of the spreading velocity and gap size in terms of the dimensionless shear rate was also studied. The dimensionless shear rate as covered in section 2.2.3.4 normalises the results by removing variable parameters such as the gap size and spreading velocity. This measure endeavours in establishing a unification of results in investigate the behaviour of these powders in terms of the dimensionless shear rate (γ^{O}*).

The dimensionless shear rate, γ^{O}*, of both samples were calculated using the D_{50} of the particles [109] and was plotted against both the bulk layer density and mass per area. The plots of the dimensionless shear rate against the mass per area provided no significant information hence were omitted in this work. However, plots demonstrating the dimensionless shear rates against the bulk layer density provided significant information, which is presented in Figures 31 and 32 for HDH and GA powders respectively.

Figure 32 displays excellent unification for GA Ti-6Al-4V powders in a form of a master curve, where the bulk layer density can be closely correlated to the dimensionless shear rate regardless of the gap size or spreading velocity. On the contrary, no correlation nor unification can be established for HDH Ti-6Al-4V powders, suggesting that the powders do not reasonably fit well or correlate with the dimensionless shear rates. The figures below illustrate powders in the intermediate flow regimes within the dimensionless shear rate range of 0.25 to 3 as introduced by Tardos et al. [110]. It is important to note that every powder may exhibit a different threshold of the dimensionless shear rate, such that 0.25 as a threshold may not be applicable to all existing powders. For instance, Figure 31 illustrates the trends for HDH powders, and it can be observed that no significant changes occur over the first two points; however, drastic fluctuations occur at the dimensionless shear rate of about 0.8.

Furthermore, powders in the intermediate flow regimes experience fluctuations within the stress and strain rates and exhibit both frictional and collisional forces, suggesting that the flow behaviour of powders is significantly affected by the changes in spreading velocity. It can also be clearly observed that an increase in the dimensionless shear rate results in reduced bulk layer densities. This is mainly due to the influence of the dimensionless shear rate on the flow behaviour of powders, where the unconfined yield strength, f_c increases when the dimensionless shear rate, γ^{O*} increases, as expressed by; $f_c \sim \gamma^{O*^n}$, where n is less than one and greater than zero. The unconfined yield strength of powders, f_c, is translated as the resistance against flow or an inverse measure of flowability. Hence, as the unconfined yield strength f_c, of powders increase, the resistance against flow increases, suggesting that the powders spreadability will deteriorate.

In summary, the dimensionless shear rate normalises the variable parameters, which include the gap size and spreading velocity, in order to achieve a unifying value to detect and compare the effects of such rates on the bulk layer density of the two samples. GA powders presented excellent unification properties, indicating reliable powders, which was not the case for HDH powders. The reliability of GA powders may be attributed to their spherical morphologies, which enhances their flow and spreading dynamics. Additionally, different powders may also exhibit different thresholds, hence 0.25 as a definite value for the intermediate flow regime may not necessarily apply to all powders. Furthermore, Mehrabi et al. also confirmed that HDH powders exhibit lower

packing fractions compared to GA powders within the radial and central zones, due to their irregular morphologies [118].

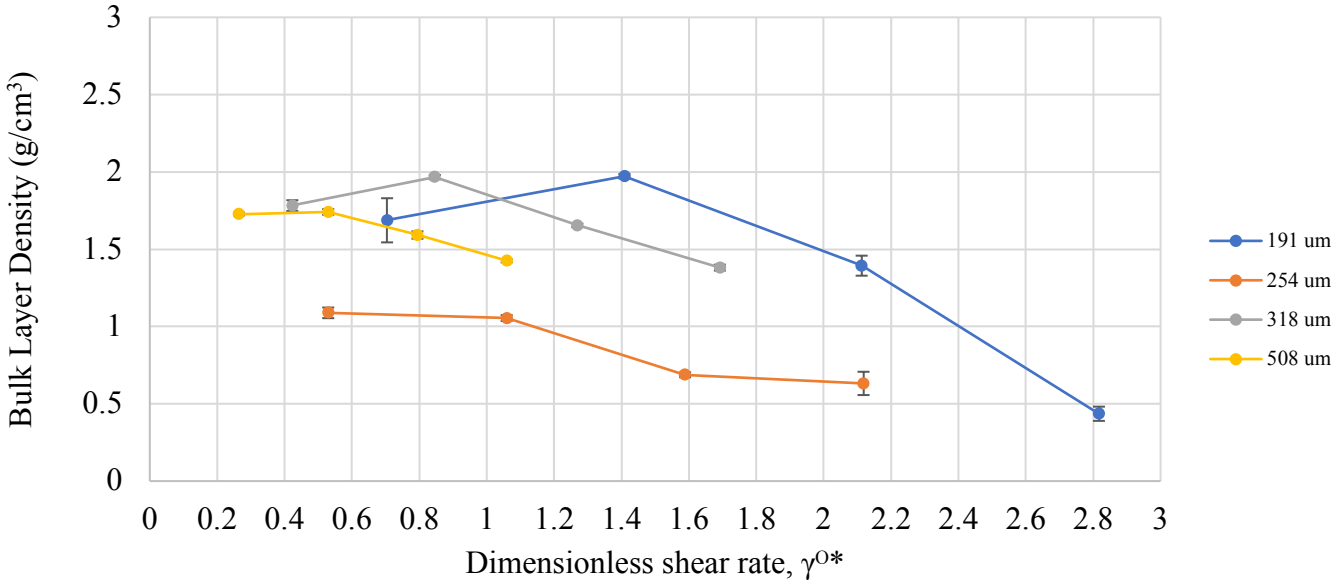

Figure 31: Dimensionless shear rate against bulk layer density(g/cm^3) of HDH Ti-6Al-4V powders

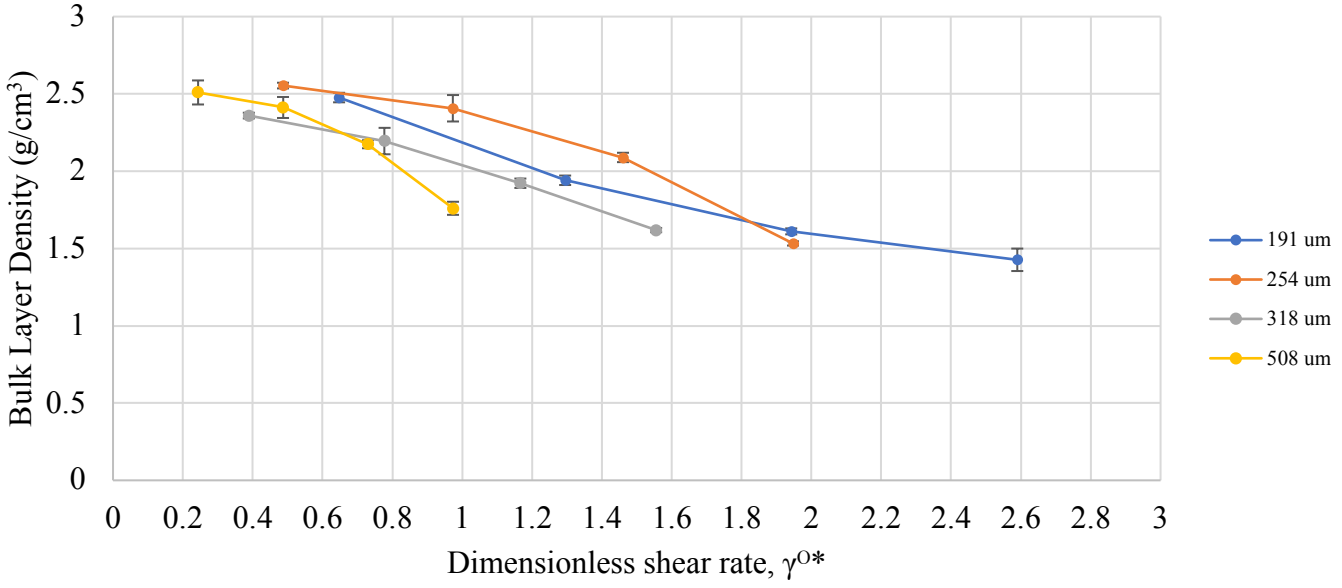

Figure 32: Dimensionless shear rate against bulk layer density(g/cm^3) of GA Ti-6Al-4V powders

CHAPTER SIX

Conclusions

6 Conclusions

Additive manufacturing has enabled the production of complex net-shaped or nearly net-shaped parts using different material such as polymers, metals, ceramics and composites which can directly be utilised as functional components [150]. Additionally, additive manufacturing as an emerging industry has facilitated the production of low-volume, high-value and complex end parts [150]. Powder bed-based additive manufacturing involves the layer-by-layer deposition of powder layers on a built plate to manufacture components, by utilising an electron beam or laser as a heat source. This phenomenon is known as powder spreadability, where unlike flowability has been minimally covered in literature. Thorough understanding of the spreading dynamics is imperative to ensure the deposition of thin and homogeneous powder layers as they play a crucial role in determining the overall quality of both the spread layer and final product.

Comparative assessment of the two samples was performed by both qualitative observations and quantitative analysis. The visual observations were in the form of captured overhead images of the spread profile to detect any changes such as jamming, wave-like texture on the spread profiles. SEM and XCT images were also provided by Mehrabi et al. [118] to inspect individual particles from the two samples. Additionally, an in-house rig was utilised to conduct spreading tests against four different gap sizes and velocities, so as to investigate the effects of such process parameters on the spreading behaviour of powders. The two metrics established for the spreadability of powders was the bulk layer density and the mass per area, where the former was deemed of more importance.

It was concluded from visual observations of SEM, XCT provided by Mehrabi et al. [118] and overhead camera that GA powders exhibited smoother surfaces rather than HDH powders due to the spherical morphologies, allowing them to pack effectively and creating homogenous layers of higher bulk densities. HDH powders exhibited elongated, irregular morphologies that can potentially lead to mechanical interlocking of particles, which impede powder flow and inevitably result in particle jamming on the powder bed.

Moreover, quantitative analysis was performed by calculating the bulk layer density and mass per area where the former metric presented more reliable results. GA powders exhibited much greater values of the bulk layer density compared to HDH powders, again owing to their spherical morphologies that enabled efficient packing creating even surface layers. It was detected that the percentage of spread increased gradually for GA powders when the gap size increased, however, this relationship was not conclusively proved for bulk layer densities across the different gap sizes. On the other hand, HDH powders performed better at lower gap sizes and spreading velocity of 100 mm/s except at the gap size of 254 μm, which will be treated as an anomaly. Additionally, the bulk layer density for GA powders decreases gradually as the spreading velocity increases suggesting a negative impact on the spreadability of powders at higher velocities.

Furthermore, the mass per area was as an attempt to measure spreadability by eliminating the gap size as a parameter to mitigate the errors resulting from variation of the gap size across the bed. The results indicated similar trends to that of the bulk layer density, however, the mass per area across the different gap sizes for both samples increased when the gap sizes increased, except for HDH powders at the gap size of 254 μm. Similarly, GA powders outperform HDH powders in regard to the higher mass per area values due to their enhanced flow behaviour.

The dimensionless shear rate was implemented in this study to compare its effects on the bulk layer density. This method normalises the variable factors which are the gap size and spreading velocity to produce a dimensionless value. It was gathered that GA powders exhibited better performance in a form of a unified master curve, indicating reliable powders. On the other hand, HDH powders did not portray trends of a master curve, suggesting degrees of heterogeneity that may indicate unreliability of powders.

Finally, the flow behaviour of powders does not provide a measure of spreadability but are still required to better understand the spreading dynamics. It is evident, from literature and the experimental tests conducted in this work, that spherical particles exhibit better spreading performance due to their enhanced flow behaviour and packing efficiency creating layers of desirable properties, in terms of smooth, even surfaces and higher densities. Figure 33 below provides a summary of the results gathered for HDH and GA Ti-6Al-4V powders.

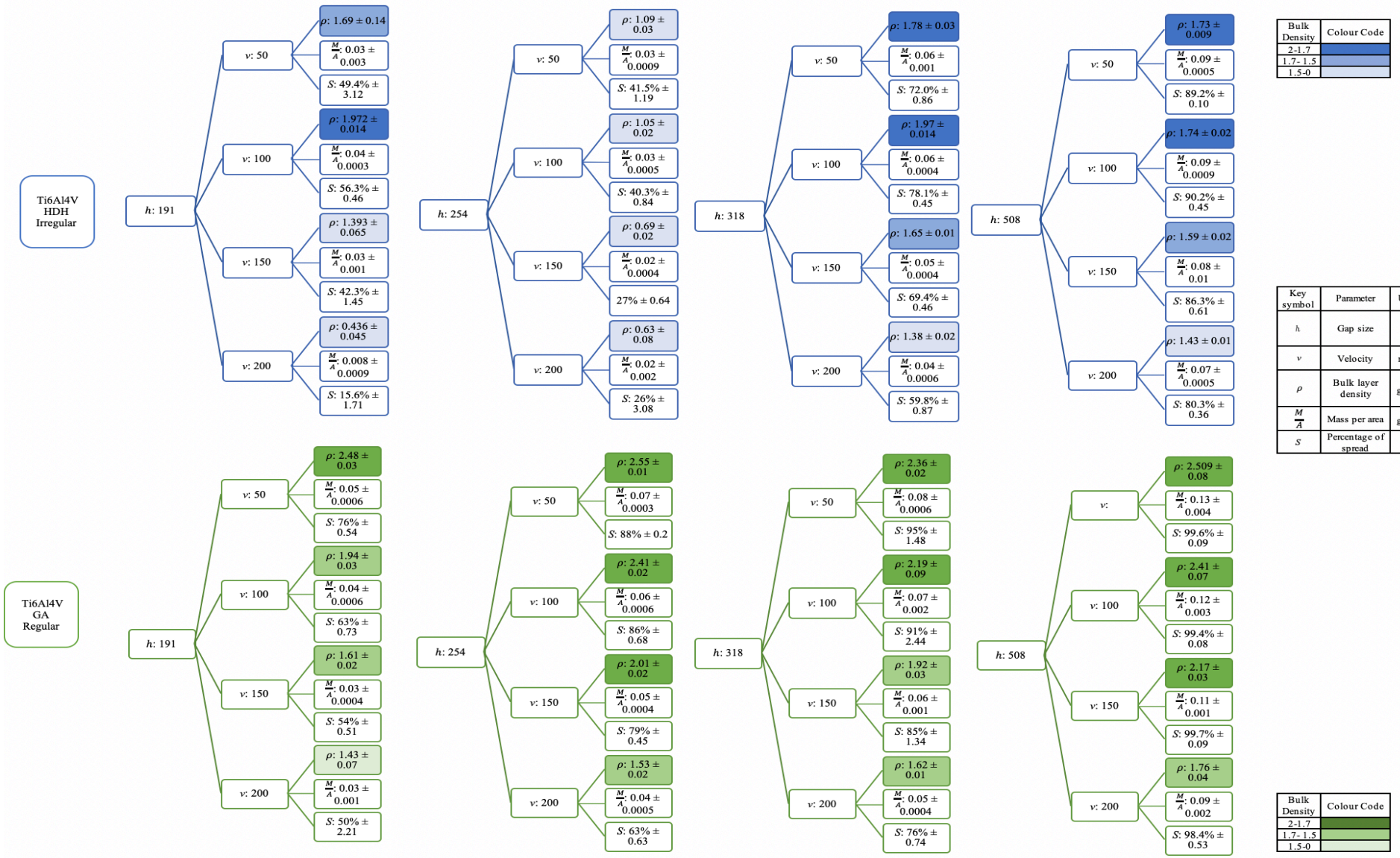

Figure 33: Summary of results for HDH and GA Ti-6Al-4V powders

CHAPTER SEVEN

Future Works

7.1 Recommendations

7 Recommendations and Future Work

The spreadability of powders is a fundamental factor affecting the quality of deposited layers, which is yet to be fully understood. To date, there is a lack of not only a definitive decision on defining the term spreadability but also viable metrics to measure this powder dynamic. The spreadability of powders is often correlated to their flowability, which may not be the correct representation of powder spreading. However, the flowability of powders should be accounted for during the spreading of thin layers. This raises the need to further develop characterisation methods to quantify and measure the spreadability of powders in additive manufacturing.

Currently, some literature covers experimental and simulation studies regarding the spreading dynamics of powders. However, the experimental work has only been limited to a single layer without any software confirming the spreading behaviour of powders. Powder spreading in PBF processes involves the layer-by-layer deposition of spread powders, hence the effects of multi-layers must be accounted for to enable the production of defect-free AM parts. Additionally, the simulation work implements very idealised powder properties such as utilising spherical shapes and eliminating any surface textures, which is not the case for true powders. Such idealisations can lead to significant inaccuracies and consequently, skew the final results.

7.1 Recommendations

The experimental work regarding the spreadability of powders should be compared to the numerical simulations for an in-depth understanding of the spreading dynamics and to further observe if such simulations support the experimental tests.

Moreover, designing a rig that emulates the coating behaviour of several layers with in-situ process measurements may provide accurate and reliable results. The multi-layer powder spreading will mimic the actual processing condition occurring in PBF processes. In-situ measurements may allow the detection of any defects occurring in real time, which may save time as it allows quality control in real time. Increasing the precision of the in-rig and amending the sharpness of the spreader is imperative in attaining accurate results.

In addition to that, external factors such as different environmental conditions can significantly influence the spreadability of powders, hence, it is imperative to test powders against such conditions. Testing powders at high relative humidity and various temperatures enables thorough analysis of the spreading behaviour. Temperature variations can be implemented by employing a hot bed as a build plate, while the humidity conditions may be controlled by utilising environment chambers.

Additionally, employing a laser profilometry or confocal microscopy enables the measurement of the thickness across the built plate, resulting in more reliable and accurate results. The effects of jamming can also be detected by employing force sensors across the built plate, where large fluctuations on the force profiles may be associated with jamming.

Furthermore, the effects of different process parameters need to be investigated all at the same time to fully assess the spreading behaviour of powders. As stated previously, process parameters such as spreading velocity, gap size, type and material of spreader need to be accounted for as powders exhibit different behaviours under different process conditions. Additionally, by utilising powders of different properties such as different particle size and shape distributions may provide valuable information regarding the differences in their spreading mechanism. Testing powders produced by different production methods enables thorough comparative analysis, which is essential for detecting differences in their spreading behaviour.

8 References

[1] D. Herzog, V. Seyda, E. Wycisk, and C. Emmelmann, "Additive manufacturing of metals," *Acta Materialia,* vol. 117, pp. 371-392, 2016/09/15/ 2016, doi: https://doi.org/10.1016/j.actamat.2016.07.019.

[2] S. H. Huang, P. Liu, A. Mokasdar, and L. Hou, "Additive manufacturing and its societal impact: a literature review," *The International Journal of Advanced Manufacturing Technology,* vol. 67, no. 5, pp. 1191-1203, 2013/07/01 2013, doi: 10.1007/s00170-012-4558-5.

[3] N. Guo and M. C. Leu, "Additive manufacturing: technology, applications and research needs," *Frontiers of Mechanical Engineering,* vol. 8, no. 3, pp. 215-243, 2013.

[4] A. C. F. o. A. M. Technologies and A. C. F. o. A. M. T. S. F. o. Terminology, *Standard terminology for additive manufacturing technologies*. Astm International, 2012.

[5] M. N. Dickson, "Soft strain sensors fabricated through additive manufacturing," *MRS Bulletin,* vol. 40, no. 6, pp. 463-463, 2015.

[6] S. F. S. Shirazi *et al.*, "A review on powder-based additive manufacturing for tissue engineering: selective laser sintering and inkjet 3D printing," *Science and Technology of Advanced Materials,* vol. 16, no. 3, p. 033502, 2015/06/20 2015, doi: 10.1088/1468-6996/16/3/033502.

[7] L. Hitzler, M. Merkel, W. Hall, and A. Öchsner, "A review of metal fabricated with laser- and powder-bed based additive manufacturing techniques: process, nomenclature, materials, achievable properties, and its utilization in the medical sector," *Advanced Engineering Materials,* vol. 20, no. 5, p. 1700658, 2018.

[8] M. Schneck *et al.*, "Evaluating the Use of Additive Manufacturing in Industry Applications," *Procedia CIRP,* vol. 81, pp. 19-23, 2019/01/01/ 2019, doi: https://doi.org/10.1016/j.procir.2019.03.004.

[9] N. Gupta, C. Weber, and S. Newsome, "Additive manufacturing: status and opportunities," *Science and Technology Policy Institute, Washington,* 2012.

[10] T. J. Horn and O. L. Harrysson, "Overview of current additive manufacturing technologies and selected applications," *Science progress,* vol. 95, no. 3, pp. 255-282, 2012.

[11] B. Schulz. "Wire Arc Additive Manufacturing Delivers Low Buy-To-Fly Ratios." Additive Manufacturing. https://www.additivemanufacturing.media/articles/wire-arc-additive-manufacturing-delivers-low-buy-to-fly-ratios (accessed 29/06, 2021).

[12] S. Beitz, R. Uerlich, T. Bokelmann, A. Diener, T. Vietor, and A. Kwade, "Influence of powder deposition on powder bed and specimen properties," *Materials,* vol. 12, no. 2, p. 297, 2019.

[13] M. Ahmed, M. Pasha, W. Nan, and M. Ghadiri, "A simple method for assessing powder spreadability for additive manufacturing," *Powder Technology,* vol. 367, pp. 671-679, 2020/05/01/ 2020, doi: https://doi.org/10.1016/j.powtec.2020.04.033.

[14] J. K. Prescott and R. A. Barnum, "On powder flowability," *Pharmaceutical technology,* vol. 24, no. 10, pp. 60-85, 2000.

[15] A. Popovich and V. Sufiiarov, "Metal Powder Additive Manufacturing," 2016.

[16] S. Wallner, "Powder Production Technologies," *BHM Berg- und Hüttenmännische Monatshefte,* vol. 164, no. 3, pp. 108-111, 2019/03/01 2019, doi: 10.1007/s00501-019-0832-2.
[17] I. Shishkovsky, *New trends in 3D printing*. BoD–Books on Demand, 2016.
[18] P. Sun, Z. Z. Fang, Y. Zhang, and Y. Xia, "Review of the Methods for Production of Spherical Ti and Ti Alloy Powder," *JOM,* vol. 69, no. 10, pp. 1853-1860, 2017/10/01 2017, doi: 10.1007/s11837-017-2513-5.
[19] A. Martín, C. M. Cepeda-Jiménez, and M. T. Pérez-Prado, "Gas atomization of γ-TiAl Alloy Powder for Additive Manufacturing," *Advanced Engineering Materials,* vol. 22, no. 1, p. 1900594, 2020.
[20] B. Rabin, G. Smolik, and G. Korth, "Characterization of entrapped gases in rapidly solidified powders," *Materials Science and Engineering: A,* vol. 124, no. 1, pp. 1-7, 1990.
[21] A. Asgarian, Z. Tang, M. Bussmann, and K. Chattopadhyay, "Water atomisation of metal powders: effect of water spray configuration," *Powder Metallurgy,* vol. 63, no. 4, pp. 288-299, 2020/08/07 2020, doi: 10.1080/00325899.2020.1802558.
[22] D. Singh *et al.*, "Continuous Manufacturing at Johnson Matthey For Pharmaceutical Applications," 2019.
[23] O. D. Neikov and V. G. Gopienko, "Chapter 18 - Production of Titanium and Titanium Alloy Powders," in *Handbook of Non-Ferrous Metal Powders (Second Edition)*, O. D. Neikov, S. S. Naboychenko, and N. A. Yefimov Eds. Oxford: Elsevier, 2019, pp. 549-570.
[24] M. Nishida, T. Tateyama, R. Tomoshige, K. Morita, and A. Chiba, "Electron microscopy studies of Ti - 47 at. % Al powder produced by plasma rotating electrode process," *Scripta Metallurgica et Materialia,* vol. 27, no. 3, pp. 335-340, 1992/08/01/ 1992, doi: https://doi.org/10.1016/0956-716X(92)90522-G.
[25] Y. Y. Kaplanskii *et al.*, "The structure and properties of pre-alloyed NiAl-Cr (Co, Hf) spherical powders produced by plasma rotating electrode processing for additive manufacturing," *Journal of materials research and technology,* vol. 7, no. 4, pp. 461-468, 2018.
[26] J. Tang, Y. Nie, Q. Lei, and Y. Li, "Characteristics and atomization behavior of Ti-6Al-4V powder produced by plasma rotating electrode process," *Advanced Powder Technology,* vol. 30, no. 10, pp. 2330-2337, 2019/10/01/ 2019, doi: https://doi.org/10.1016/j.apt.2019.07.015.
[27] M. N. Ahsan, A. J. Pinkerton, R. J. Moat, and J. Shackleton, "A comparative study of laser direct metal deposition characteristics using gas and plasma-atomized Ti–6Al–4V powders," *Materials Science and Engineering: A,* vol. 528, no. 25-26, pp. 7648-7657, 2011.
[28] T. DebRoy *et al.*, "Additive manufacturing of metallic components – Process, structure and properties," *Progress in Materials Science,* vol. 92, pp. 112-224, 2018/03/01/ 2018, doi: https://doi.org/10.1016/j.pmatsci.2017.10.001.
[29] P. Sun, Z. Z. Fang, Y. Xia, Y. Zhang, and C. Zhou, "A novel method for production of spherical Ti-6Al-4V powder for additive manufacturing," *Powder Technology,* vol. 301, pp. 331-335, 2016/11/01/ 2016, doi: https://doi.org/10.1016/j.powtec.2016.06.022.

[30] M. Entezarian, F. Allaire, P. Tsantrizos, and R. A. L. Drew, "Plasma atomization: A new process for the production of fine, spherical powders," *JOM,* Article vol. 48, no. 6, pp. 53-55, 1996, doi: 10.1007/BF03222969.

[31] S. Zherebtsov, M. Murzinova, G. Salishchev, and S. L. Semiatin, "Spheroidization of the lamellar microstructure in Ti–6Al–4V alloy during warm deformation and annealing," *Acta Materialia,* vol. 59, no. 10, pp. 4138-4150, 2011/06/01/ 2011, doi: https://doi.org/10.1016/j.actamat.2011.03.037.

[32] Z. K. Snow, "Understanding Powder Spreadability in Powder Bed Fusion Additive Manufacturing," 2018.

[33] M. Boulos, "Plasma power can make better powders," *Metal Powder Report,* vol. 59, no. 5, pp. 16-21, 2004.

[34] B. Dzur, "Plasma puts heat into spherical powder production," *Metal Powder Report,* vol. 63, no. 2, pp. 12-15, 2008.

[35] C. McCracken, D. Barbis, and R. Deeter, "Key characteristics of hydride–dehydride titanium powder," *Powder metallurgy,* vol. 54, no. 3, pp. 180-183, 2011.

[36] X. C. Goso and A. Kale, "Production of titanium metal powder by the HDH process," *Journal of the Southern African Institute of Mining and Metallurgy,* vol. 111, pp. 203-210, 03/01 2011.

[37] M. Yan and P. Yu, "An Overview of densification, microstructure and mechanical property of additively manufactured Ti-6Al-4V—Comparison among selective laser melting, electron beam melting, laser metal deposition and selective laser sintering, and with conventional powder," *Sintering techniques of materials,* 2015.

[38] Y. P. Dong *et al.*, "Cost-affordable Ti-6Al-4V for additive manufacturing: Powder modification, compositional modulation and laser in-situ alloying," *Additive Manufacturing,* vol. 37, p. 101699, 2021/01/01/ 2021, doi: https://doi.org/10.1016/j.addma.2020.101699.

[39] V. S. Bhattiprolu, K. W. Johnson, O. C. Ozdemir, and G. A. Crawford, "Influence of feedstock powder and cold spray processing parameters on microstructure and mechanical properties of Ti-6Al-4V cold spray depositions," *Surface and Coatings Technology,* vol. 335, pp. 1-12, 2018/02/15/ 2018, doi: https://doi.org/10.1016/j.surfcoat.2017.12.014.

[40] J. A. Slotwinski, E. J. Garboczi, P. E. Stutzman, C. F. Ferraris, S. S. Watson, and M. A. Peltz, "Characterization of metal powders used for additive manufacturing," *Journal of research of the National Institute of Standards and Technology,* vol. 119, p. 460, 2014.

[41] C. Meier, R. Weissbach, J. Weinberg, W. A. Wall, and A. J. Hart, "Critical influences of particle size and adhesion on the powder layer uniformity in metal additive manufacturing," *Journal of Materials Processing Technology,* vol. 266, pp. 484-501, 2019.

[42] N. Karapatis, G. Egger, P. Gygax, and R. Glardon, "Optimization of powder layer density in selective laser sintering," in *1999 International Solid Freeform Fabrication Symposium*, 1999.

[43] A. Streek, P. Regenfuss, R. Ebert, and H. Exner, "Laser micro sintering–a quality leap through improvement of powder packing," in *2008 International Solid Freeform Fabrication Symposium*, 2008.

[44] Y. Ma, T. M. Evans, N. Philips, and N. Cunningham, "Numerical simulation of the effect of fine fraction on the flowability of powders in additive manufacturing," *Powder Technology,* vol. 360, pp. 608-621, 2020.
[45] A. Cooke and J. Slotwinski, *Properties of metal powders for additive manufacturing: a review of the state of the art of metal powder property testing*. US Department of Commerce, National Institute of Standards and Technology, 2012.
[46] A. B. Spierings and G. Levy, "Comparison of density of stainless steel 316L parts produced with selective laser melting using different powder grades," in *Proceedings of the Annual International Solid Freeform Fabrication Symposium*, 2009: Austin, TX, pp. 342-353.
[47] E. C. Santos, M. Shiomi, K. Osakada, and T. Laoui, "Rapid manufacturing of metal components by laser forming," *International Journal of Machine Tools and Manufacture,* vol. 46, no. 12-13, pp. 1459-1468, 2006.
[48] A. Simchi, "The role of particle size on the laser sintering of iron powder," *Metallurgical and Materials Transactions B,* vol. 35, no. 5, pp. 937-948, 2004.
[49] M. Krantz, H. Zhang, and J. Zhu, "Characterization of powder flow: Static and dynamic testing," *Powder Technology,* vol. 194, no. 3, pp. 239-245, 2009/09/15/ 2009, doi: https://doi.org/10.1016/j.powtec.2009.05.001.
[50] Y. Shi, Z. Li, H. Sun, S. Huang, and F. Zeng, "Effect of the properties of the polymer materials on the quality of selective laser sintering parts," *Proceedings of the Institution of Mechanical Engineers, Part L: Journal of Materials: Design and Applications,* vol. 218, no. 3, pp. 247-252, 2004, doi: 10.1177/146442070421800308.
[51] C. Körner, E. Attar, and P. Heinl, "Mesoscopic simulation of selective beam melting processes," *Journal of Materials Processing Technology,* vol. 211, no. 6, pp. 978-987, 2011.
[52] A. T. Sutton, C. S. Kriewall, M. C. Leu, and J. W. Newkirk, "Powder characterisation techniques and effects of powder characteristics on part properties in powder-bed fusion processes," *Virtual and physical prototyping,* vol. 12, no. 1, pp. 3-29, 2017.
[53] Y. Lee and W. Zhang, "Mesoscopic simulation of heat transfer and fluid flow in laser powder bed additive manufacturing," in *International solid free form fabrication symposium, Austin*, 2015, pp. 1154-1165.
[54] A. B. Spierings, N. Herres, and G. Levy, "Influence of the particle size distribution on surface quality and mechanical properties in AM steel parts," *Rapid Prototyping Journal,* 2011.
[55] S. Ziegelmeier *et al.*, "An experimental study into the effects of bulk and flow behaviour of laser sintering polymer powders on resulting part properties," *Journal of Materials Processing Technology,* vol. 215, pp. 239-250, 2015/01/01/ 2015, doi: https://doi.org/10.1016/j.jmatprotec.2014.07.029.
[56] A. J. Forsyth, S. Hutton, M. J. Rhodes, and C. F. Osborne, "Effect of applied interparticle force on the static and dynamic angles of repose of spherical granular material," *Physical Review E,* vol. 63, no. 3, p. 031302, 2001.
[57] H. Chen, Q. Wei, Y. Zhang, F. Chen, Y. Shi, and W. Yan, "Powder-spreading mechanisms in powder-bed-based additive manufacturing: Experiments and computational

modeling," *Acta Materialia,* vol. 179, pp. 158-171, 2019/10/15/ 2019, doi: https://doi.org/10.1016/j.actamat.2019.08.030.
[58] K. Abd-Elghany and D. Bourell, "Property evaluation of 304L stainless steel fabricated by selective laser melting," *Rapid Prototyping Journal,* 2012.
[59] B. Liu, R. Wildman, C. Tuck, I. Ashcroft, and R. Hague, "Investigation the effect of particle size distribution on processing parameters optimisation in selective laser melting process," *Additive manufacturing research group, Loughborough University,* pp. 227-238, 2011.
[60] A. Averardi, C. Cola, S. E. Zeltmann, and N. Gupta, "Effect of particle size distribution on the packing of powder beds: A critical discussion relevant to additive manufacturing," *Materials Today Communications,* vol. 24, p. 100964, 2020.
[61] Q. B. Nguyen, M. L. S. Nai, Z. Zhu, C.-N. Sun, J. Wei, and W. Zhou, "Characteristics of Inconel Powders for Powder-Bed Additive Manufacturing," *Engineering,* vol. 3, no. 5, pp. 695-700, 2017/10/01/ 2017, doi: https://doi.org/10.1016/J.ENG.2017.05.012.
[62] E. J. R. Parteli and T. Pöschel, "Particle-based simulation of powder application in additive manufacturing," *Powder Technology,* vol. 288, pp. 96-102, 2016/01/01/ 2016, doi: https://doi.org/10.1016/j.powtec.2015.10.035.
[63] J. A. Muñiz-Lerma, A. Nommeots-Nomm, K. E. Waters, and M. Brochu, "A Comprehensive Approach to Powder Feedstock Characterization for Powder Bed Fusion Additive Manufacturing: A Case Study on AlSi7Mg," *Materials,* vol. 11, no. 12, p. 2386, 2018. [Online]. Available: https://www.mdpi.com/1996-1944/11/12/2386.
[64] G. Jacob, G. Jacob, C. U. Brown, and A. Donmez, *The influence of spreading metal powders with different particle size distributions on the powder bed density in laser-based powder bed fusion processes*. US Department of Commerce, National Institute of Standards and Technology, 2018.
[65] M. A. Kaleem, M. Z. Alam, M. Khan, S. H. I. Jaffery, and B. Rashid, "An experimental investigation on accuracy of Hausner Ratio and Carr Index of powders in additive manufacturing processes," *Metal Powder Report,* 2020/07/14/ 2020, doi: https://doi.org/10.1016/j.mprp.2020.06.061.
[66] H. Attar *et al.*, "Effect of Powder Particle Shape on the Properties of In Situ Ti–TiB Composite Materials Produced by Selective Laser Melting," *Journal of Materials Science & Technology,* vol. 31, no. 10, pp. 1001-1005, 2015/10/01/ 2015, doi: https://doi.org/10.1016/j.jmst.2015.08.007.
[67] S. Berretta, O. Ghita, and K. E. Evans, "Morphology of polymeric powders in Laser Sintering (LS): From Polyamide to new PEEK powders," *European Polymer Journal,* vol. 59, pp. 218-229, 2014/10/01/ 2014, doi: https://doi.org/10.1016/j.eurpolymj.2014.08.004.
[68] L. Cordova, T. Bor, M. de Smit, M. Campos, and T. Tinga, "Measuring the spreadability of pre-treated and moisturized powders for laser powder bed fusion," *AddItive manufacturing,* vol. 32, p. 101082, 2020.
[69] G. S. Upadhyaya, *Powder metallurgy technology*. Cambridge Int Science Publishing, 1997.
[70] S. Vock, B. Klöden, A. Kirchner, T. Weißgärber, and B. Kieback, "Powders for powder bed fusion: a review," *Progress in Additive Manufacturing,* pp. 1-15, 2019.

[71] E. O. Olakanmi, "Selective laser sintering/melting (SLS/SLM) of pure Al, Al–Mg, and Al–Si powders: Effect of processing conditions and powder properties," *Journal of Materials Processing Technology,* vol. 213, no. 8, pp. 1387-1405, 2013/08/01/ 2013, doi: https://doi.org/10.1016/j.jmatprotec.2013.03.009.

[72] A. B. Spierings, M. Voegtlin, T. Bauer, and K. Wegener, "Powder flowability characterisation methodology for powder-bed-based metal additive manufacturing," *Progress in Additive Manufacturing,* vol. 1, no. 1, pp. 9-20, 2016.

[73] J. W. Carson, B. H. Pittenger, and I. Jenike & Johanson, "Bulk Properties of Powders " *ASM Handbook: Powder Metal Technologies and Applications,* vol. 7, pp. 287-301, 1998, doi: 10.1361/asmhba0001530.

[74] M. Van den Eynde, L. Verbelen, and P. Van Puyvelde, "Assessing polymer powder flow for the application of laser sintering," *Powder Technology,* vol. 286, pp. 151-155, 2015/12/01/ 2015, doi: https://doi.org/10.1016/j.powtec.2015.08.004.

[75] B. Utela, D. Storti, R. Anderson, and M. Ganter, "A review of process development steps for new material systems in three dimensional printing (3DP)," *Journal of Manufacturing Processes,* vol. 10, no. 2, pp. 96-104, 2008/07/01/ 2008, doi: https://doi.org/10.1016/j.jmapro.2009.03.002.

[76] C. Pleass and S. Jothi, "Influence of powder characteristics and additive manufacturing process parameters on the microstructure and mechanical behaviour of Inconel 625 fabricated by Selective Laser Melting," *Additive Manufacturing,* vol. 24, pp. 419-431, 2018/12/01/ 2018, doi: https://doi.org/10.1016/j.addma.2018.09.023.

[77] Z. Snow, R. Martukanitz, and S. Joshi, "On the development of powder spreadability metrics and feedstock requirements for powder bed fusion additive manufacturing," *Additive Manufacturing,* vol. 28, pp. 78-86, 2019.

[78] A. B. Spierings, "Powder Spreadability and Characterization of Sc- and Zr-modified Aluminium Alloys processed by Selective Laser Melting. Quality Management System for additive manufacturing," ETH Zurich, 2018. [Online]. Available: http://hdl.handle.net/20.500.11850/253924

[79] E. Olson, "Particle shape factors and their use in image analysis part 1: theory," *Journal of GXP Compliance,* vol. 15, no. 3, p. 85, 2011.

[80] A. Strondl, O. Lyckfeldt, H. Brodin, and U. Ackelid, "Characterization and Control of Powder Properties for Additive Manufacturing," *JOM,* vol. 67, no. 3, pp. 549-554, 2015/03/01 2015, doi: 10.1007/s11837-015-1304-0.

[81] X. L. Deng and R. N. Davé, "Dynamic simulation of particle packing influenced by size, aspect ratio and surface energy," *Granular Matter,* vol. 15, no. 4, pp. 401-415, 2013.

[82] D. Schiochet Nasato and T. Pöschel, "Influence of particle shape in additive manufacturing: Discrete element simulations of polyamide 11 and polyamide 12," *Additive Manufacturing,* vol. 36, p. 101421, 2020/12/01/ 2020, doi: https://doi.org/10.1016/j.addma.2020.101421.

[83] S. Haeri, Y. Wang, O. Ghita, and J. Sun, "Discrete element simulation and experimental study of powder spreading process in additive manufacturing," *Powder Technology,* vol. 306, pp. 45-54, 2017.

[84] Y. Y. Sun, S. Gulizia, C. H. Oh, C. Doblin, Y. F. Yang, and M. Qian, "Manipulation and Characterization of a Novel Titanium Powder Precursor for Additive Manufacturing

Applications," *JOM,* vol. 67, no. 3, pp. 564-572, 2015/03/01 2015, doi: 10.1007/s11837-015-1301-3.
[85] J. Landauer, M. Kuhn, D. S. Nasato, P. Foerst, and H. Briesen, "Particle shape matters – Using 3D printed particles to investigate fundamental particle and packing properties," *Powder Technology,* vol. 361, pp. 711-718, 2020/02/01/ 2020, doi: https://doi.org/10.1016/j.powtec.2019.11.051.
[86] A. Standard, "Standard test methods for flow rate of metal powders using the hall flowmeter funnel," 2013.
[87] D. Geldart, E. Abdullah, A. Hassanpour, L. Nwoke, and I. Wouters, "Characterization of powder flowability using measurement of angle of repose," *China Particuology,* vol. 4, no. 3-4, pp. 104-107, 2006.
[88] R. L. Carr, "Classifying flow properties of solids," *Chem. Eng.,* vol. 1, pp. 69-72, 1965.
[89] D. McGlinchey, *Characterisation of bulk solids*. John Wiley & Sons, 2009.
[90] A. B. Spierings, *Powder Spreadability and Characterization of Sc-and Zr-modified Aluminium Alloys Processed by Selective Laser Melting: Quality Management System for Additive Manufacturing*. ETH Zurich, 2018.
[91] E. C. Abdullah and D. Geldart, "The use of bulk density measurements as flowability indicators," *Powder Technology,* vol. 102, no. 2, pp. 151-165, 1999/03/03/ 1999, doi: https://doi.org/10.1016/S0032-5910(98)00208-3.
[92] A. Chi-Ying Wong, "Characterisation of the flowability of glass beads by bulk densities ratio," *Chemical Engineering Science,* vol. 55, no. 18, pp. 3855-3859, 2000/09/15/ 2000, doi: https://doi.org/10.1016/S0009-2509(00)00048-8.
[93] H. P. Tang, M. Qian, N. Liu, X. Z. Zhang, G. Y. Yang, and J. Wang, "Effect of Powder Reuse Times on Additive Manufacturing of Ti-6Al-4V by Selective Electron Beam Melting," *JOM,* vol. 67, no. 3, pp. 555-563, 2015/03/01 2015, doi: 10.1007/s11837-015-1300-4.
[94] L. Markusson, "Powder Characterization for Additive Manufacturing Processes," ed, 2017.
[95] A. M. Rausch, V. E. Küng, C. Pobel, M. Markl, and C. Körner, "Predictive Simulation of Process Windows for Powder Bed Fusion Additive Manufacturing: Influence of the Powder Bulk Density," *Materials,* vol. 10, no. 10, p. 1117, 2017. [Online]. Available: https://www.mdpi.com/1996-1944/10/10/1117.
[96] G. Jacob, A. Donmez, J. Slotwinski, and S. Moylan, "Measurement of powder bed density in powder bed fusion additive manufacturing processes," *Measurement Science and Technology,* vol. 27, no. 11, p. 115601, 2016/10/05 2016, doi: 10.1088/0957-0233/27/11/115601.
[97] M. Schmid and K. Wegener, "Additive Manufacturing: Polymers Applicable for Laser Sintering (LS)," *Procedia Engineering,* vol. 149, pp. 457-464, 2016/01/01/ 2016, doi: https://doi.org/10.1016/j.proeng.2016.06.692.
[98] A. Amado, M. Schmid, and K. Wegener, "Flowability of SLS powders at elevated temperature," ETH Zurich, 2014.
[99] P. Karapatis, "A sub-process approach of selective laser sintering," EPFL, 2002.
[100] R. O. Grey and J. K. Beddow, "On the Hausner Ratio and its relationship to some properties of metal powders," *Powder Technology,* vol. 2, no. 6, pp. 323-326, 1969/09/01/ 1969, doi: https://doi.org/10.1016/0032-5910(69)80024-0.

[101] R. P. Zou and A. B. Yu, "Evaluation of the packing characteristics of mono-sized non-spherical particles," *Powder Technology,* vol. 88, no. 1, pp. 71-79, 1996/07/01/ 1996, doi: https://doi.org/10.1016/0032-5910(96)03106-3.
[102] A. Zocca, C. M. Gomes, T. Mühler, and J. Günster, "Powder-bed stabilization for powder-based additive manufacturing," *Advances in Mechanical Engineering,* vol. 6, p. 491581, 2014.
[103] A. W. Jenike, "Storage and flow of solids, bulletin no. 123," *Bulletin of the University of Utah,* vol. 53, no. 26, p. 198, 1964.
[104] K. Johanson, "Effect of particle shape on unconfined yield strength," *Powder Technology,* vol. 194, no. 3, pp. 246-251, 2009/09/15/ 2009, doi: https://doi.org/10.1016/j.powtec.2009.05.004.
[105] D. Schulze, "Flow properties of powders and bulk solids," *Braunschweig/Wolfenbu ttel, Germany: University of Applied Sciences,* 2006.
[106] J. A. Slotwinski and E. J. Garboczi, "Metrology needs for metal additive manufacturing powders," *Jom,* vol. 67, no. 3, pp. 538-543, 2015.
[107] P. Mellin, O. Lyckfeldt, P. Harlin, H. Brodin, H. Blom, and A. Strondl, "Evaluating flowability of additive manufacturing powders, using the Gustavsson flow meter," *Metal Powder Report,* vol. 72, no. 5, pp. 322-326, 2017/09/01/ 2017, doi: https://doi.org/10.1016/j.mprp.2017.06.003.
[108] D. Schulze, "Measuring powder flowability: a comparison of test methods-part I," *Powder and Bulk Engineering,* vol. 10, pp. 45-61, 1996.
[109] A. Hassanpour, C. Hare, and M. Pasha, *Powder flow : theory, characterisation and application*. London: Royal Society of Chemistry, 2019.
[110] G. I. Tardos, S. McNamara, and I. Talu, "Slow and intermediate flow of a frictional bulk powder in the Couette geometry," *Powder Technology,* vol. 131, no. 1, pp. 23-39, 2003/03/03/ 2003, doi: https://doi.org/10.1016/S0032-5910(02)00315-7.
[111] A. Thompson, N. Senin, I. Maskery, L. Körner, S. Lawes, and R. Leach, "Internal surface measurement of metal powder bed fusion parts," *Additive Manufacturing,* vol. 20, pp. 126-133, 2018/03/01/ 2018, doi: https://doi.org/10.1016/j.addma.2018.01.003.
[112] J. M. Benson and E. Snyders, "The need for powder characterisation in the additive manufacturing industry and the establishment of a national facility," *South African Journal of Industrial Engineering,* vol. 26, no. 2, pp. 104-114, 2015.
[113] R. Cunningham *et al.*, "Analyzing the effects of powder and post-processing on porosity and properties of electron beam melted Ti-6Al-4V," *Materials Research Letters,* vol. 5, no. 7, pp. 516-525, 2017.
[114] O. D. Neikov, "Atomization and granulation," in *Handbook of non-ferrous metal powders*, 2009, pp. 102-142.
[115] H. Galarraga, D. A. Lados, R. R. Dehoff, M. M. Kirka, and P. Nandwana, "Effects of the microstructure and porosity on properties of Ti-6Al-4V ELI alloy fabricated by electron beam melting (EBM)," *Additive Manufacturing,* vol. 10, pp. 47-57, 2016.
[116] M. Iebba *et al.*, "Influence of powder characteristics on formation of porosity in additive manufacturing of Ti-6Al-4V components," *Journal of Materials Engineering and Performance,* vol. 26, no. 8, pp. 4138-4147, 2017.

[117] G. Kerckhofs, G. Pyka, M. Moesen, S. Van Bael, J. Schrooten, and M. Wevers, "High-resolution microfocus X-ray computed tomography for 3D surface roughness measurements of additive manufactured porous materials," *Advanced Engineering Materials,* vol. 15, no. 3, pp. 153-158, 2013.
[118] M. Mehrabi, A. Hassanpour, and A. Bayly, "An X-ray microtomography study of particle morphology and the packing behaviour of metal powders during filling, compaction and ball indentation processes," *Powder Technology,* vol. 385, pp. 250-263, 2021/06/01/ 2021, doi: https://doi.org/10.1016/j.powtec.2021.02.069.
[119] S. Özbilen, "Satellite formation mechanism in gas atomised powders," *Powder Metallurgy,* vol. 42, no. 1, pp. 70-78, 1999.
[120] R. J. Hebert, "Metallurgical aspects of powder bed metal additive manufacturing," *Journal of Materials Science,* vol. 51, no. 3, pp. 1165-1175, 2016.
[121] G. Pyka, G. Kerckhofs, I. Papantoniou, M. Speirs, J. Schrooten, and M. Wevers, "Surface Roughness and Morphology Customization of Additive Manufactured Open Porous Ti6Al4V Structures," *Materials,* vol. 6, no. 10, pp. 4737-4757, 2013. [Online]. Available: https://www.mdpi.com/1996-1944/6/10/4737.
[122] H. C. Hamaker, "The London—van der Waals attraction between spherical particles," *physica,* vol. 4, no. 10, pp. 1058-1072, 1937.
[123] F. Chu *et al.*, "Influence of satellite and agglomeration of powder on the processability of AlSi10Mg powder in Laser Powder Bed Fusion," *Journal of Materials Research and Technology,* vol. 11, pp. 2059-2073, 2021/03/01/ 2021, doi: https://doi.org/10.1016/j.jmrt.2021.02.015.
[124] L. E. Thomas-Seale, J. C. Kirkman-Brown, M. M. Attallah, D. M. Espino, and D. E. Shepherd, "The barriers to the progression of additive manufacture: Perspectives from UK industry," *International Journal of Production Economics,* vol. 198, pp. 104-118, 2018.
[125] L. I. Escano *et al.*, "Revealing particle-scale powder spreading dynamics in powder-bed-based additive manufacturing process by high-speed x-ray imaging," *Scientific reports,* vol. 8, no. 1, pp. 1-11, 2018.
[126] C. A. Chatham, T. E. Long, and C. B. Williams, "A review of the process physics and material screening methods for polymer powder bed fusion additive manufacturing," *Progress in Polymer Science,* vol. 93, pp. 68-95, 2019/06/01/ 2019, doi: https://doi.org/10.1016/j.progpolymsci.2019.03.003.
[127] S. Berretta, O. Ghita, K. E. Evans, A. Anderson, and C. Newman, "Size, shape and flow of powders for use in Selective Laser Sintering (SLS)," *High Value Manufacturing: Advanced Research in Virtual and Rapid Prototyping,* p. 49, 2013.
[128] R. Esmaeilizadeh, U. Ali, A. Keshavarzkermani, Y. Mahmoodkhani, E. Marzbanrad, and E. Toyserkani, "On the effect of spatter particles distribution on the quality of Hastelloy X parts made by laser powder-bed fusion additive manufacturing," *Journal of Manufacturing Processes,* vol. 37, pp. 11-20, 2019/01/01/ 2019, doi: https://doi.org/10.1016/j.jmapro.2018.11.012.
[129] J. M. Contreras, A. Jiménez-Morales, and J. M. Torralba, "Improvement of rheological properties of Inconel 718 MIM feedstock using tailored particle size distributions,"

Powder Metallurgy, vol. 51, no. 2, pp. 103-106, 2008/06/01 2008, doi: 10.1179/174329008X313342.
[130] W. Nan *et al.*, "Jamming during particle spreading in additive manufacturing," *Powder Technology,* vol. 338, pp. 253-262, 2018.
[131] H. Chen, Y. Chen, Y. Liu, Q. Wei, Y. Shi, and W. Yan, "Packing quality of powder layer during counter-rolling-type powder spreading process in additive manufacturing," *International Journal of Machine Tools and Manufacture,* vol. 153, p. 103553, 2020.
[132] S. Haeri, "Optimisation of blade type spreaders for powder bed preparation in Additive Manufacturing using DEM simulations," *Powder Technology,* vol. 321, pp. 94-104, 2017.
[133] A. Budding and T. H. J. Vaneker, "New Strategies for Powder Compaction in Powder-based Rapid Prototyping Techniques," *Procedia CIRP,* vol. 6, pp. 527-532, 2013/01/01/ 2013, doi: https://doi.org/10.1016/j.procir.2013.03.100.
[134] Y. M. Fouda and A. E. Bayly, "A DEM study of powder spreading in additive layer manufacturing," *Granular Matter,* vol. 22, no. 1, pp. 1-18, 2020.
[135] W. Nan and M. Ghadiri, "Numerical simulation of powder flow during spreading in additive manufacturing," *Powder Technology,* vol. 342, pp. 801-807, 2019/01/15/ 2019, doi: https://doi.org/10.1016/j.powtec.2018.10.056.
[136] Z. Xiang, M. Yin, Z. Deng, X. Mei, and G. Yin, "Simulation of forming process of powder bed for additive manufacturing," *Journal of Manufacturing Science and Engineering,* vol. 138, no. 8, 2016.
[137] Y. Shi and Y. Zhang, "Simulation of random packing of spherical particles with different size distributions," *Applied Physics A,* vol. 92, no. 3, pp. 621-626, 2008.
[138] P. S. Desai and C. F. Higgs, "Spreading process maps for powder-bed additive manufacturing derived from physics model-based machine learning," *Metals,* vol. 9, no. 11, p. 1176, 2019.
[139] M. Shaheen, A. Thornton, S. Luding, and T. Weinhart, "Discrete particle simulation of the spreading process in additive manufacturing," in *8th International Conference on Discrete Element Methods, DEM 2019: MS-03: Open-source development*, 2019: University of Twente, pp. 263-263.
[140] Y. Sun, M. Aindow, and R. J. Hebert, "Comparison of virgin Ti-6Al-4V powders for additive manufacturing," *Additive Manufacturing,* vol. 21, pp. 544-555, 2018/05/01/ 2018, doi: https://doi.org/10.1016/j.addma.2018.02.011.
[141] G. Chen, S. Y. Zhao, P. Tan, J. Wang, C. S. Xiang, and H. P. Tang, "A comparative study of Ti-6Al-4V powders for additive manufacturing by gas atomization, plasma rotating electrode process and plasma atomization," *Powder Technology,* vol. 333, pp. 38-46, 2018/06/15/ 2018, doi: https://doi.org/10.1016/j.powtec.2018.04.013.
[142] H. Gong, K. Rafi, H. Gu, T. Starr, and B. Stucker, "Analysis of defect generation in Ti–6Al–4V parts made using powder bed fusion additive manufacturing processes," *Additive Manufacturing,* vol. 1-4, pp. 87-98, 2014/10/01/ 2014, doi: https://doi.org/10.1016/j.addma.2014.08.002.
[143] H. Gong *et al.*, "Melt pool characterization for selective laser melting of Ti-6Al-4V pre-alloyed powder," in *Solid freeform fabrication symposium*, 2014, pp. 256-267.

[144] C.-J. Kong, C. J. Tuck, I. A. Ashcroft, R. D. Wildman, and R. Hague, "High density Ti6Al4V via SLM processing: microstructure and mechanical properties," in *International Solid Freeform Fabrication Symposium*, 2011, vol. 36, pp. 475-483.
[145] D. Drake, "An approach for defining the key quality characteristics of metal powder for powder bed fusion and directed energy deposition," *Colorado school of mines,* 2018.
[146] W. Xu, S. Sun, J. Elambasseril, Q. Liu, M. Brandt, and M. Qian, "Ti-6Al-4V additively manufactured by selective laser melting with superior mechanical properties," *Jom,* vol. 67, no. 3, pp. 668-673, 2015.
[147] K. Higashitani, H. Makino, and S. Matsusaka, *Powder Technology Handbook*, 4th ed. ed. Boca Raton: CRC Press LLC, 2019.
[148] S. Tammas-Williams, H. Zhao, F. Léonard, F. Derguti, I. Todd, and P. B. Prangnell, "XCT analysis of the influence of melt strategies on defect population in Ti–6Al–4V components manufactured by Selective Electron Beam Melting," *Materials Characterization,* vol. 102, pp. 47-61, 2015/04/01/ 2015, doi: https://doi.org/10.1016/j.matchar.2015.02.008.
[149] M. Neikter *et al.*, "Defect characterization of electron beam melted Ti-6Al-4V and Alloy 718 with X-ray microtomography," *Aeronautics and Aerospace Open Access Journal,* vol. 2, no. 3, pp. 139-145, 2018.
[150] F. Calignano *et al.*, "Overview on Additive Manufacturing Technologies," *Proceedings of the IEEE,* vol. 105, no. 4, pp. 593-612, 2017, doi: 10.1109/JPROC.2016.2625098.

Appendix

- Sample excel spreadsheet for calculating the layer bulk density and mass per area.

Sample 2: Ti6Al4V GA- Regular
PSD: 25-130um

Date: 27/01/2021
Time: 11:00am

Gap size: 318 um
Amount: 4 grams
Speed: 200 mm/s= 4000 RPM

Weight of the empty container: 2.4674g

Iterations	Weight of powder after taring (g)	Weight of powder in Container after feeding (g)	Weight of the powder from wall of feeder + previous amount (g)	Weight of collected powder after spreading (dropped powder) (g)	Weight of spreaded powder in new container (g)	percentage of spread powder%	Losses	Percentage losses%
1	4.0071	0	0	0.9313	3.0368	75.78548077	0.9703	24.214519
2	4.0075	0	0	0.9682	3.0088	75.07922645	0.9987	24.920773
3	4.0069	0	0	0.9635	3.0035	74.95819711	1.0034	25.041802
4	4.0074	0	0	0.9072	3.0671	76.53590857	0.9403	23.464091
5	4.0078	0	0	0.8964	3.0769	76.77279305	0.9309	23.227206
Average	**4.0074**					**75.82632119**	**0.968325**	**24.16346**
						Standard Deviation		
						0.736584163		

Standard Deviation

Iterations	Data	Standard Deviation
1	75.78548077	0
2	75.07922645	0.353127161
3	74.95819711	0.364819822
4	76.53590857	0.631074463
5	76.77279305	0.736584163

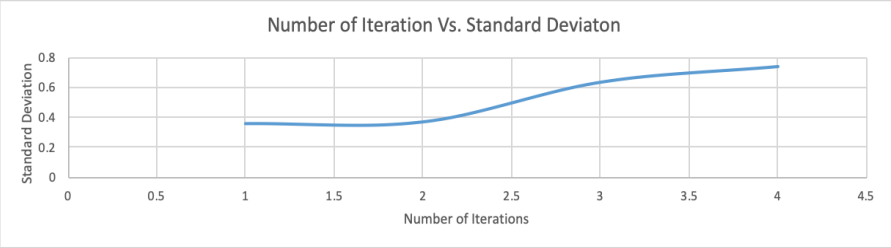

Time
14:00
14:30

Density Calculations from the Spreadability 0.0318

Iteration	Area (mm^2)	Volume (cm^3)	Density (g/cm^3)	Mass per area (g/cm^2)
1	5919.044	1.882255992	1.613383096	0.051305582
2	5826.347	1.852778346	1.623939532	0.051641277
3	5785.943	1.839929874	1.63239917	0.051910294
4	5916.362	1.881403116	1.630219475	0.051840979
5	6065.295	1.92876381	1.595270496	0.050729602
Average Density			**1.619042354**	**0.051485547**
			0.013597377	0.000432397

- Calculation of the dimensionless shear rate.

HDH Powders

Dimensionless Shear Rate					
Gap Size	**Velocity**	**γ°= (Velocity/Gap size)**	**D[v,0.5]**	**g**	**γ^{O}***
mm	**mm/s**	**s^{-1}**	**mm**	**mms^{-2}**	**$=\gamma^{\circ}(d/g)^{1/2}$**
0.508	50	98.4	0.07100	9810	0.265
	100	196.9	0.07100	9810	0.530
	150	295.3	0.07100	9810	0.794
	200	393.7	0.07100	9810	1.059
0.318	50	157.2	0.07100	9810	0.423
	100	314.5	0.07100	9810	0.846
	150	471.7	0.07100	9810	1.269
	200	628.9	0.07100	9810	1.692
0.254	50	196.9	0.07100	9810	0.530
	100	393.7	0.07100	9810	1.059
	150	590.6	0.07100	9810	1.589
	200	787.4	0.07100	9810	2.118
0.191	50	261.8	0.07100	9810	0.704
	100	523.6	0.07100	9810	1.409
	150	785.3	0.07100	9810	2.113
	200	1047.1	0.07100	9810	2.817

GA Powders

	Dimensionless Shear Rate				
Gap Size	**Velocity**	**γ°= (Velocity/Gap size)**	**D[v,0.5]**	**g**	**γ^{o*}**
mm	mm/s	s^{-1}	mm	mms^{-2}	$=\gamma^{\circ}(d/g)^{1/2}$
0.508	50	98.4	0.06	9810	0.243
	100	196.9	0.06	9810	0.487
	150	295.3	0.06	9810	0.730
	200	393.7	0.06	9810	0.974
0.318	50	157.2	0.06	9810	0.389
	100	314.5	0.06	9810	0.778
	150	471.7	0.06	9810	1.167
	200	628.9	0.06	9810	1.555
0.254	50	196.9	0.06	9810	0.487
	100	393.7	0.06	9810	0.974
	150	590.6	0.06	9810	1.460
	200	787.4	0.06	9810	1.947
0.191	50	261.8	0.06	9810	0.647
	100	523.6	0.06	9810	1.295
	150	785.3	0.06	9810	1.942
	200	1047.1	0.06	9810	2.590

- Calculating the angle of repose on the build

HDH TiAl4V at 191 μm with 50 mm/s

Iteration	H(left),mm	B(Left), mm	AoR (Left), Radians	AoR (Left), Degrees	H (Right), mm	B (Right), mm	AoR (Right), Radians	AoR (Right), Degrees	AoR (Average), Degrees
1	15.304	24.73	0.5541599	31.751025	13.92	27.027	0.4756075	27.250302	29.500663
2	12.097	25.968	0.4359502	24.978108	12.581	23.872	0.4850285	27.790087	26.384098
3	14.25	25.374	0.5117044	29.318501	13.5	24.124	0.5101904	29.231756	29.275128
4	14.739	26.738	0.5037931	28.865221	13.043	24.912	0.4823198	27.634888	28.250054
5	13.037	26.565	0.4562271	26.139889	13.318	26.498	0.4657286	26.684284	26.412086
								Average	27.964406

GA TiAl4V at 191 μm with 50 mm/s

Iteration	H(left),mm	B(Left), mm	AoR (Left), Radians	AoR (Left), Degrees	H (Right), mm	B (Right), mm	AoR (Right), Radians	AoR (Right), Degrees	AoR (Average), Degrees
1	10.185	23.521	0.4086417	23.413446	9.817	24.445	0.381881	21.880168	22.646807
2	8.632	26.462	0.3153201	18.066513	9.907	24.482	0.3845211	22.031439	20.048976
3	10.346	23.275	0.4182801	23.965687	10.001	25.344	0.3758513	21.534696	22.750191
4	10.325	23.572	0.4128466	23.654365	10.411	26.5	0.374343	21.448271	22.551318
5	9.034	26.932	0.323643	18.543379	10.229	26.25	0.371575	21.289678	19.916529
								Average	21.582764